

ABSTRACT

Title of Thesis: **REVEALING THE STRUCTURAL
AND FUNCTIONAL
PROPERTIES OF NON-
CANONICAL K6-LINKED
POLYUBIQUITIN CHAINS.**

Apurva Chaturvedi, Doctor of Philosophy, 2017

Thesis Directed By: Professor David Fushman,
Department of Chemistry and Biochemistry

Ubiquitin is an important protein modifier in eukaryotes, which tags the proteins and signals them to different pathways in the cell. It has been shown that polyubiquitin chains of different linkages act as distinct cellular signals. Non-canonical K6-linked polyubiquitin chains have been linked to breast and ovarian tumor suppressor protein BRCA1. However, detailed structural and binding studies of these chains had been hampered by the absence of an efficient way to synthesize them. We developed and optimized both non-enzymatic and enzymatic methods to synthesize K6-linked

polyubiquitin chains. Dynamics of K6-linked diubiquitin chains were studied by solution NMR and ensemble analysis. We determined that K6-linked diubiquitin is present in at least of two conformations in solution. The conformers we determined from the analysis of solution data suggested the structural ability of K6-linked diubiquitin to bind protein receptors from both proteasomal degradation signaling pathway (hHR23a UBA2) and DNA Damage Repair pathway (Rap80 tUIM). In order to elucidate the pathway it is involved in, we performed NMR binding assays to determine which of these proteins K6-linked diubiquitin binds. We found that this diubiquitin binds both Rap80 tUIM and hHR23a UBA2 with a high affinity, suggesting that it has the functionality to be part of both DNA repair pathway and proteasomal signaling pathway. Thus, our studies with K6-linked diubiquitin have revealed that due to their conformational heterogeneity, these chains have the capability to be part of both proteasomal degradation signaling and DNA damage repair pathways.

REVEALING THE STRUCTURAL AND FUNCTIONAL
PROPERTIES OF NON-CANONICAL K6-LINKED
POLYUBIQUITIN CHAINS.

by

Apurva Chaturvedi

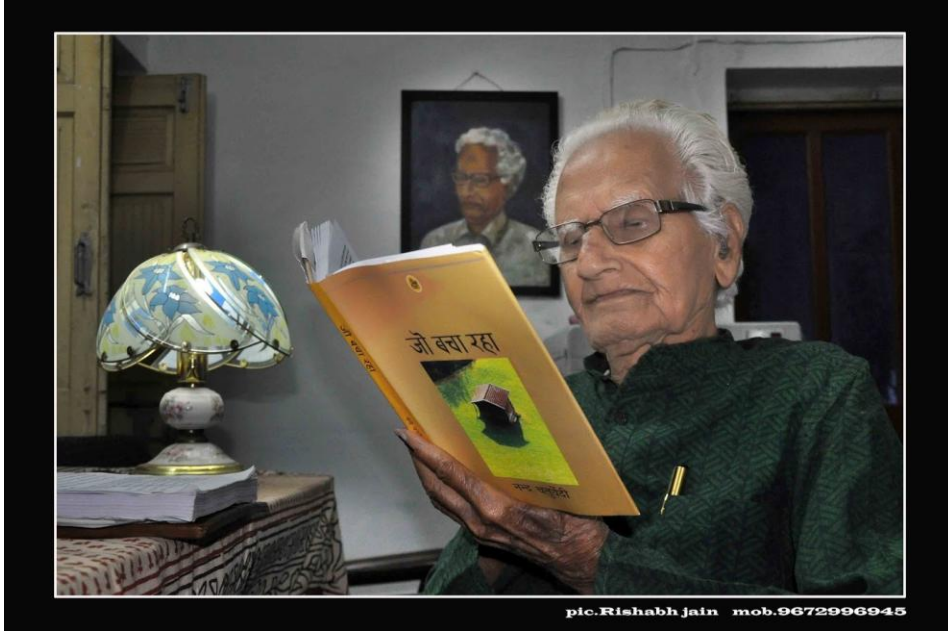
Thesis submitted to the Faculty of the Graduate School of the
University of Maryland, College Park, in partial fulfillment
of the requirements for the degree of
Doctor of Philosophy
2017

Advisory Committee:
Professor David Fushman, Chair
Professor Douglas Julin
Professor John Orban
Professor Paul Paukstelis
Professor Sergei Sukharev

© Copyright by
Apurva Chaturvedi
2017

Dedication

I dedicate this work to Da. I could not be there during his last days but his memories will always be with me.



आशा बलवती है राजन!

The hope is potent o, king!

Acknowledgements

I am grateful to Dr. Fushman for guiding, motivating and supporting me towards my PhD. He helped me grow as a researcher over the years and has taught me valuable life lessons.

I would also like to thank my committee members for their input and help through the years and especially in recent days with the thesis.

I thank Dr. Carlos Castaneda for teaching me everything I know about ubiquitin chemistry and mentoring me through the initial stages of my graduate school. I also thank him for his collaborations and input on the K6-linked diubiquitin project.

I am really grateful to Dr. Urszula Nowicka who taught me how to setup my first NMR experiment and for sharing her scientific expertise with me over the years. I thank her for help with assignment of Rap80 tUIM and for major contributions to the yeast Ddi1UBL story. Also, for being an awesome friend and a fellow concert/ play/ opera/ ballet-goer.

I thank Dr. Rajesh Singh who was always there to help and advise me about everything through the years.

I am also grateful to Adithya Sundar for being a great classmate, labmate, roommate and friend. Adi and Dulith Abeykoon have taught me how to be more pragmatic, which has helped me through some tough times. I will always be thankful for that.

I would like to thank Lillian Hallmark and Westley Pawloski for helping with the human Ddi1Ubl project.

I want to acknowledge Emma Dixon for providing me with K27- linked diubiquitin chains labeled on the proximal domain for my studies. I thank Dr Tanuja Kashyap for providing K11-linked diubiquitin chains. I also want to thank all my collaborators on different projects that are mentioned in this work.

I want to thank Dr. Daoning Zhang for his support through my PhD.

I acknowledge all my current and former labmates for helping me over the years.

I am most grateful to my parents for being supportive and for helping me emotionally as I pursued my degree far away from home. I thank them for making sure I am doing well even when I could not talk to them that often.

I thank my brother Sugandh, who has always pushed me to try my best and is one of the biggest reasons towards me pursuing a PhD. I am also thankful for bringing the positivity of Sonali bhabhi and Palash into my life. Watching Palash's smiling photos and videos got me through these last few months.

I am also thankful of my extended family here that has made me feel like home in this foreign land. I would like to thank Preeti Didi, Vijaya Bua, Ankur Bhaiya, Sheshai and Gaurav jijaji for their support.

I want to thank Sapna Desai who has believed in me these last few years while I was "almost done with my PhD". For being understanding of the rigors of PhD. and not complaining (that much) when during her holidays instead of going out, I asked her to sit with me in lab as I setup experiments. Thanks for always being there.

I also want to thank my friends Dr. Malini Iyer and Dr. Nikhil Patil for their emotional support via conference calls.

I thank my friend Maria Teresa Perez for all her help through the years. It was great to share the writing process with you. I am sure you are going to get it done soon.

I thank Shahnawaz Zaheer, Apurv Mittal, Romina Heymann, Dr. Aaron Geller and Dr. Karina Herrera-Guzmann for their friendship and support.

I have to give a special mention to Dr. Kyle Anderson who has shown me what being successful means.

I also want to thank all the animal friends who have showered me with their love. Especially, Bianka, Chumchum, Moose, Helmut and Otto, who have been instrumental in my emotional well-being during PhD.

I thank all my other friends and family for always being there for me.

Table of Contents

Dedication	ii
Acknowledgements	iii
Table of Contents	vi
List of Tables.....	viii
List of Figures	ix
List of Abbreviations.....	xv
Chapter 1: Introduction	1
1.1 Ubiquitin and polyubiquitin chains.....	1
1.1.1 Assembly and disassembly of polyubiquitin chains	3
1.1.2 Ubiquitin Binding Domains and Ubiquitin-Like Domains.....	5
1.2 Diversity of Polyubiquitin Chains	7
1.2.1 <i>In Vitro</i> Synthesis of Non-Canonical Chains.....	9
1.3 K6-linked polyubiquitin chains.....	9
1.3.1 Structural Information.....	9
1.3.2 Functional Information	11
1.4 K27-linked polyubiquitin chain	12
1.4.1 Structural Information.....	12
1.4.2 Functional Information	14
1.5 Summary of the Work.....	15
Chapter 2: Structure of K6-linked Ubiquitin Chains	18
2.1 Synthesizing K6-linked diubiquitin using non-enzymatic method.....	18
2.2 Relaxation/RDC derived models	21
2.3 Ensemble Analysis.....	31
2.4 pH effect on structure of K6-Ub ₂	33
Chapter 3: Binding Studies of K6-Linked Diubiquitin.....	36
3.1 Introduction.....	36
3.2 Synthesis of K6-linked chains by enzymatic method.....	37
3.3 Interaction of K6-Ub ₂ with Rap80 tUIM.....	39
3.3.1 Binding affinity of Rap80 tUIM to K6-Ub ₂	41
3.3.2 Directionality of binding.....	50
3.3.3 Mimicking the effect of Rap80 tUIM Phosphorylation.....	52
3.3.4 Salt effect	55
Section 3.4 Interaction of K6-Ub ₂ with hHR23a UBA2.....	59
3.4.1 Binding affinity of hHR23a UBA2 to K6-Ub ₂	60
3.4.2 Directionality of hHR23a UBA2 with K6-Ub ₂ interaction.....	65
Chapter 4: Studying K27-Ub₂	71
4.1 Introduction.....	71

4.2 Interaction of K27-Ub ₂ with Rap80 tUIM	73
4.2.1 Binding affinity of K27-Ub ₂ to Rap80.....	73
4.2.2 Directionality of binding of K27-Ub ₂ to Rap80	75
4.3 DUB inhibition by K27-Ub ₂	77
Chapter 5: Binding studies of yeast Ddi1UBL	79
5.1 Charge Dependency of Yeast Ddi1UBL Binding to Ubiquitin	79
5.2 Yeast Ddi1UBL Binding to Different Diubiquitin Chains	80
Chapter 6: Binding studies of human Ddi1UBL	97
6.1 Introduction.....	97
6.2 hDdi1UBL binding to Ubiquitin.....	98
6.3 hDdi1UBL binding to K48-Ub ₂	103
Chapter 7: Materials and methods	106
7.1 Protein Constructs.....	106
7.2 Protein purification	107
7.3 Polyubiquitin Chains generation and purification:	107
7.4 NMR experiments.....	108
7.4.1 NMR binding assays	109
7.4.2 PRE Experiments	109
7.5 DUB inhibition assays	110
Chapter 8: Discussion and Future Direction	111
8.1 Discussion	111
8.2 Future directions	115
8.3 Conclusion	116
Appendices	119
Bibliography	145

List of Tables

Table 1-1. Percentage abundance <i>in vivo</i> of ubiquitin chains linked via different lysines ³⁰	8
Table 2-1. Overall rotational diffusion tensor characteristics of K6-linked diubiquitin determined from ¹⁵ N relaxation data for the two ubiquitin units.....	25
Table 2-2. Alignment tensor characteristics for K6-linked diubiquitin determined from the RDCs for the two ubiquitin units.	28
Table 3-1. Summary of K _d s from all titrations of K6-Ub ₂ and Rap80 tUIM.....	58
Table 5-1. Summary of K _d s for yDdi1UBL and diubiquitin binding studies.	96
Table i. Overall rotational diffusion tensor characteristics of ubiquitin tail variants determined from ¹⁵ N relaxation data.....	143
Table ii. Alignment tensor characteristics for ubiquitin tail variants determined from the RDCs.....	144
Table iii. Rhombicity values of the tail variants.	144

List of Figures

Figure 1-1. Cartoon representation of ubiquitin structure.	2
Figure 1-2. Difference in K48- and K63-linked diubiquitin conformations lead to different binding mode to the same ligand.	3
Figure 1-3. Assembly and disassembly of ubiquitin chains and various proteins involved in different ubiquitin signaling pathway.	4
Figure 1-4. A comparison of γ Ddi1UBL and Ub and their interaction..	6
Figure 1-5. Classification of polyubiquitin chains according to linkage.	7
Figure 1-6. K6-linked diubiquitin crystal structure (PDB 2XK5).	10
Figure 1-7. Structural models of K27-Ub ₂ derived from residual dipolar couplings (A) and ¹⁵ N relaxation (B) ⁴¹	13
Figure 1-8. Three sets of 2-conformer ensembles for K27-Ub ₂ from SES analysis that fit best to experimental data.	14
Figure 2-1. Scheme of the assembly of K6-Linked Ub ₂ from wild type ubiquitin and K6(Boc) ubiquitin by non-enzymatic method.	19
Figure 2-2. ESI-MS checkpoints at different stages of the non-enzymatic synthesis of K6-linked diubiquitin ¹⁵ N labeled at distal domain.	20
Figure 2-3. Coomassie-stained 15% SDS PAGE gel of the chemical condensation reaction of K6-linked Ub ₂ ¹⁵ N labeled on the distal Ub.	20
Figure 2-4. ESI-MS of purified K6-linked diubiquitin ¹⁵ N labeled at proximal (left) and distal (right) domain.	21
Figure 2-5. Overlay of ¹ H - ¹⁵ N SOFAST HMQC spectra of the distal Ub of K6-linked diubiquitin (blue) and monoubiquitin (red).	22
Figure 2-6. Chemical Shift Perturbations of ¹⁵ N labeled K6(Boc) Ub (A), ¹⁵ N proximal labeled K6-linked diubiquitin (B), ¹⁵ N distal labeled K6-linked diubiquitin (C) with reference to WT ubiquitin and ¹⁵ N proximal labeled K6-linked diubiquitin with reference to ¹⁵ N labeled K6(Boc) Ub (D).	23
Figure 2-7. Relaxation rates (R ₁ and R ₂) and heteronuclear NOE of distal (left) and proximal (right) domains of K6-linked diubiquitin.	25
Figure 2-8. Correlation plots of experimental ratio of ¹⁵ N relaxation rates (R ₁ /R ₂) of distal domain (A) and proximal domain (B) of K6-linked diubiquitin with the calculated ratio using NH vectors from the solution NMR structure of ubiquitin (PDB:1D3Z) and fit to the fully anisotropic model of overall rotational diffusion tensors.	26
Figure 2-9. Relaxation derived structure (A) and correlation plot of ¹⁵ N relaxation rates (R ₁ /R ₂) of both domains of K6-linked diubiquitin simultaneously with the calculated ratio using NH vectors from the relaxation derived structure and fit to the fully anisotropic model of overall rotational diffusion tensors (B).	27
Figure 2-10. Correlation plots of experimental RDC data of K6-linked diubiquitin, proximal domain (left) and (b) distal domain (right) compared with the predicted values using NH vectors from the solution NMR structure of ubiquitin monomer (PDB:1D3Z).	29
Figure 2-11. Correlation plots of experimental RDC data of K6-linked diubiquitin distal domain (A), proximal domain (B) and both domains simultaneously (C)	

compared with the calculated values using NH vectors from respective individual domains from K6-linked diubiquitin crystal structure or the whole crystal structure (PDB:2XK5).	30
Figure 2-12. Comparison of K6-linked diubiquitin crystal structure (PDB 2XK5) (A), ¹⁵ N-Relaxation derived structural model (B) and PATIDOCK generated RDC optimized structural model (C).	31
Figure 2-13. 2-conformer ensemble reproduces experimental RDC data extremely well.....	32
Figure 2-14. Two sets of 2-conformer ensembles of K6-Ub ₂ that are in excellent agreement with experimental data.	33
Figure 2-15. Comparison of CSPs of K6-Ub ₂ labeled on the distal domain at pH 6.8 (top left) and pH 4.5 (top right) with CSPs of K48-Ub ₂ labeled on the distal domain at pH 6.8 (bottom left) and pH 4.5 (bottom right) ⁵⁴	34
Figure 2-16. Crystal structure of K6-Ub ₂ (PDB 2XK5) showing H68 (orange sticks) on proximal domain (green) and H68 (orange sticks) on the distal domain (blue). ...	35
Figure 3-1. K6-Ub ₂ has conformers that illustrate its potential to bind to both Rap80 tUIM and hHR23a UBA2.	37
Figure 3-2. Enzymatic method to synthesize all-natural K6-Ub ₂	38
Figure 3-3. Coomassie-stained 15% SDS PAGE gel of the enzymatic reaction of K6-linked Ub ₂ ¹⁵ N labeled on the distal Ub.....	39
Figure 3-4. Overview of Rap80 tUIM structure.	40
Figure 3-5. Possible modes of Rap80 tUIM binding to K6-Ub ₂	41
Figure 3-6. Interaction of K6-Ub ₂ with Rap80 tUIM.	42
Figure 3-7. Titration fit of K6-Ub ₂ labeled on the proximal (left) and distal (right) domain upon addition of his-tagged Rap80 tUIM (Y).....	43
Figure 3-8. A. CSP plot of ¹⁵ N labeled ubiquitin upon addition of his-tagged Rap80 tUIM (Y) at saturation.	44
Figure 3-9. Comparison of CSP plots of K6-Ub ₂ , ¹⁵ N labeled on the proximal domain upon addition of his-tagged Rap80 UIM1 (Y) at saturation (left) and upon addition of his-tagged Rap80 tUIM (Y) at saturation (right)..	45
Figure 3-10. Expected stoichiometry of the binding showing 2 UIM1 binding to each domain of K6-Ub ₂ (Left).	46
Figure 3-11. A. CSP plot of ¹⁵ N labeled his-tagged Rap80 tUIM(Y) upon addition of K6-Ub ₂ at saturation.	47
Figure 3-12. Titration fit of ¹⁵ N labeled his-tagged Rap80 tUIM(Y) upon addition of K6-Ub ₂	48
Figure 3-13. ITC titration analysis of K6-Ub ₂ binding to Rap80tUIM..	49
Figure 3-14. Determined directionality of Rap80 tUIM binding to K6-Ub ₂	50
Figure 3-15. PRE effect measured on ¹⁵ N labeled K6-Ub ₂ on proximal domain (left) and distal domain (right) upon addition of Rap80 tUIM with MTSL attached at position C121.	51
Figure 3-16. PRE effect measured on ¹⁵ N labeled Rap80 tUIM upon addition of K6-Ub ₂ with MTSL attached on K6C of distal domain.....	52
Figure 3-17. Comparison of CSP plots of K6-Ub ₂ , ¹⁵ N labeled on the distal domain upon addition of his-tagged Rap80 tUIM (Y) at saturation (left) and upon addition of his-tagged S101E Rap80 tUIM (Y) at saturation (right)..	53

Figure 3-18. Comparison of CSP plots of K6-Ub ₂ , ¹⁵ N labeled on the proximal domain upon addition of his-tagged Rap80 tUIM (Y) at saturation (top left) and upon addition of his-tagged S101E Rap80 tUIM (Y) at saturation (top right).....	54
Figure 3-19. Titration fit of K6-Ub ₂ labeled on the proximal (left) and distal (right) domain upon addition of his tagged S101E Rap80 tUIM (Y).	55
Figure 3-20. CSP plot of K6-Ub ₂ , ¹⁵ N labeled on the distal domain upon addition of his-tagged Rap80 tUIM (Y) at saturation in presence (top left) or absence of salt (top right) and upon addition of his-tagged S101E Rap80 tUIM (Y) at saturation in the presence (bottom left) or absence of salt (bottom right).....	56
Figure 3-21. Titration fit of K6-Ub ₂ labeled on the proximal (top left) upon addition of his-tagged Rap80 tUIM(Y) in PBS pH 7.4 buffer, distal domain upon addition of his-tagged Rap80 tUIM (Y) (top right) and his-tagged S101E Rap80 tUIM (Y) (bottom) in PBS pH 7.4 buffer.....	57
Figure 3-22. Structure and function of hHR23a UBA2.....	59
Figure 3-23. Studying the interaction of K6-Ub ₂ with hHR23a UBA2, observing K6-Ub ₂	61
Figure 3-24. CSP plot of K6-Ub ₂ , ¹⁵ N labeled on the proximal domain upon addition of hHR23a UBA2 at saturation (top left) and distal domain upon addition of hHR23a UBA2 at saturation (bottom left) compared with CSP plot of K48-Ub ₂ , ¹⁵ N labeled on the distal domain upon addition of hHR23a UBA2 at saturation (top right) and proximal domain upon addition of hHR23a UBA2 at saturation (bottom right).....	62
Figure 3-25. Titration fit of K6-Ub ₂ labeled on the proximal domain (left) upon addition of hHR23a UBA2 and distal domain upon addition of hHR23a UBA2 using KDFIT global.....	63
Figure 3-26. Titration fit of K6-Ub ₂ labeled on the distal domain upon addition of hHR23a UBA2, original fit (left) and adjusted (multiply ligand by 0.75) fit (right)..	63
Figure 3-27. CSP plot of ¹⁵ N labeled hHR23a UBA2 upon addition of K6-Ub ₂ (top left and bottom left) and of mono ubiquitin (top right) and K48-Ub ₂ (bottom right) at saturation.....	64
Figure 3-28. CSPs more than 0.15 ppm on ¹⁵ N labeled hHR23a UBA2 upon addition of Ub, K48-Ub ₂ or K6-Ub ₂ mapped on the surface representation of the structure of hHR23a UBA2 (PDB 1DV0) (left).....	65
Figure 3-29. PRE effect measured on ¹⁵ N labeled hHR23a UBA2 upon addition of K6-Ub ₂ with MTSL attached at position Cys6 of the distal domain.	66
Figure 3-30. Reconstructed position of the spin label on Cys6 of the distal domain of K6-Ub ₂ with respect to the hHR23a UBA2 domain generated from SLFIT added onto the PDB structure of hHR23a UBA2 (1DV0).	67
Figure 3-31. Reconstructed position of the spin label on Cys6 of the distal domain of K6-Ub ₂ with respect to the hHR23a UBA2 domain generated from SLFIT assuming two positions for the spin label added onto the PDB structure of hHR23a UBA2 (1DV0)..	67
Figure 3-32. Reconstructed position of the spin label on Cys6 of the distal domain of K6-Ub ₂ with respect to the hHR23a UBA2 domain after removing residues 24-28 of the UBA2 domain, generated from SLFIT added onto the PDB 1DV0 (left).	68

Figure 3-33. PRE effect measured on K6-Ub ₂ labeled on distal domain (top) and proximal domain (bottom) upon addition of hHR23a UBA2 with MTSL attached at position C334.....	69
Figure 3-34. Conformer from SASSIE generated ensemble whose coordinates gave the best fit of the PRE data on K6-Ub ₂ labeled on distal domain (green) and proximal domain (blue) upon addition of hHR23a UBA2 with MTSL attached at position C334.....	70
Figure 4-1. Three sets of two-conformer ensembles of K27-Ub ₂	72
Figure 4-2. Conformer of K27-Ub ₂ (left) with similar Ub/Ub orientation as Rap80 tUIM bound K63-Ub ₂ (right).	73
Figure 4-3. CSP plot of K27-Ub ₂ , ¹⁵ N labeled on the distal domain upon addition of his-tagged Rap80 tUIM(Y) at saturation (top left) and proximal domain upon addition of his-tagged Rap80 tUIM(Y) at saturation (top right).....	74
Figure 4-4. Titration fit of K27-Ub ₂ labeled on the distal domain (left) and proximal domain (right) upon addition of his-tagged Rap80 UIM1 (Y) using KDFIT global.	75
Figure 4-5. Determine directionality of Rap80 tUIM binding to K27-Ub ₂ using Paramagnetic Relaxation Enhancement (PRE) measurements.....	76
Figure 4-6. PRE effect on K27-Ub ₂ labeled on distal domain (top) and proximal domain (bottom) upon addition of his-tagged Rap80 tUIM with MTSL attached at position C121.....	77
Figure 4-7. K27-Ub ₂ inhibits IsoT/USP5 DUB activity towards K48-Ub ₂ (left) and K63-Ub ₂ (right).....	78
Figure 5-1. Cartoon representation of domain composition of Ddi1 in yeast ²⁸	79
Figure 5-2. Charge-charge interactions are critical for interaction between ubiquitin and yDdi1UBL.....	80
Figure 5-3. CSP plot of ¹⁵ N labeled yDdi1UBL upon addition of K48-Ub ₂ (top left) and of K63-Ub ₂ (top right) at saturation.	81
Figure 5-4. Alignment of the sequence of the α -helix in yDdi1UBL with the sequence of amino acids that compose α -helix of Ub and UBL domains of shuttle proteins: Rad23 and Dsk2.....	82
Figure 5-5. CSP plot of ¹⁵ N labeled yDdi1UBL_SK upon addition of K48-Ub ₂ (left) and of K63-Ub ₂ (right) at saturation.	83
Figure 5-6. Comparison between CSP plot of ¹⁵ N labeled yDdi1UBL_K upon addition of K48-Ub ₂ at saturation (left) and CSP plot of ¹⁵ N labeled yDdi1UBL upon addition of K48-Ub ₂ (right).....	84
Figure 5-7. Titration fit of ¹⁵ N labeled yDdi1UBL upon addition of K48-Ub ₂ (left) and K63-Ub ₂ (right)	85
Figure 5-8. ITC titration analysis of yDdi1UBL and K48-Ub ₂ binding.....	85
Figure 5-9. Titration fit of ¹⁵ N labeled yDdi1UBL_SK upon addition of K48-Ub ₂ (A) and K63-Ub ₂ (B) using KDFIT global.....	86
Figure 5-10. CSP plot of ¹⁵ N labeled K48-Ub ₂ on the proximal (left) and distal (right) domain upon addition of yDdi1UBL at saturation..	87
Figure 5-11. Titration fit of K48-Ub ₂ ¹⁵ N labeled on proximal domain (left) and distal domain (right) upon addition of yDdi1UBL.	88

Figure 5-12. Titration fit of K48-Ub ₂ ¹⁵ N labeled on proximal domain (left) and distal domain (right) upon addition of yDdi1UBL using KDFIT global after multiplying the ligand concentration by 0.8.....	88
Figure 5-13. PRE effect on yDdi1UBL upon addition of K48-Ub ₂ with MTSL attached at position T12C on the proximal domain (top) and K48C on the distal domain (bottom). Position of the spin label fitted using the coordinates from the PDB structure of yDdi1UBL (2MRP).....	89
Figure 5-14. PRE effect on yDdi1UBL_SK upon addition of K48-Ub ₂ with MTSL attached at position T12C on the proximal domain (top) and K48C on the distal domain (bottom).....	91
Figure 5-15. Reconstructed positions of spin labels generated using SLFIT and yDdi1UBL structure from PDB 2MRP..	92
Figure 5-16. CSP plot of ¹⁵ N labeled yDdi1UBL upon addition of K6-Ub ₂ at saturation.....	93
Figure 5-17. Titration fit of ¹⁵ N labeled yDdi1UBL upon addition of K6-Ub ₂	93
Figure 5-18. CSP plot of ¹⁵ N labeled yDdi1UBL upon addition of K27-Ub ₂ at saturation (left).....	94
Figure 5-19. CSP plot of ¹⁵ N labeled yDdi1UBL upon addition of K11-Ub ₂ at saturation (top left).....	95
Figure 6-1. Ddi1 gene structure and domain conservation among eukaryotes.....	97
Figure 6-2. A “classical” shuttle protein (e.g. Dsk2) employs a ubiquitin-associated (UBA) domain to recognize and bind polyubiquitinated tag on a substrate protein and a ubiquitin-like (UBL) domain to target it to the proteasome..	98
Figure 6-3. Overlay of ¹⁵ N WT Ub spectrum by itself (blue) and after addition of GST-tagged hDdi1UBL at 1:1 (red) and 1:2 (green) ratio.	99
Figure 6-4. ¹ H- ¹⁵ N SOFAST HMQC spectrum of ¹⁵ N labeled hDdi1UBL.....	100
Figure 6-5. CSP plot of ¹⁵ N labeled Ub upon addition of hDdi1UBL at saturation.	101
Figure 6-6. CSP plot of ¹⁵ N labeled Ub upon addition of yDdi1UBL ²⁸ (left) and hDdi1UBL (right) at saturation.....	101
Figure 6-7. Titration fit of ¹⁵ N ubiquitin upon addition of hDdi1UBL.	102
Figure 6-8. Titration fit of ¹⁵ N labeled hDdi1UBL upon addition of ubiquitin, using KDFIT global.....	103
Figure 6-9. ITC titration analysis of hDdi1UBL and K48-Ub ₂ binding.	104
Figure 8-1. Conformer from SASSIE generated ensemble whose coordinates gave the best fit of the PRE effect on K6-Ub ₂ labeled on distal domain (green) and proximal domain (cyan) upon addition of hHR23a UBA2 with MTSL attached at position C334.....	112
Figure i. Crystals from K6-Ub ₂ : Rap80 tUIM mix formed in 0.05M Zinc acetate dihydrate +20% w/v Polyethylene glycol 3,350 (left) and 0.2 M Sodium acetate trihydrate pH 7.0+20% w/v Polyethylene glycol 3,350 (right).	119
Figure ii. 15% SDS PAGE of crystals formed in 0.05M Zinc acetate dihydrate +20% w/v Polyethylene glycol 3,350.....	120
Figure iii. Titration fit of ¹⁵ N labeled Ddi1UBA with ubiquitin in the presence (left) and absence (right) of salt.	120

Figure iv. Cartoon structural representation of ubiquitin indicating the residues missing in Ub62 (K63-G76) in red (PDB: 1D3Z).	121
Figure v. Coomassie-stained 15% SDS PAGE gel of Ub62 (left).	122
Figure vi. Comparison of ^1H - ^{15}N SOFAST HMQC spectra of wild type ubiquitin (red) and Ub62 (blue).	123
Figure vii. Comparison of ^1H - ^{15}N SOFAST HMQC spectra of Ub62 purified using acid precipitation plus anion exchange chromatography (red) and purified using heat precipitation plus cation exchange chromatography (blue).	124
Figure viii. Comparison of ^1H - ^{15}N SOFAST HMQC spectra of Ub62 before (red) and after (blue) the addition of ubiquilin-1 UBA in a 1:1 molar ratio.	125
Figure ix. Comparison of ^1H - ^{15}N SOFAST HMQC spectra of Ub62 before denaturation by 8M urea (blue) and after denaturation/refolding (red).	125
Figure x. Circular dichroism spectrum of Ub62 at 30 °C.	126
Figure xi. Circular dichroism spectra of Ub62 at different temperatures.	127
Figure xii. Change in ellipticity of Ub62 at 222nm as a function of temperature.	127
Figure xiii. Comparison of the ^1H - ^{15}N SOFAST HMQC spectra of Ub62 before (blue) and after (red) adding the C-terminal peptide.	128
Figure xiv. Comparison of the ^1H - ^{15}N SOFAST HMQC spectra of Ub62 with C-terminal peptide in 20mM NaP pH 6.8 (blue) and upon addition of 10% v/v acetic acid (red).	129
Figure xv. Comparison of ^1H - ^{15}N SOFAST HMQC spectra of Ub62 before (blue) and after (red) denaturing by increasing the temperature to 72 °C and refolding back by reducing temperature to 23 °C.	130
Figure xvi. Comparison of the ^1H - ^{15}N SOFAST HMQC spectra of Ub62 with C-terminal peptide before (blue) and after (red) denaturing by 8M Urea and refolding in 20 mM NaP pH 6.8.	131
Figure xvii. Schematic representation of attaching either strep-tag TM II or biotin hydrazide to K6-linked polyubiquitin chains in order to immobilize the chains for pull-down assays.	132
Figure xviii. Deconvoluted ESI-MS of the following reaction: 5mgs of UbCOSR in 500 μl 0.1M MES buffer + 25 μl of 50 mM Hydrazide biotin solution (EZ-Link Hydrazide Biotin from Thermo Scientific in DMSO).	134
Figure xix. Deconvoluted ESI-MS of the following reaction: 5mgs of UbCOSR in 500 μl 0.1 M MES buffer + 25 μl of 50 mM Hydrazide biotin solution (EZ-Link Hydrazide Biotin from Thermo Scientific in DMSO).	134
Figure xx. Deconvoluted ESI-MS of the following reaction 2.5 mgs ^{15}N WT Ub in 970 μl 0.1 M MES buffer pH 4.8 + 25 μl 50 mM Biotin hydrazide in DMSO + 12.5 μl of 100 mg/ml EDC solution in 0.1M MES buffer pH 4.8.	135
Figure xxi. Deconvoluted ESI-MS of the following reaction: 2.5 mgs Unlabeled WT Ub in 970 μl 20 mM NaP buffer pH 8 + 25 μl 50mM Biotin hydrazide in DMSO +12.5 μl of 100 mg/ml EDC solution in 20 mM NaP buffer pH 8.	136
Figure xxii. Deconvoluted ESI-MS of the following reaction: ~5 mgs Unlabeled UbCOSR Alloc + DMSO 87.5 μl + DIEA 10 μl + AgNO ₃ 2.5 μl + H-OSu 2.5 μl .	138
Figure xxiii. Growth curve of WT yeast and PEP4 ⁻ yeast (top), PEP4 ⁻ yeast protein profile at different time points during its growth curve (bottom).	140

List of Abbreviations

1D3Z- PDB id of RDC optimized structure of monoubiquitin

26S- 26S proteasome.

χ^2 test- A statistical method assessing the goodness of fit between experimental values and values that are back-calculated.

τ_c - overall rotational correlation time.

μM - Micromolar

AgNO_3 - Silver nitrate.

Alloc- Allyloxycarbonyl.

ALTENS- A program for determining the alignment tensor of a molecule from residual dipolar coupling (RDC) data, using singular value decomposition.

APBS-Adaptive Poisson Boltzmann solver.

ATP- Adenosine triphosphate.

BARD1- BRCA1-associated RING domain protein 1, E3 ubiquitin ligase.

Boc- tert-Butyloxycarbonyl.

BRCA1- Breast cancer type 1 protein.

cal- calorie.

CSP- Chemical shift perturbation.

D- Overall rotational diffusion tensors, determined here from relaxation data.

Da- Dalton, 1 g/mol.

Ddi1- DNA damage-inducible protein 1.

Ddi1UBL- Ubiquitin-like domain of DNA damage-inducible protein 1.

Ddi1UBL_K- L31K mutant of Ddi1UBL.

Ddi1UBL_SK- A30S, L31K mutant of Ddi1UBL.

DDR- DNA Damage Repair.

DNA- Deoxyribonucleic acid.

DUB- Deubiquitinating enzyme.

E1- Ubiquitin activating enzyme.

E2- Ubiquitin conjugating enzyme.

E3- Ubiquitin ligase.

ESI-MS- Electrospray ionization-mass spectrometry.

hDdi1UBL- Ubiquitin-like domain of DNA damage-inducible protein 1 in humans.

hHR23a UBA2- Human homolog of yeast protein Rad23, ubiquitin-associated domain 2.

IsoT- Isopeptidase T, USP5, deubiquitinase that cleaves all polyubiquitin chains with a free C-terminus except K27-Ub₂.

ITC- Isothermal titration calorimetry.

K6 alloc- Ubiquitin with all amino groups protected using alloc group except K6.

K6(Boc)- Ubiquitin with K6 amino group protected by boc group.

kcal- Kilocalorie.

M1- Amino terminus of ubiquitin.

MESNA- Sodium 2-mercaptoethanesulfonate, $C_2H_5NaO_3S_2$.

Miro1- Mitochondrial Rho GTPase 1.

mM- Millimolar

ms- Milliseconds.

MTSL- Methyl methanesulfonothioate, a nitroxide spin-label.

MW- Molecular weight.

NleL- Non-LEE-encoded ligase, E3 ubiquitin ligase.

NMR- Nuclear magnetic resonance.

NIST- National institute of standards and technology.

ns- Nanoseconds.

hnNOE- Heteronuclear nuclear Overhauser effect.

hOtuB1- Otubain1, K48-linkage specific deubiquitinase.

K_d - Dissociation constant of binding.

KDFIT- A program for determining the K_d from CSPs of NMR binding assays.

PATIDOCK- A program for predicting the alignment tensor of a molecule and the residual dipolar couplings (RDCs) under steric alignment caused by planar objects, and for determining the alignment tensor from experimental RDC data using singular value decomposition.

PBS- Phosphate-buffered saline.

PDB- Protein data bank.

PolyUb- Polyubiquitin.

ppm- Parts per million

PRC1- Polycomb transcriptional repressive complex 1.

PRE- Paramagnetic relaxation enhancement.

Rad23 UBL- Ubiquitin-like domain of Rad23, UV excision repair protein.

Q value- Quality factor.

r- Pearson's correlation coefficient.

Rap80 tUIM - Receptor associated protein 80 tandem ubiquitin interacting motif.

RDC- Residual dipolar coupling.

RING1B- Ring Finger Protein 1, Really Interesting New Gene 1 Protein, E3 Ubiquitin Transferase.

ROTDIF- A program for determining the overall rotational diffusion tensor of a molecule from spin-relaxation data.

RVP- Retroviral protease fold domain.

S- Alignment tensor from RDC data.

SANS- Small-angle neutron scattering.

SASSIE- A program to construct ensembles of biomolecular structures that are consistent with experimental scattering data.

SES- Sparse ensemble selection. A program for recovering a representative conformational ensemble of a macromolecule from (underdetermined) experimental data using sparse-ensemble selection (SES) combined with multi-orthogonal matching pursuit (Multi-OMP).

SOFAST HMQC- Selective optimized flip angle short transient heteronuclear multiple quantum coherence.

SPHP- A high performance cation column.

T1 relaxation- Spin-lattice relaxation time.

T2 relaxation- Transverse relaxation time.

TCEP- Tris(2-carboxyethyl)phosphine, reducing agent.

TFA- Trifluoroacetic acid.

Ub- Ubiquitin.

Ub₂- Diubiquitin.

Ub₃- Triubiquitin.

UBA- Ubiquitin-associated domain.

UbCA- Fully allocated thioesterified ubiquitin.

UbC^{H7}- Ubiquitin-conjugating enzyme H7, E2 conjugating enzyme.

UbCOSR- Thioesterified ubiquitin.

UBD- Ubiquitin binding domain.

UBL- Ubiquitin-like domain.

UIM- Ubiquitin interacting motif.

WT- wild type, no mutations.

yDdi1UBL- Ubiquitin-like domain of DNA damage-inducible protein 1 in yeast.

YUH1- C-terminal hydrolase, it removes the excess residue (after G76) from Ub C-terminal tail.

Chapter 1: Introduction

1.1 Ubiquitin and polyubiquitin chains

Ubiquitin is a 76 amino acids protein found in all eukaryotes. As its name suggests, it is a ubiquitous molecule and is involved in various processes in the cell. Its diverse functions have been attributed to it being conjugated to target proteins in different forms^{1,2}. Defects in different ubiquitin-mediated pathways are implicated in diseases like malignancies and neurodegenerative disorders. Therefore, understanding these various signals is imperative in treating these syndromes^{3,4}.

Ubiquitin (Ub) can form different linkages owing to the fact that the ϵ -amino group of all seven lysine residues (K6, K11, K27, K29, K33, K48 and K63) and the amino terminus of ubiquitin (M1) can form an isopeptide bond with the C-terminal glycine of the subsequent ubiquitin. Ubiquitin monomers of the chains are distinguished as proximal and distal. The ubiquitin that has a free C-terminus is referred to as the "proximal unit" and the one that doesn't use any of its amino groups for the isopeptide linkage is called "distal unit"⁵. Additionally, ubiquitin can be attached via isopeptide bond to lysine residues of target protein as a monomer or a polymer of different lengths (ranging from 2-10) and linkages. Target proteins can be "tagged" by Ub monomer through monoubiquitination (single ubiquitin) or multiubiquitination (multiple ubiquitins conjugated to different lysine residues of the target protein), both of which have been shown to be involved in DNA repair and protein trafficking⁶⁻⁸. Furthermore, differently linked polyubiquitin chains can tag various target proteins depending on the signaling pathway they are involved in. For

instance, K48- and K11-linked chains target proteins for proteasomal degradation while those linked through K63 are known to be a part of DNA repair⁹⁻¹³. These diverse signals have been hypothesized to originate due to the different chain conformations that are formed depending on which of the seven lysines on the ubiquitin are used². Additionally to chain conformation, there is a canonical hydrophobic patch on one side of the ubiquitin surface formed by L8, I44 and V70 that is involved in the interaction with a majority of Ub-receptors, and therefore it is important for determining specific signal^{14,15} (Figure 1-1).

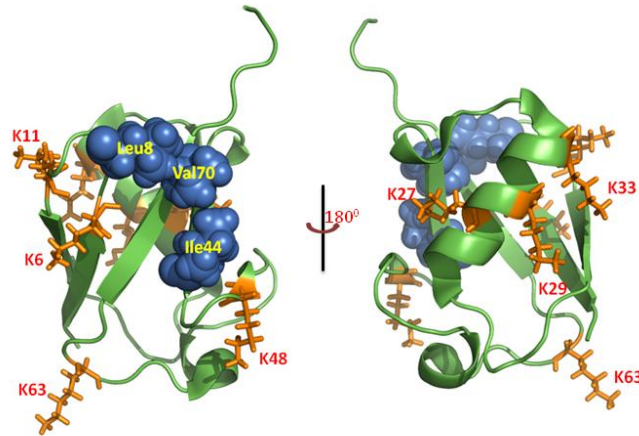


Figure 1-1. Cartoon representation of ubiquitin structure. Shown is the NMR solution structure of ubiquitin (PDB: 1D3Z) with lysine residues as orange sticks and canonical hydrophobic patch as blue spheres.

Depending on which linkage is formed, the availability of the hydrophobic patch determines the ability of the ubiquitin chain to interact with different ubiquitin binding receptors. For example, K48-linked dimer and tetramer have been shown to be able to form a "closed" conformation under physiological conditions, which means their hydrophobic patches interact with each other and form an interface while K63-linked chains tend to form an "open" extended conformation, where both hydrophobic patches are ligand accessible¹⁶⁻¹⁸. As shown in Figure 1-2, due to the closed

conformation, K48-linked dimer binds to one of the ubiquitin-associated domains, UBA2, of proteasomal shuttle protein hHR23a (human homologue of yeast protein Rad23) in a "sandwich mode", with one UBA2 interacting with both domains of the diubiquitin. By contrast, K63-linked dimer binds as two monomeric subunits both having accessible hydrophobic patches and thus can interact with two hHR23a UBA2s at the same time^{19,20}

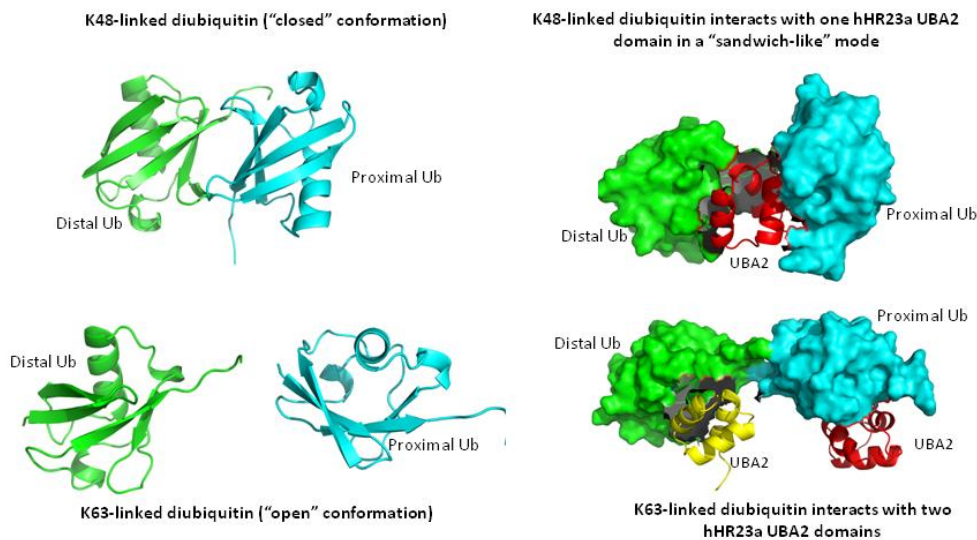


Figure 1-2. Difference in K48- and K63-linked diubiquitin conformations lead to different binding mode to the same ligand. The distal domain of ubiquitin is indicated in green and proximal domain of ubiquitin is indicated in cyan. The ligand, UBA2 domain, is indicated in red and yellow. An open conformation reflects a conformation where there is no interface between the hydrophobic patches on the two ubiquitin moieties of the diubiquitin.

1.1.1 Assembly and disassembly of polyubiquitin chains

The polyubiquitin chains are made and attached to the substrate *in vivo* using a sequential ATP dependent enzyme system consisting of ubiquitin C-terminal activating enzyme E1, ubiquitin conjugating enzyme E2, which extends the ubiquitin chain and along with ubiquitin ligase E3 ubiquitinates substrates (Figure 1-3). The chains can exist in both anchored form (attached to the substrate) or unanchored form. To synthesize unanchored chains, sometimes E1 and E2 are sufficient. There are only

two E1 enzymes (UBA1 and UBA6) for making all ubiquitin linkages while there are many more E2 and E3 enzymes present in the cells²¹. E2 enzymes are usually specific to the lysine that is used to make the chains while E3 enzymes are specific to the substrate^{22,23}.

The modifications by ubiquitinating enzymes can be reversed by deubiquitinating enzymes (DUBs) present in the cells (Figure 1-3). These ubiquitin specific proteases remove the ubiquitin(s) from the substrate protein and also disassemble free polymeric chains. Some DUBs have the capability to preferentially recognize specific ubiquitin linkages while others are more promiscuous²⁴.

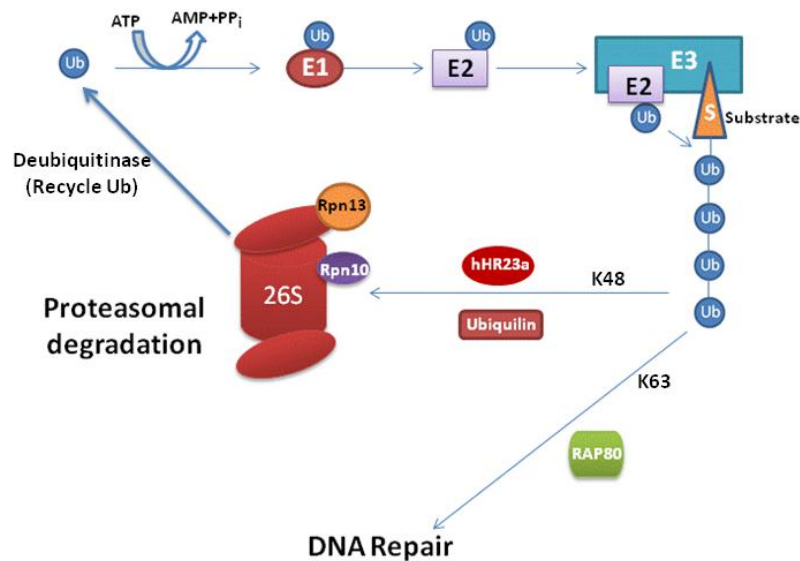


Figure 1-3. Assembly and disassembly of ubiquitin chains and various proteins involved in different ubiquitin signaling pathway. Ub indicates ubiquitin, E1 is activating enzyme, E2 is conjugating enzyme, E3 indicates ubiquitin ligase, S indicates the substrate to be ubiquitinated, K48 indicates K48-linked polyubiquitin chains attached to the substrate, K63 indicates K63-linked polyubiquitin chains attached to the substrate, hHR23a and ubiquilin are proteasomal shuttles, Rap80 is a receptor involved in DNA repair pathway, 26S indicates the whole 26S proteasome, Rpn 10 and Rpn13 indicates receptors on the proteasome.

1.1.2 Ubiquitin Binding Domains and Ubiquitin-Like Domains

Once ubiquitin tags its target proteins by the sequential enzyme machinery explained above, it interacts non-covalently with different receptors called Ubiquitin Binding Domains (UBDs). These domains are able to bind specifically to polyubiquitin chains of different linkages and help translate these signals into distinct outcomes. A group of receptors act as proteasomal shuttle proteins that recognize polyubiquitin chains linked via specific linkage and bring the ubiquitinated substrate to the proteasome for degradation. The proteasomal shuttle proteins typically contain an N-terminal ubiquitin-like domain (UBL) and a C-terminal ubiquitin-associated domain (UBA). It has been hypothesized that the UBL-UBA shuttle proteins utilize their UBL domain to interact with the proteasome (primarily through the Rpn1 subunit), and their UBA domain(s) to interact with Ub moieties on ubiquitinated proteins.

In humans, UBA (Ub-associated) domains of shuttle receptors hHR23A and human homologue of Dsk2, Ubiquilin-1, both of which deliver ubiquitinated substrates to the proteasome for degradation, bind with different levels of specificity to K48-linked chains (Figure 1-3). hHR23A UBAs bind preferentially to K48-linked chains whereas Ubiquilin-1 UBA binding is linkage non-specific^{25,26}. Receptor-associated protein 80 (RAP80) has been shown to be a part of DNA repair and interact preferentially with K63-linked chains²⁷ (Figure 1-3).

DNA damage-inducible protein 1 (Ddi1), like hHR23A, is believed to belong to a family of shuttle proteins targeting polyubiquitinated substrates for proteasomal degradation. Our lab determined the structure and binding properties of the ubiquitin-

like (UBL) and ubiquitin-associated (UBA) domains of Ddi1 from *Saccharomyces cerevisiae*. Former lab member and co-author Dr. Urszula Nowicka showed that Ddi1UBL has an ubiquitin-like fold but due to its negatively charged β -sheet surface, the positively charged residues of ubiquitin recognize it (Figure 1-4). Ddi1UBL can thus bind both ubiquitin and proteasome, suggesting a novel mechanism for Ddi1 as a proteasomal shuttle²⁸.

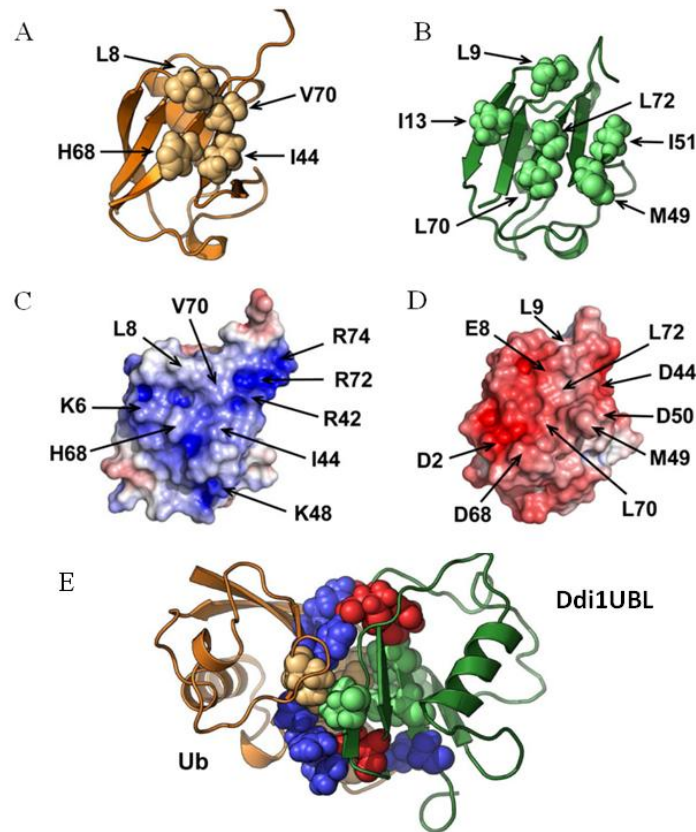


Figure 1-4. A comparison of yDdi1UBL and Ub and their interaction (A) Sphere representation of the hydrophobic patch residues on Ub surface. (B) Sphere representation of the residues on the surface of yDdi1UBL that form the hydrophobic surface patch. (C–D) Surface electrostatic potential (positive is blue, negative is red) of Ub (C) and Ddi1UBL (D), calculated using Adaptive Poisson Boltzmann Solver (APBS)²⁹. The coloring range is ± 4 kT/e for Ub and ± 8 kT/e for Ddi1UBL. Both proteins are oriented similarly, with the β -sheet surface facing the reader. Location of charged side chains and major hydrophobic residues on the surface of each protein is indicated with arrows. (E) The Ub:Ddi1UBL interface is formed by both hydrophobic and polar/charged amino acids (shown as spheres colored orange and blue, respectively, for Ub, green and red for Ddi1UBL). Ribbon colors are as in (A–B)²⁸.

1.2 Diversity of Polyubiquitin Chains

Polyubiquitin chains can be classified according to their linkage. Polyubiquitin chains containing linkages via a single amino group are termed homogenous and those that contain linkages via more than one amino group are called heterogeneous. They can also be classified according to their linkage topology. Chains where only one of the amino groups of one ubiquitin is covalently attached to the C-terminus of another ubiquitin are referred to as unbranched chains, while they are called branched chains when multiple ubiquitins are covalently attached to different lysines on a single ubiquitin. Moreover, chains that contain proteins other than ubiquitin (Ubiquitin-like proteins, UBL e.g. Rub1³⁰) are known as heterologous or mixed chains⁵ (Figure 1-5).

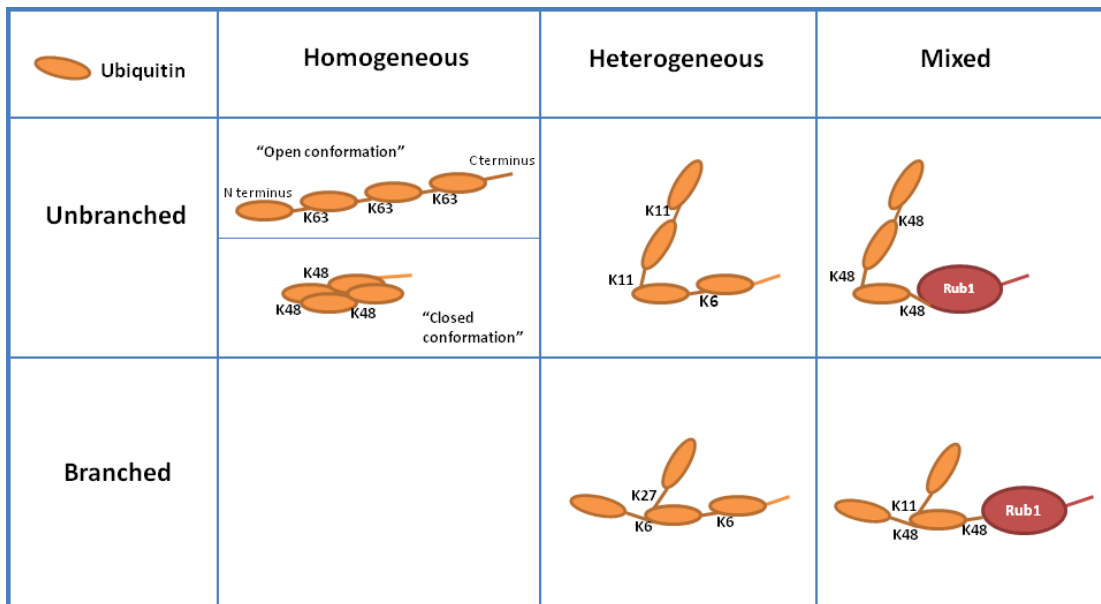


Figure 1-5. Classification of polyubiquitin chains according to linkage. Orange oval shapes indicate ubiquitin, red oval shapes represent Rub1 but can be substituted by other ubiquitin-like (UBL) proteins. K48, K63, K6, K11 and K27 indicate presence of isopeptide linkage via that lysine.

Another way of classification of polyubiquitin chains is according to their abundance in cells as canonical chains: K48- and K63-linked and non-canonical chains: K6-, K11-, K27-, K29- and K33-linked. The relative abundance of the chains has been analyzed using mass-spectrometry based proteomics approach in yeast and it has been found that K48-linked chains have the highest abundance, followed by equal abundance of K63-linked and K11-linked. K6-, K27- and K33-linked chains are present in lower abundance compared to the others while K29 linkage has been shown to be present only in branched chains³¹ (Table 1-1). But one has to take this data with a grain of salt, since the more abundant species mask the presence of lesser populated species in mass spectrometry analyses and skew the results by underestimating the abundance of lesser populated species³².

	Lysine Linkage	Percent Abundance
Canonical Linkages	K48	29.1% ± 1.9%
	K63	16.3% ± 0.2%
Non-canonical Linkages	K11	28.0% ± 1.4%
	K6	10.9% ± 1.9%
	K27	9.0% ± 0.1%
	K29	3.2% ± 0.1%
	K33	3.5% ± 0.1%

Table 1-1. Percentage abundance *in vivo* of ubiquitin chains linked via different lysines in yeast³¹.

1.2.1 *In Vitro* Synthesis of Non-Canonical Chains

Even though it has been shown that all the chains are present *in vivo*, non-canonical chains have not been as well studied as the canonical chains, mainly because of the inability to synthesize them *in vitro*. The specific E2s that are required to synthesize these chains are not known, thus there is a need to use some alternative method to enzymatic synthesis. Methods have been proposed in which ubiquitin is chemically synthesized and conjugated to another ubiquitin using native chemical ligation³³, but this is a very laborious process and is restricted by the fact that very few labs have the apparatus needed to perform chemical synthesis of whole ubiquitin chains. Also using this technology, individual chains could not be isotopically labeled since the cost of doing that using chemical synthesis is prohibitive. Our lab has developed a method to synthesize any polyubiquitin chains by incorporating one protective group, tert-Butyloxycarbonyl (boc), as a genetically incorporated unnatural amino acid, Lys(Boc) and another orthogonal protective group allyloxycarbonyl (alloc) protecting all other amino groups along with silver-mediated condensation reaction³⁴. Using this method, we have made all the non-canonical dimers with both proximal and distal Ub ¹⁵N- labeled and some heterogeneous trimers (K11, K33-Ub₃, K6, K27-Ub₃).

1.3 K6-linked polyubiquitin chains

1.3.1 Structural Information

K6-linked diubiquitin is one of the polyubiquitin chains that could not be studied extensively until non-enzymatic methods to make polyubiquitin chains were

developed. Recently, few attempts of gaining some insights about possible K6-linked polyubiquitin structures have been made. Using molecular modeling, Fushman and Walker were first to predict that K6-linked diubiquitin is capable of forming interface between its two units (proximal and distal)³⁵. The crystal structure of K6-linked ubiquitin dimer (PDB 2XK5) by Virdee *et al.*³⁶ confirm the computationally predicted possibility of a closed conformer. Based on the crystal structure, K6-linked ubiquitin dimer forms an interface and attains an "asymmetric closed conformation". It is shown that the hydrophobic patch on the proximal subunit, consisting mainly of I44 and V70 (I44 hydrophobic patch) interacts with a different hydrophobic patch consisting of L71, I36 and L8 (I36 hydrophobic patch) on the distal domain (Figure 1-6).

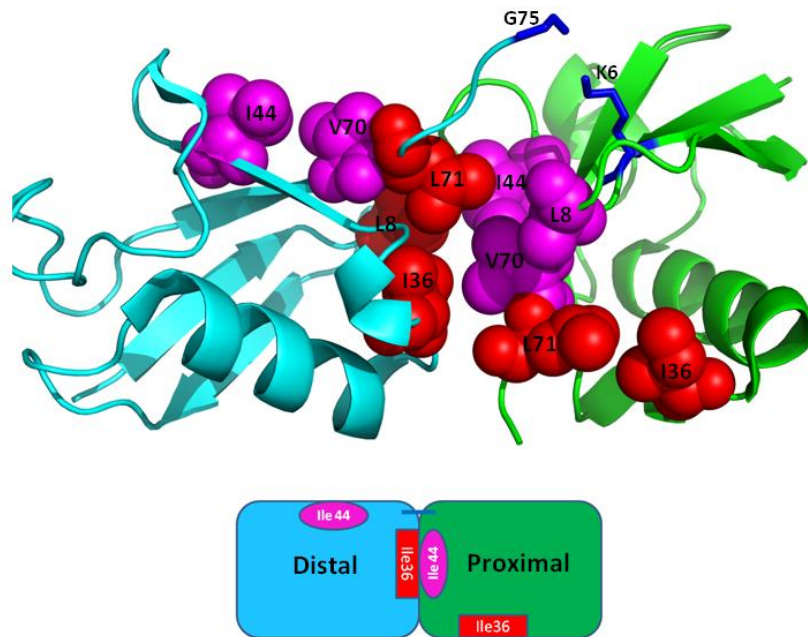


Figure 1-6. K6-linked diubiquitin crystal structure (PDB 2XK5). The distal subunit is shown in cyan and proximal domain is shown in green. Cartoon representation (top) of the structure with I36 hydrophobic patch indicated by red spheres and I44 hydrophobic patch by magenta spheres. K6 of the proximal domain and G75 of the distal domain are represented by blue sticks. Schematic drawing (below) showing the "asymmetric closed conformation" of K6-linked diubiquitin³⁶.

1.3.2 Functional Information

Interestingly, despite limited opportunities to study K6-linked polyubiquitin chains *in vitro*, some *in vivo* studies of K6-linked polyubiquitin chains have been performed. Based on mass spectrometric and mutational studies, K6-linked diubiquitin has been shown to be formed by autoubiquitination of E3 ligase BRCA1-BARD1^{37,38}. BRCA1 is a breast and ovarian tumor suppressor and forms a heterodimer with BARD1 to form an E3 ligase, which has been known to play an important role in DNA repair. Sobhian *et al.* have shown through coimmunoprecipitation that the UBD RAP80, which interacts with K63-linked polyubiquitin, interacts with endogenous BRCA1³⁹. They also hypothesized that K6-linked chains may interact preferably with RAP80, however direct interaction between these two proteins has not been observed. Moreover, it has also been shown that K6-linked polyubiquitin chains are recognized and disassembled at the proteasome. Thus, it is hypothesized that they play a role in proteasomal degradation³¹. In addition to the above function, it has been shown that branched K6-linkage containing polyubiquitin chains are involved in autoubiquitination of RING1B, which is an integral component of Polycomb transcriptional Repressive Complex 1 (PRC1), required for developmental gene regulation, ageing and cancer⁴⁰. Thus, we can see that K6-linked polyubiquitin has an important role in the cell. Furthermore, comprehensive studies of structure and dynamics of K6-linked polyubiquitin chain will help to understand how this polyubiquitin is able to carry out its biological functions.

1.4 K27-linked polyubiquitin chain

1.4.1 Structural Information

K27-linked diubiquitin chains like other non-canonical chains had not been studied structurally due to absence of a known enzymatic assembly to synthesize these chains *in vitro*. Since our lab developed the non-enzymatic method to synthesize polyubiquitin chains, we have been able to study and determine the structure of K27-Ub₂ using solution NMR, small-angle neutron scattering (SANS) and *in silico* ensemble modeling^{41,42}.

Using the solution NMR data, ex-lab member Dr. Carlos Castañeda determined structural models of K27-Ub₂ based on residual dipolar couplings (RDC) and ¹⁵N relaxation. Both these models show that the two ubiquitin units have their canonical hydrophobic patches (L8, I44, V70) positioned in a manner that could allow simultaneous interaction of both units with a receptor (Figure 1-7).

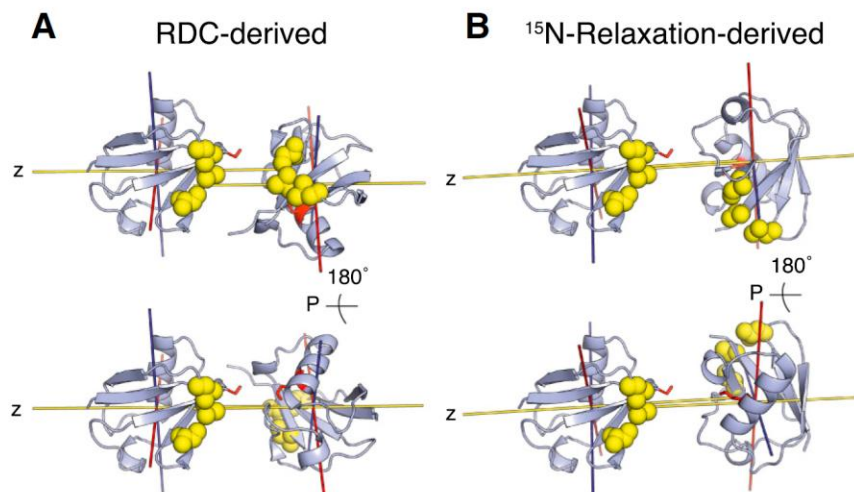


Figure 1-7. Structural models of K27-Ub₂ derived from residual dipolar couplings (A) and ¹⁵N relaxation (B)⁴¹. The yellow balls represent the canonical hydrophobic patch. In all structural models, distal domain is on the left and proximal domain is on the right. Due to orientational degeneracy of the data, two structures are shown for each Ub₂, differing by a 180° rotation of the proximal ubiquitin about the z axis of the corresponding tensor.

Using the solution NMR derived models and sparse ensemble selection (SES) method, Dr. Castañeda determined that K27-Ub₂ exists in more than one conformational state, and that two-conformer state is the minimal ensemble that agrees with the experimental data most likely is populated as two-conformer state in solution (Figure 1-8). Interestingly, the major conformer in all of these ensembles is similar to the RDC-derived and ¹⁵N relaxation-derived structural models.

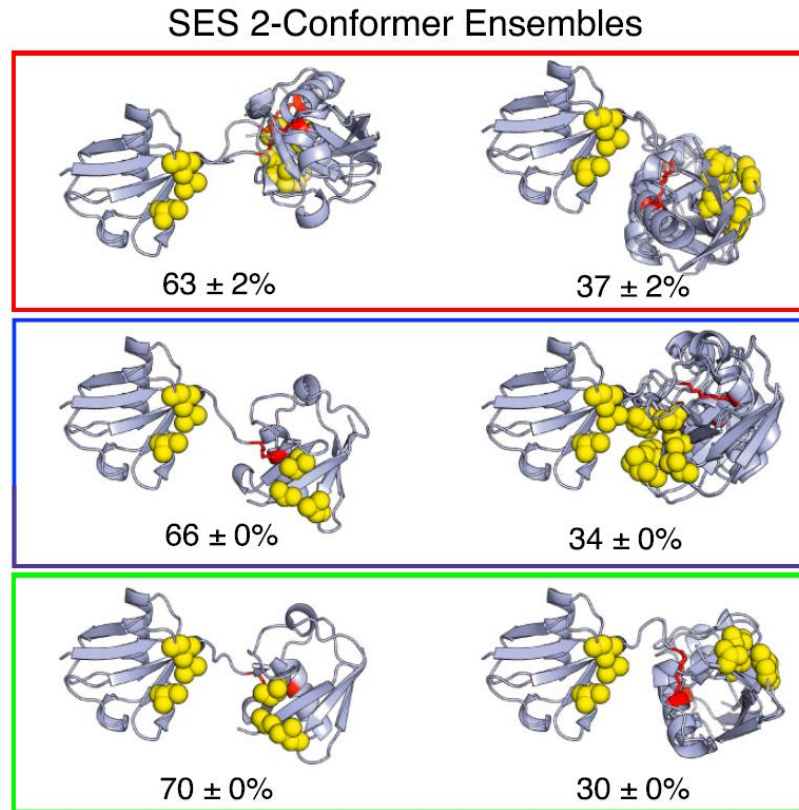


Figure 1-8. Three sets of 2-conformer ensembles for K27-Ub₂ from SES analysis that fit best to experimental data. Numbers below the structures indicate the population weight of each conformer in the ensemble⁴¹. In all structural models, distal domain is on the left and proximal domain is on the right.

1.4.2 Functional Information

Recent studies have shown that K27-linked polyubiquitin chains are involved in non-proteolytic functions. K27-linked polyUb has been observed on mitochondrial trafficking protein Miro1 helping slow down its degradation by the proteasome⁴³. PolyUb chains linked via K27 are also involved in the regulation of innate immunity⁴³⁻⁴⁶. Gatti *et al.* have also shown that K27 on the ubiquitin is essential for DNA damaged induced chromatin ubiquitination. They showed that histones belonging to the H2A family are targets of this modification and crucial players of

DNA damage response including Rap80 directly interact with the K27-linked ubiquitin⁴⁷. Using information from the structural data, Dr. Castañeda showed that K27-Ub₂ may be specifically recognized by K48-selective receptor UBA2 domain from proteasomal shuttle protein hHR23a. Another ex-lab member Emma Dixon observed that K27-Ub₂ chains are refractive to most deubiquitinating enzymes⁴¹.

1.5 Summary of the Work

The primary aim of this work was to elucidate the structure and function of K6-linked diubiquitin. We also focused on K27-linked diubiquitin and possible role of these chains in DNA damage repair (DDR) pathway. Furthermore, we aim to understand the binding properties of ubiquitin-like domain of DNA damage-inducible protein 1 (Ddi1UBL) from both yeast and humans with ubiquitin in order to illuminate its possible function in the proteasomal degradation pathway as a shuttle protein.

We developed and optimized both non-enzymatic and enzymatic methods to synthesize K6-linked polyubiquitin chains. Utilizing these methods, we generated K6-Ub₂ to study its structure and function by solution NMR techniques. From the solution NMR measurements, small-angle neutron scattering (SANS), and *in silico* ensemble generation we determined population-weighted conformational ensembles of K6-linked diubiquitin. We demonstrated that the crystal structure of K6-Ub₂ obtained by Virdee *et al.*³⁶ represents only one of the conformers populated in solution and that K6-linked diubiquitin exists in solution as at least two conformers. The conformers we determined from the analysis of solution data suggested the structural ability of K6-Ub₂ to bind proteins from both proteasomal degradation signaling pathway (hHR23a) and DDR pathway (Rap80). We performed NMR

binding assays to determine which of these proteins K6-Ub₂ binds and in order to elucidate the pathway it is involved in. For our binding studies, we used the ubiquitin binding domains of both proteins that have been shown to contain linkage-specific polyubiquitin binding preferences. hHR23a has the ubiquitin-associated domain 2 (hHR23a UBA2) that binds tightly to K48-Ub₂ and Rap80 contains a tandem ubiquitin interacting motif (Rap80 tUIM) that binds specifically to K63-Ub₂. We observed that K6-Ub₂ binds tightly to both hHR23a UBA2 and Rap80 tUIM, indicating that it has the functional capability to be involved in both pathways.

Our group has shown that in solution K27-Ub₂ exists in at least two conformers and the structural analysis of these conformers suggested the capability to bind both hHR23a UBA and Rap80 tUIM. Castañeda *et al.* have already shown that K27-Ub₂ binds hHR23a UBA2 tightly. Here, we demonstrate that it has high binding affinity for Rap80 tUIM too.

Our studies with K6- and K27-Ub₂ have revealed that due to their conformational heterogeneity, these chains have the capability to be part of both proteasomal degradation signaling and DNA damage repair pathways.

We also performed studies with Ddi1UBL from both yeast and humans. We studied how charges on ubiquitin surface affect its interaction with yeast Ddi1UBL (yDdi1UBL). From mutational studies we determined that binding between yDdi1UBL and ubiquitin is dramatically reduced when all three positive charges near the hydrophobic surface of ubiquitin (K6, R42 and R72) are mutated to either neutral (A) or negative (E) charged amino acids. We also demonstrated that yDdi1UBL binds tighter to K48-Ub₂ than monoubiquitin and other diubiquitin chains we tested

(K63-, K6-, K27- and K11-Ub₂s). We also demonstrated that this linkage specificity is removed by a single mutation (L31K) in the putative ubiquitin interacting motif (UIM) on the “back side” of yDdi1UBL, suggesting that this putative UIM might be responsible for the preferential binding to K48-linked chains. Furthermore, we illustrated a directionality in the binding of K48-Ub₂ to yDdi1UBL, wherein the proximal domain binds the “front side” β -sheet surface similar to monoubiquitin, while the distal domain binds the “back side” putative UIM.

Our binding studies with human Ddi1UBL (hDdi1UBL) confirmed that the surprising functionality of yDdi1UBL to bind ubiquitin is conserved across the species. Moreover, we showed that the property of Ddi1UBL to bind tighter to K48-Ub₂ compared to monoubiquitin is also conserved. These results give more credence to the alternative proteasomal shuttle model proposed by Nowicka *et al.*

Chapter 2: Structure of K6-linked Ubiquitin Chains

2.1 Synthesizing K6-linked diubiquitin using non-enzymatic method

We successfully synthesized all-natural K6-linked diubiquitins ^{15}N labeled at proximal or distal domain using the non-enzymatic method mentioned above. Using K6-linked diubiquitin ^{15}N labeled at the distal domain as an example, we demonstrate the steps of the performed synthesis with its checkpoints. Following the scheme shown in Figure 2-1, we first thioesterified the ^{15}N labeled wild type ubiquitin using E1 enzyme and sodium 2-mercaptoethanesulfonate (MESNA, $\text{C}_2\text{H}_5\text{NaO}_3\text{S}_2$). The next step was to protect all the amino groups of the thioesterified ubiquitin (UbCOSR) using allyloxycarbonyl (alloc) group. Electrospray ionization-mass spectrometry (ESI-MS) was used to confirm the molecular mass change (Figure 2-2).

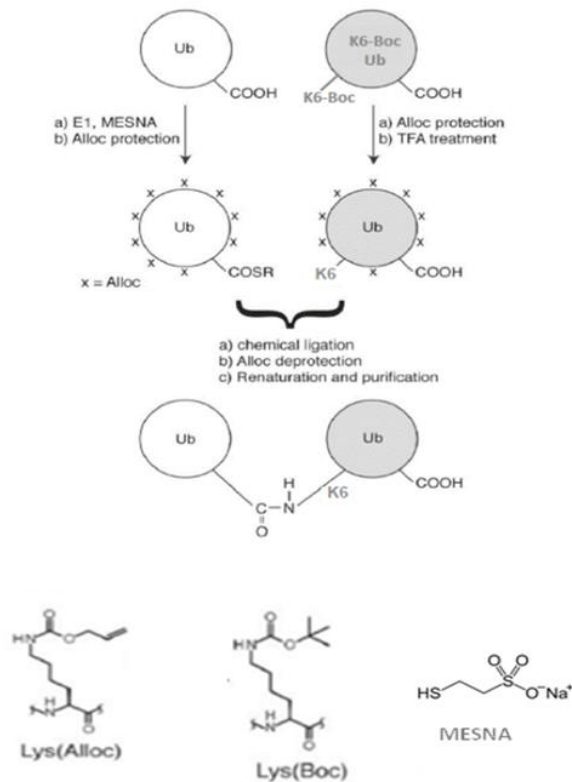


Figure 2-1. Scheme of the assembly of K6-Linked Ub₂ from wild type ubiquitin and K6(Boc) ubiquitin by non-enzymatic method. The different shades of the monomers represent selective isotopic labeling. The structures of MESNA, Lys(Alloc) and Lys(Boc) are shown.

Furthermore, we protected all the amino groups of K6(Boc) ubiquitin using the same method and then removed the Boc group from K6 by means of trifluoroacetic acid (TFA) treatment. ESI-MS showed that both the addition of alloc groups and removal of Boc group were successful (Figure 2-2).

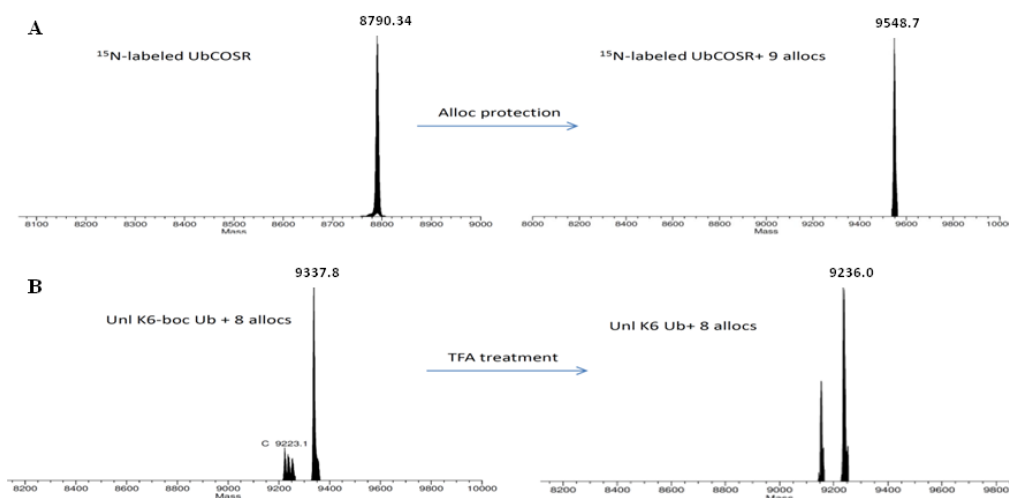


Figure 2-2. ESI-MS checkpoints at different stages of the non-enzymatic synthesis of K6-linked diubiquitin ¹⁵N labeled at distal domain. All masses shown above are in Da. A. Alloc protection of ¹⁵N labeled thioesterified ubiquitin (¹⁵N labeled Ub + SR = 8665 Da + 124 Da = 8789 Da). Addition of 9 alloc (1 alloc=84 Da) groups changes the molecular weight of UbCOSR (8789 Da) to 9547 Da. B. Removal of Boc group (~100 Da) by TFA treatment of allocated unlabeled (Unl) K6(Boc) Ub (9338 Da) gives the product allocated Unl K6 Ub (9236 Da). UbCOSR- thioesterified ubiquitin, TFA-trifluoroacetic acid, SR- thioester.

In the next stage of synthesis, we performed silver-mediated condensation reaction and after 16 hours the dimer presence was observed (Figure 2-3).

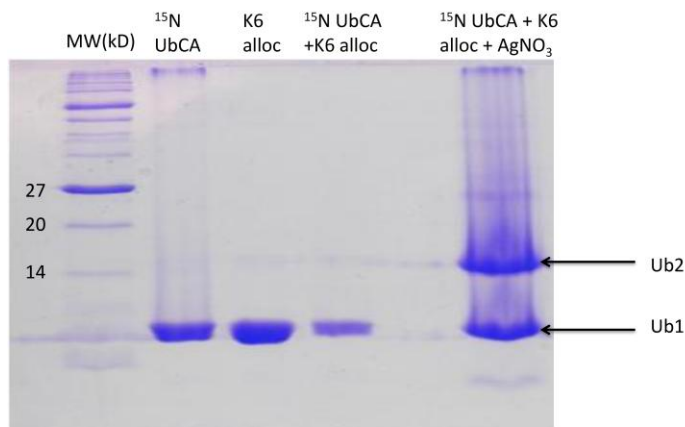


Figure 2-3. Coomassie-stained 15% SDS PAGE gel of the chemical condensation reaction of K6-linked Ub₂ ¹⁵N labeled on the distal Ub. UbCA- fully allocated thioesterified ubiquitin, K6 alloc- ubiquitin with all amino groups protected using alloc groups except K6, AgNO₃- silver nitrate, Ub1- monoubiquitin, Ub2- diubiquitin.

Once the chemical condensation reaction was successful, we removed all the allocs from the sample by incubating it in the presence of ruthenium-catalyst and

thiophenol followed by unfolding and refolding of the proteins. Finally, we separated the dimer from other contaminants by size exclusion chromatography. Purity of the final product was additionally verified using ESI-MS, where only one species was observed and its molecular weight corresponded to that of an ubiquitin dimer with one unit ^{15}N labeled (Figure 2-4).

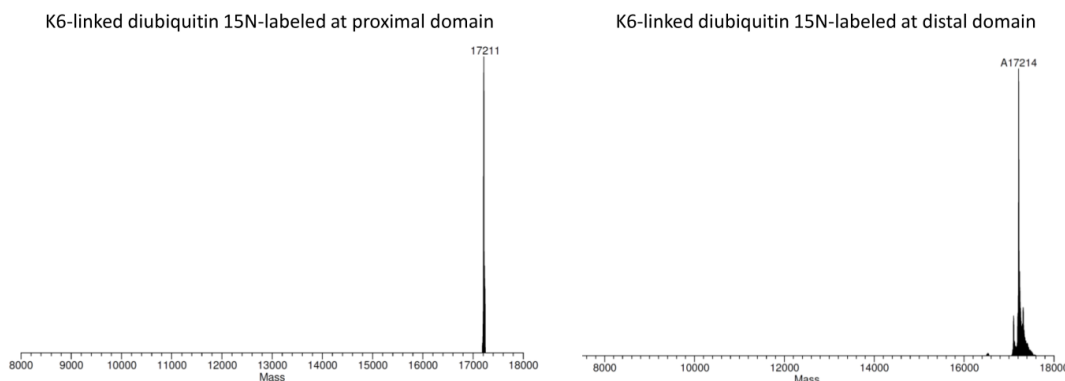


Figure 2-4. ESI-MS of purified K6-linked diubiquitin ^{15}N labeled at proximal (left) and distal (right) domain. The expected mass of the diubiquitin (^{15}N labeled ubiquitin + unlabeled ubiquitin- H_2O =8665 Da +8565 Da -18 Da=17212 Da) is observed.

2.2 Relaxation/RDC derived models

Once the dimers (^{15}N labeled at either proximal or distal domain) were purified, we collected a ^1H - ^{15}N SOFAST HMQC spectrum to confirm that they are properly folded. The ^1H - ^{15}N SOFAST HMQC spectra of the diubiquitins and monoubiquitin were used to compare the changes in peaks positions in the spectra. As an example, overlay of the ^1H - ^{15}N SOFAST HMQC spectrum of K6-linked diubiquitin ^{15}N labeled at distal domain with the ^1H - ^{15}N SOFAST HMQC spectrum of wild type ubiquitin is shown (Figure 2-5). The biggest perturbations in the chemical shifts are observed for residue G76 since in the case of wild type ubiquitin it

is free while in the dimer, the distal domain G76 is involved in isopeptide linkage formation with ϵ -amine of K6.

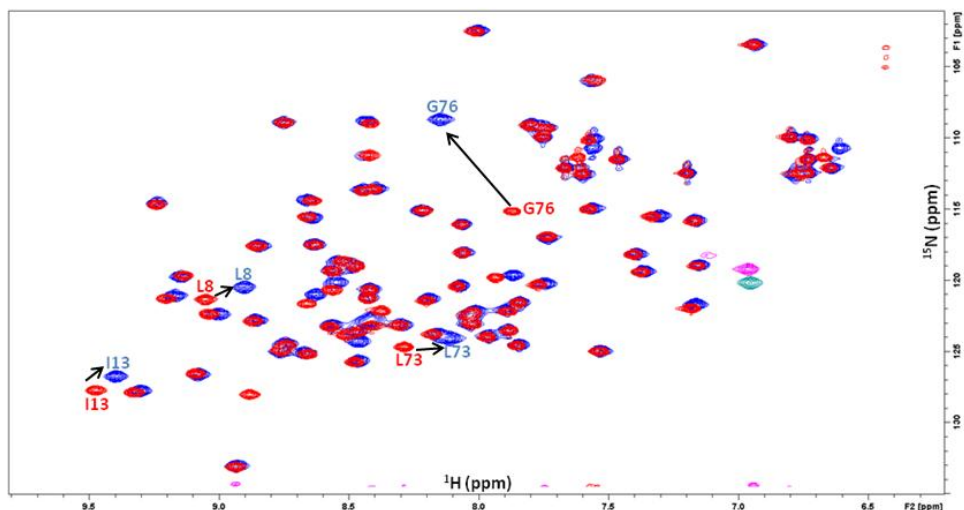


Figure 2-5. Overlay of ^1H - ^{15}N SOFAST HMQC spectra of the distal Ub of K6-linked diubiquitin (blue) and monoubiquitin (red). Several residues showing noticeable signal shifts are indicated. The black arrow indicates the direction of the signal shift.

The changes in chemical shifts were quantified as chemical shift perturbations (CSP) and plotted against residue number. The CSPs of both proximal domain and distal domain (Figure 2-6(C)) of the ubiquitin dimer versus wild type ubiquitin are numerous and well spread out. In the proximal domain (Figure 2-6(B)), significant CSPs are seen in the residues surrounding the hydrophobic patch (L8, I44, V70). CSPs shown by distal domain (Figure 2-6(C)) are the highest at G76 due to its participation in isopeptide linkage. However, residues around L8 also show very high perturbations and significant perturbations are seen at I36 as well. There are minor perturbations in the region surrounding I44 and V70. These CSPs indicate formation of the interface between distal and proximal domain.

It is important to confirm that the CSPs shown by the proximal domain are not only due to addition of another ubiquitin unit at K6 but due to interaction with the

distal domain. We calculated CSPs of ^{15}N labeled K6(Boc) versus ^{15}N labeled wild type ubiquitin and found that the spread of CSPs are markedly different. In K6(Boc) ubiquitin (Figure 2-6(A)), the CSPs are observed mostly around K6 while in the proximal domain additional to the area surrounding K6, CSPs around I44 and V70 are observed (Figure 2-6(B)). Thus, the CSP pattern shown by proximal domain is most likely due to the interaction between the two domains.

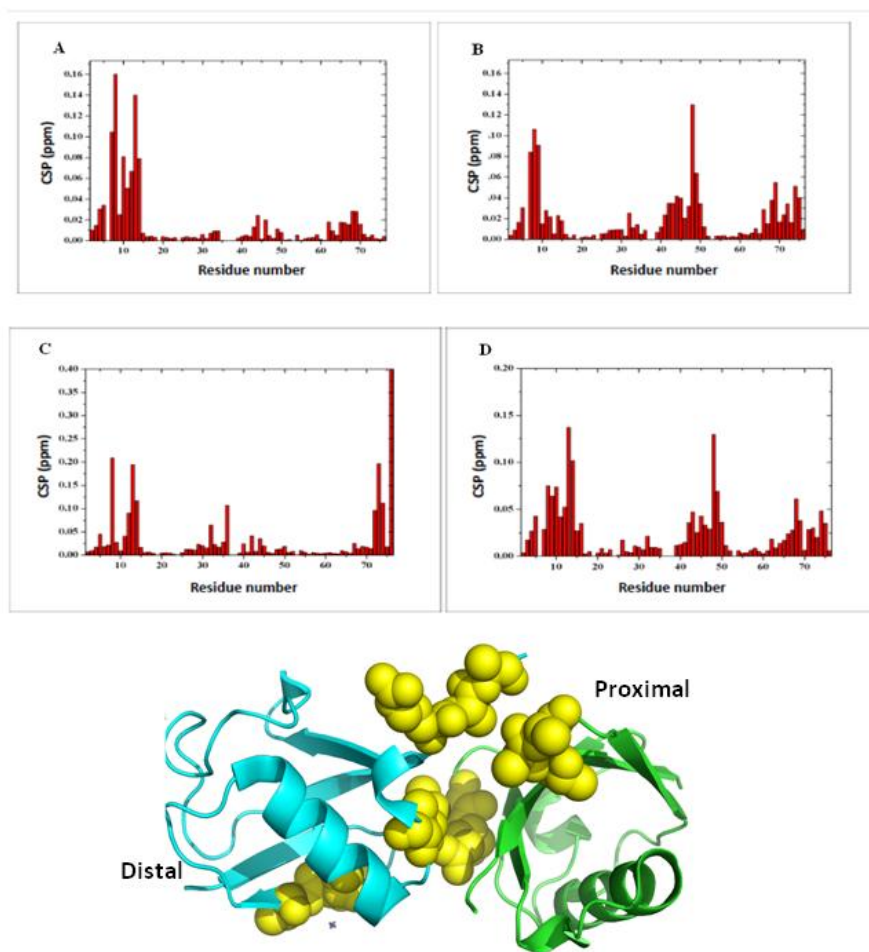


Figure 2-6. Chemical Shift Perturbations of ^{15}N labeled K6(Boc) Ub (A), ^{15}N proximal labeled K6-linked diubiquitin (B), ^{15}N distal labeled K6-linked diubiquitin (C) with reference to WT ubiquitin and ^{15}N proximal labeled K6-linked diubiquitin with reference to ^{15}N labeled K6(Boc) Ub (D). CSPs greater than 0.06 of K6-Ub₂ ^{15}N labeled on proximal and distal domain with reference to WT ubiquitin mapped onto the structural cartoon representation of K6-Ub₂ crystal structure (PDB: 2XK5).

^{15}N relaxation experiments and ^1H - ^{15}N NOE were obtained for both domains (Figure 2-7). Loss of flexibility in G76 of the distal domain (indicated by higher NOE that is comparable to those in the loops) compared to proximal domain confirms that G76 of the distal domain is restricted in mobility, likely as the result of its involvement in the isopeptide linkage. G76 of the proximal is the only residue to show a negative heteronuclear NOE indicating very high flexibility.

The average ^{15}N T_1 (Spin-lattice relaxation time) of both proximal and distal domain from R_1 was calculated and is between 700-715 ms, which matches the T_1 of an ubiquitin dimer¹⁶. Also, the ^1H T_2 (Transverse relaxation time) values of both domains are ~23.5 ms while that of monoubiquitin is known to be around 50 ms¹⁶. Finally, overall rotational correlation times (τ_c) obtained from our relaxation data (Table 2-1) for both ubiquitin domains (~8.4 ns) is twice that of ubiquitin monomer (4.2 ns)¹⁶. All this data indicate that both domains of K6-linked diubiquitin tumble as one unit, to a first approximation, instead of two completely independent entities.

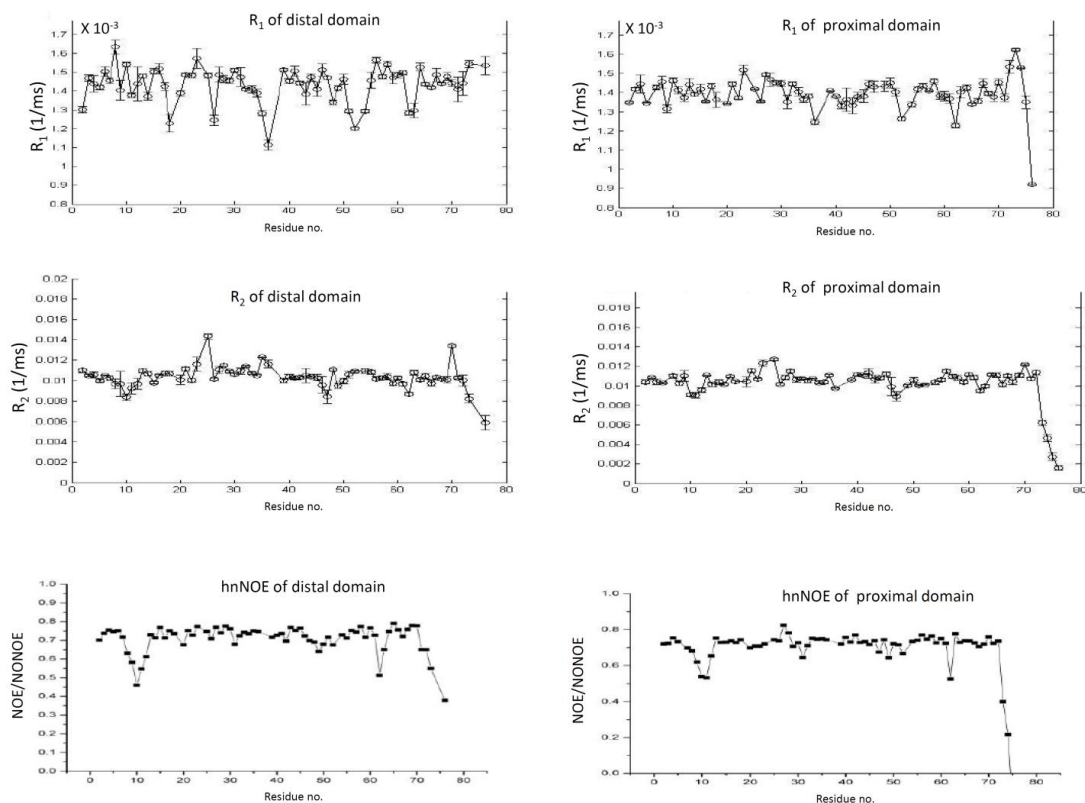


Figure 2-7. Relaxation rates (R_1 and R_2) and heteronuclear NOE of distal (left) and proximal (right) domains of K6-linked diubiquitin.

We determined the overall rotational diffusion tensor of each ubiquitin domain separately by using the program ROTDIF⁴⁸ (Table 2-1).

K6-linked diubiquitin unit	$D_{xx} \times 10^7$ $\text{rad}^2\text{s}^{-1}$	$D_{yy} \times 10^7$ $\text{rad}^2\text{s}^{-1}$	$D_{zz} \times 10^7$ $\text{rad}^2\text{s}^{-1}$	τ_c in ns	α in deg	β in deg	γ in deg
Proximal	1.80 (0.05)	2.00 (0.05)	2.10 (0.06)	8.46 (0.13)	135 (26)	106 (21)	38 (9)
Distal	1.63 (0.10)	1.79 (0.07)	2.65 (0.13)	8.25 (0.25)	125 (10)	153 (5)	169 (19)

Table 2-1. Overall rotational diffusion tensor characteristics of K6-linked diubiquitin determined from ^{15}N relaxation data for the two ubiquitin units. Atom coordinates for each Ub domain were taken from PDB: 1D3Z. D_{xx} , D_{yy} , D_{zz} represent the principal components of the overall rotational diffusion tensors along the x, y and z principal axes respectively. τ_c represents the overall rotational correlation time. α , β , γ represent Euler angles that determine the orientation of the principal axes of the overall rotational diffusion tensor with respect to the coordinate frame of the protein. Numbers in the parentheses represent standard deviations.

The correlation between the experimental ratio of the backbone ^{15}N relaxation rates (R_1/R_2) and the calculated ratio using atomic coordinates of NMR solution structure of ubiquitin 1D3Z is good (~ 0.9) for both distal and proximal domains (Figure 2-8).

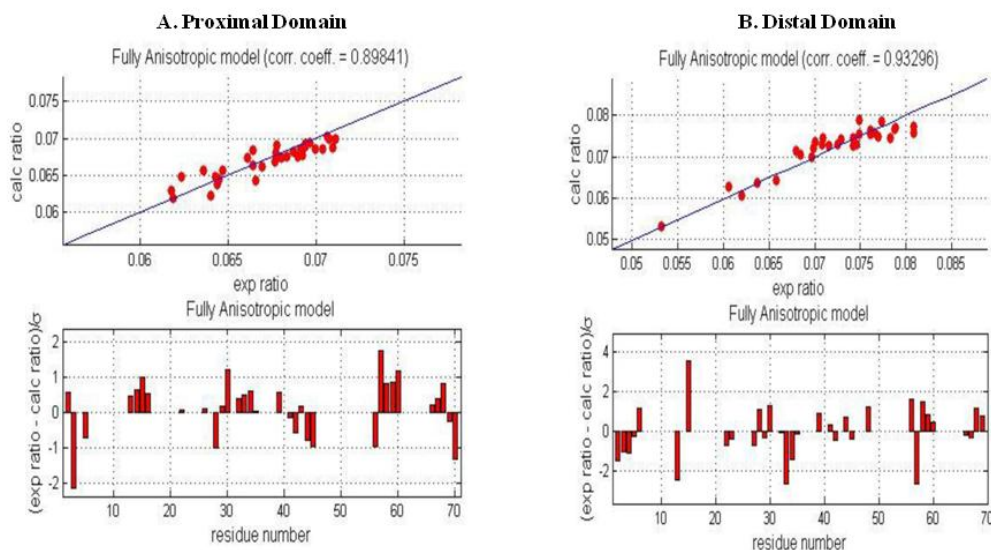


Figure 2-8. Correlation plots of experimental ratio of ^{15}N relaxation rates (R_1/R_2) of distal domain (A) and proximal domain (B) of K6-linked diubiquitin with the calculated ratio using NH vectors from the solution NMR structure of ubiquitin (PDB:1D3Z) and fit to the fully anisotropic model of overall rotational diffusion tensors.

The Euler angles (α , β , γ) shown in Table 2-1 are used to characterize the principal axes frame of the diffusion tensors with respect to the coordinate frame of the 1D3Z structure. Assuming that there is no interdomain mobility, we used these angles to determine the orientation of the two domains relative to each other. The centers of mass of the domains were set apart by an arbitrary distance of 17 \AA and using the atomic coordinates of 1D3Z, eight different structures (due to degeneracy of the diffusion tensor with respect to 180° rotations around the axes) were generated by rotating the distal and proximal domains so that their diffusion tensors match. Out of

these, only two have the orientation and position that would allow formation of the isopeptide linkage between the G76 of the distal domain and K6 of the proximal domain. In Figure 2-9(A), one of the two structures is shown. When this relaxation-derived structure was used to calculate the ratio of the relaxation rates for both domains together, the correlation was reasonable (0.78) although not ideal (Figure 2-9(B)).

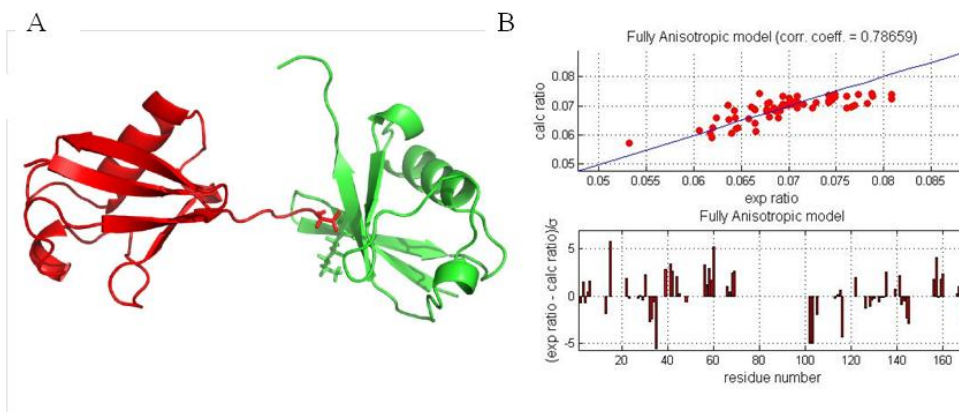


Figure 2-9. Relaxation derived structure (A) and correlation plot of ^{15}N relaxation rates (R_1/R_2) of both domains of K6-linked diubiquitin simultaneously with the calculated ratio using NH vectors from the relaxation derived structure and fit to the fully anisotropic model of overall rotational diffusion tensors (B).

Since the correlation of experimental data with the relaxation derived structure was not ideal, we utilized residual dipolar coupling, which is an orthogonal physical property, to independently determine relative orientation of the two domains. We determined residual dipolar couplings by taking the difference of the measured ^1H - ^{15}N couplings in the presence and absence of the alignment medium (C_{12}E_5 and hexanol, molar ratio 0.85)⁴⁹. Using MATLAB program ALTENS¹⁶, the alignment tensors (S) were calculated for both domains individually (Table 2-2).

K6-linked diubiquitin unit	S_{xx} in Hz	S_{yy} in Hz	S_{zz} in Hz	α in deg	β in deg	γ in deg	Q
Proximal	-1.78 (0.67)	-14.71 (0.72)	16.45 (0.61)	236 (2)	136 (1)	214 (3)	0.124
Distal	13.07 (0.61)	19.07 (0.70)	-32.141 (0.76)	298 (2)	30 (1)	108 (6)	0.085

Table 2-2. Alignment tensor characteristics for K6-linked diubiquitin determined from the RDCs for the two ubiquitin units. Atom coordinates for each Ub domain were taken from PDB: 1D3Z. S_{xx} , S_{yy} , S_{zz} represent the principal components of the alignment tensors along the x, y and z axes respectively. α , β , γ represent Euler angles that determine the orientation of the principal axes of the alignment tensor with respect to the coordinate frame of the protein. Q indicates quality factor. Quality factors⁵⁰ report on the residuals between the experimental and back-calculated values, with low Q reflecting excellent agreement. Numbers in the parentheses represent standard deviations.

Both distal and proximal domains showed excellent agreement between the experimental RDCs and the back calculated RDCs using the atomic coordinates of monoubiquitin structure (PDB: 1D3Z) (Figure 2-10).

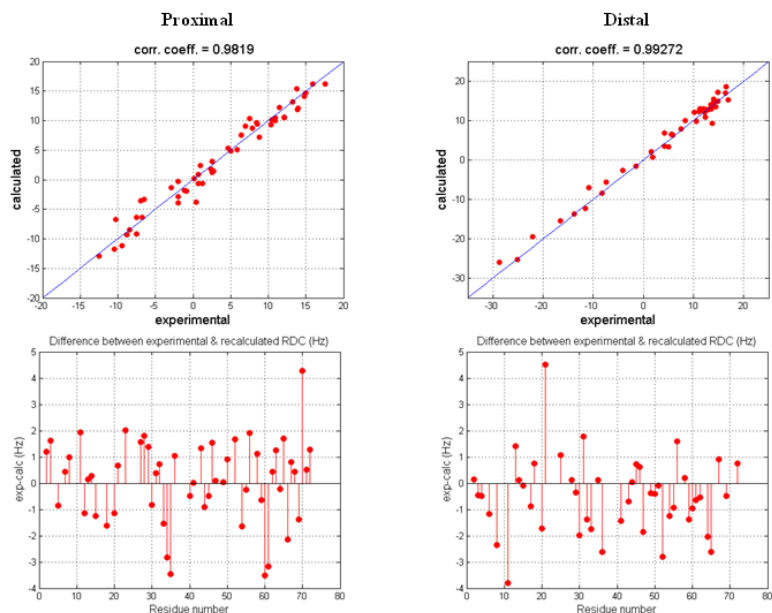


Figure 2-10. Correlation plots of experimental RDC data of K6-linked diubiquitin, proximal domain (left) and (b) distal domain (right) compared with the predicted values using NH vectors from the solution NMR structure of ubiquitin monomer (PDB:1D3Z). The bottom plots show residuals of the fit.

Like in relaxation data, the Euler angles (α , β , γ) are also used to characterize the principal axes frame of the alignment tensors with respect to atomic coordinates of the ubiquitin NMR structure. Assuming that the alignment tensors for both domains are similar (i.e. there is no interdomain mobility), we can use the above angles to generate RDC structures. We used the program PATIDOCK⁵¹ to generate 8 structures based on the RDC data. Correlation of our experimental RDC data of both domains simultaneously with the calculated RDC values using atomic coordinates of the PATIDOCK generated structure was in good agreement (correlation coefficient of 0.92) but not as good as with individual domains (Figure 2-11(D)). However, there is a noticeable decrease in correlation when the experimental RDC data for individual domains or both domains together is compared with calculated RDCs based on atomic coordinates of the respective individual domains from K6-linked diubiquitin crystal structure or the whole crystal structure (PDB 2XK5) (Figure 2-11(A-C)).

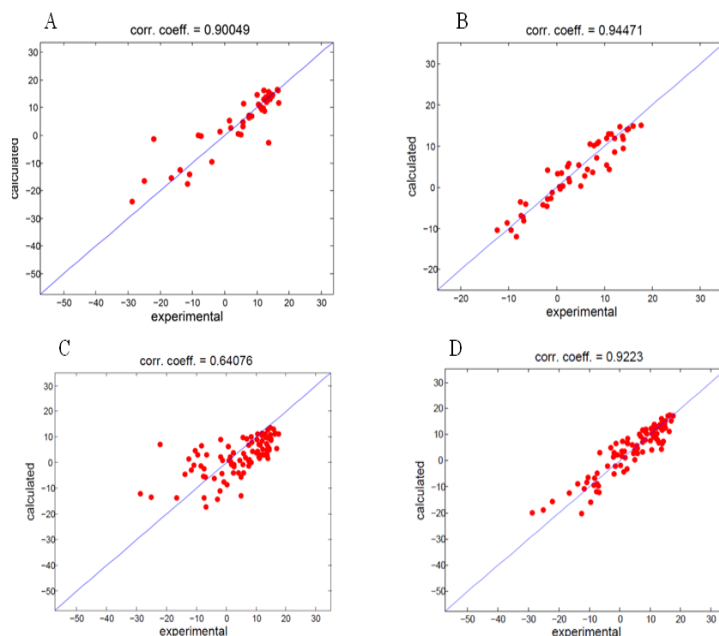


Figure 2-11. Correlation plots of experimental RDC data of K6-linked diubiquitin distal domain (A), proximal domain (B) and both domains simultaneously (C) compared with the calculated values using NH vectors from respective individual domains from K6-linked diubiquitin crystal structure or the whole crystal structure (PDB:2XK5). Correlation plots of experimental RDC data of both domains of K6-linked diubiquitin at the same time with calculated values using atomic coordinates from the RDC-optimized structure generated using PATIDOCK (D).

Finally, our NMR data delivered information about the dynamics of the K6-linked diubiquitin in solution, therefore models built based on this data reflect more physiologically relevant conformations. Comparative analysis of RDC derived solution structure, relaxation derived solution structure and crystal structure of K6-linked diubiquitin (PDB 2XK5) were performed by keeping the distal domain of both models similarly positioned, showed noticeable difference in the orientation of the proximal domain between the crystal structure and the solution NMR derived models (Figure 2-12).

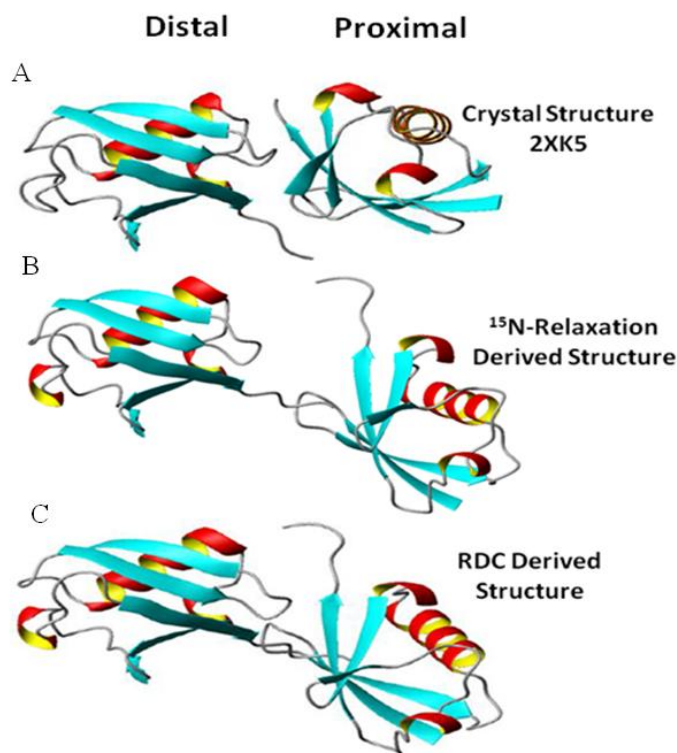


Figure 2-12. Comparison of K6-linked diubiquitin crystal structure (PDB 2XK5) (A), ¹⁵N-Relaxation derived structural model (B) and PATIDOCK generated RDC optimized structural model (C). Distal domains of the models are aligned to each other.

2.3 Ensemble Analysis

My former labmate Dr. Carlos Castañeda performed the ensemble analysis. All the work based on the ensemble mentioned in this subsection is performed by him and is published in a peer-reviewed article in which I am a co-author⁴².

While the single structure representations for K6-Ub₂ derived from the RDC and ¹⁵N relaxation data are similar to the crystal structure, Castañeda *et al.*⁴² showed that neither this single conformation nor the crystal structure alone is sufficient to fit the solution data (high Q values, low correlation coefficient). Sparse ensemble selection (SES) analysis⁵² was performed on *in silico* generated ensemble (SASSIE⁵³) of K6-Ub₂. From the analysis, it was determined that a two-conformer ensemble

reproduces experimental RDC data extremely well ($Q = 0.06$, $r = 0.99$) (Figure 2-13). For K6-Ub₂, the results for 2- and 3-conformer ensembles are essentially indistinguishable in terms of correlation coefficients and Q values.

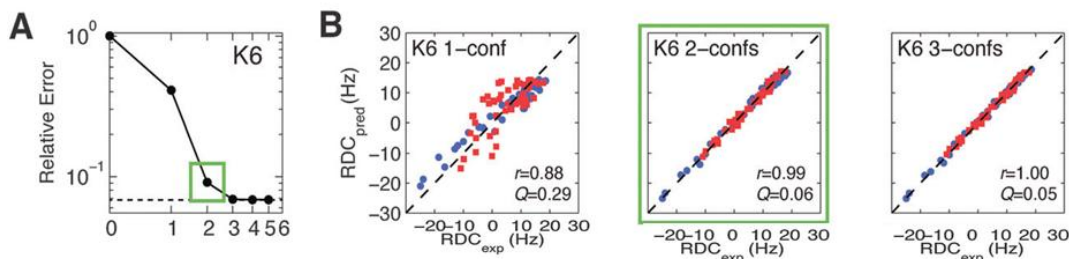


Figure 2-13. 2-conformer ensemble reproduces experimental RDC data extremely well. (A) I-Curve analysis to determine the optimal number of conformers (indicated by green square) for K6-Ub₂ ensemble solutions. **(B)** Agreement between experimental RDCs for both Ubs taken together vs. RDCs predicted from 1-conformer, 2-conformer, and 3-conformer ensembles. Data for the distal and proximal Ubs are colored blue and red, respectively. Pearson's correlation coefficient (r) and quality factor (Q) values are indicated inside each plot.⁴²

Figure 2-14 shows the two sets of 2-conformer ensembles that are in excellent agreement with experimental RDCs. Surprisingly, the major conformer of the second (blue) ensemble is compact and strikingly similar to the crystal structure of K6-Ub₂ (Figure 2-14(C)). The analysis revealed that similar to K48-Ub₂, even in K6-Ub₂ the compact conformer is in equilibrium with a more open conformer. Moreover, the more open conformer might be capable of forming a sandwich-like ligand binding mode similar to how K48-Ub₂ binds hHR23a UBA2. Interestingly, this open conformer is the major conformer for the first (red) ensemble in Figure 2-14(A), while the other more compact conformer is different from the crystal structure in how the Ub units are oriented with respect to each other. It is striking that this second conformer resembles the ligand-bound structure of K63-Ub₂. Both ensembles of K6-Ub₂ are in reasonable agreement with the (small-angle neutron scattering) SANS data (Figure 2-14(D)) with the first (red) ensemble showing better agreement than the

second (blue). These structural ensembles reflect the flexibility of K6-Ub₂ and highlight the ability of the chain to adopt multiple Ub/Ub orientations that might be competent to bind different ligands.

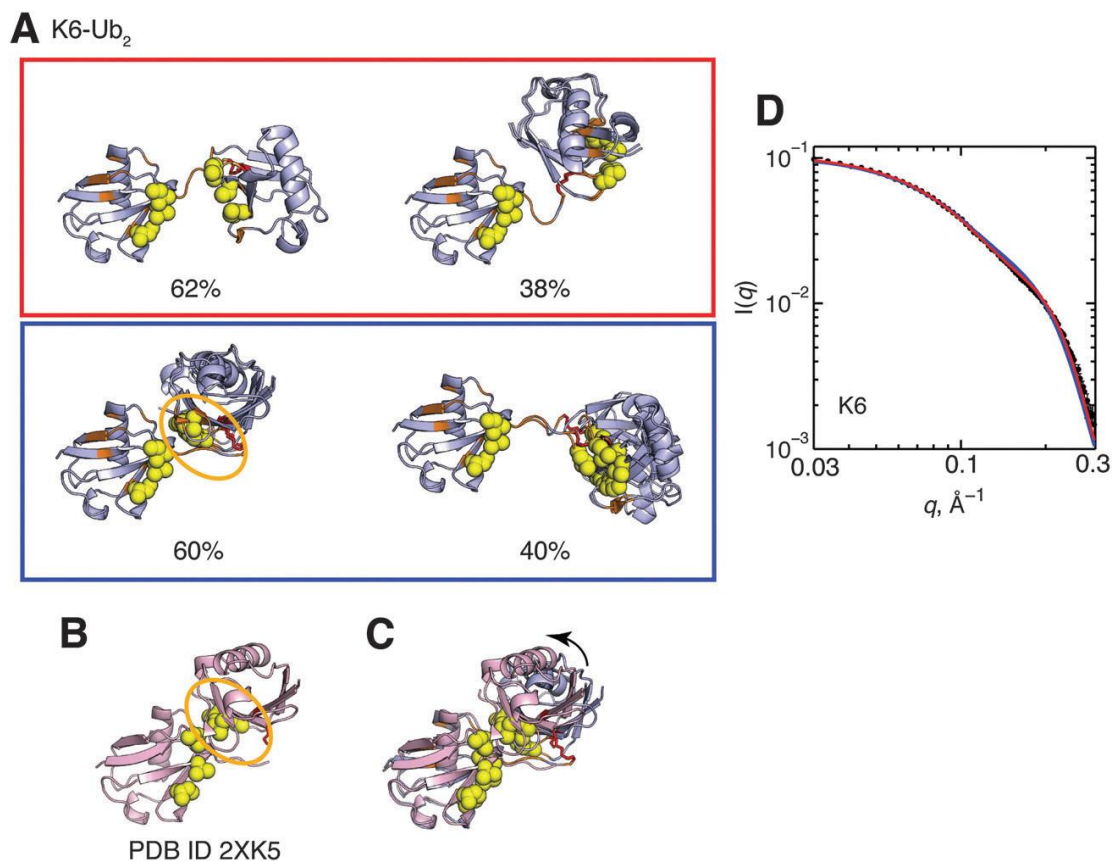


Figure 2-14. Two sets of 2-conformer ensembles of K6-Ub₂ that are in excellent agreement with experimental data. (A) Two-conformer ensembles of K6-Ub₂. For each conformer, residues with CSPs > 0.04 ppm are colored orange. Numbers below the structures indicate population weights of each conformer. (B) Crystal structure of K6-Ub₂ (PDB ID 2XK5). (C) Overlay of the crystal structure of K6-Ub₂ (pink) and the blue ensemble's conformer of the highest population weight from panel A (light blue). The arrow highlights orientational difference for the proximal Ub between the light blue and pink structures. (D) Agreement between experimental (black circles) and predicted SANS $I(q)$ profiles from the conformational ensembles shown in panel A. The $I(q)$ curve for each ensemble is color-coded according to panel A.⁴²

2.4 pH effect on structure of K6-Ub₂

Since it is known that K48-Ub₂ loses its interface at low pH (acidic conditions)¹⁶, we wanted to test if the same happens with K6-Ub₂. When the pH of

the buffer was lowered to 4.5, although the CSPs in the distal domain were reduced, the region around L8 still showed minor CSPs (Figure 2-15).

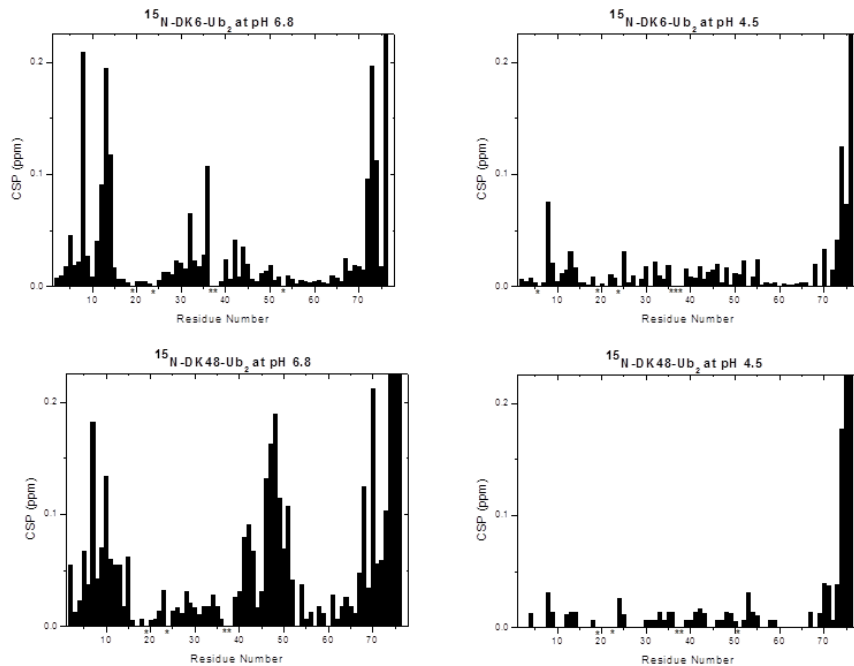


Figure 2-15. Comparison of CSPs of K6-Ub₂ labeled on the distal domain at pH 6.8 (top left) and pH 4.5 (top right) with CSPs of K48-Ub₂ labeled on the distal domain at pH 6.8 (bottom left) and pH 4.5 (bottom right)⁵⁴.

It can be interpreted to mean that even though K6-Ub₂ at lower pH tends to be more populated in the open conformation than it is at neutral pH, there is still a partial interface at the lower pH. This could be due to the fact that unlike in K48-Ub₂, the H68 on both domains of K6-Ub₂ are not part of the interface but only the H68 on the proximal domain is part of the interface while H68 on the distal domain is further away (Figure 2-16).

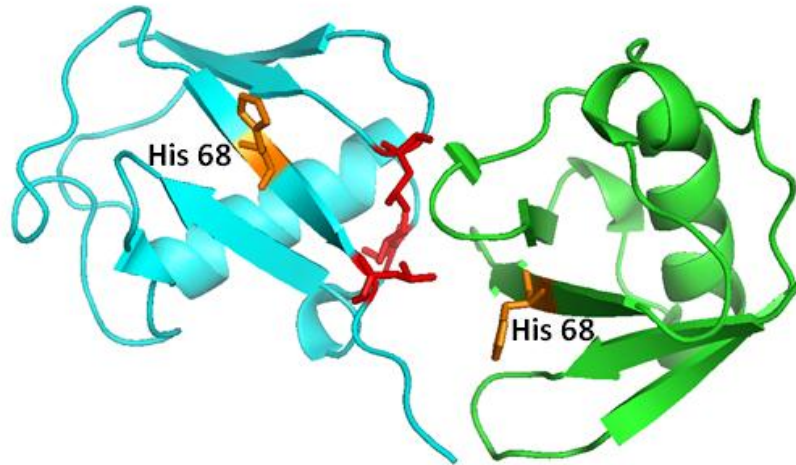


Figure 2-16. Crystal structure of K6-Ub₂ (PDB 2XK5) showing H68 (orange sticks) on proximal domain (green) and H68 (orange sticks) on the distal domain (blue). The hydrophobic patch (L8, I36 and L71) on the distal domain involved in the interface is also shown (red sticks).

Chapter 3: Binding Studies of K6-Linked Diubiquitin

3.1 Introduction

As mentioned in the previous chapter, the SES analysis showed that RDC data for K6-Ub₂ can be reproduced if there is a minimum of two-conformer ensemble⁴². The results of the SES analysis indicated that there are at least two sets of two-conformer ensemble that fit the experimental RDC data. Interestingly, the minor conformer of the first set (shown inside the red box in Figure 2-14 (A)) is similar to the bound state of Rap80 tUIM to K63-Ub₂ (Figure 3-1 (A)). As mentioned before, previous studies have shown that K6-linked chains are auto-ubiquitinated onto BRCA1-BARD1^{37,38} while Sobhian *et al.* showed that BRCA1 co-immunoprecipitates with Rap80. Direct interactions between Rap80 and K6-Ub₂ has not been discovered yet but these *in vivo* studies of K6-linked polyubiquitin chains show that it might be part of the DNA repair pathway involving Rap80. Therefore, the presence of the conformer resembling the Rap80 tUIM bound state of K63-Ub₂ led us to study the interaction between Rap80 tUIM and K6-Ub₂ exhaustively.

Moreover, the major conformer of the set in the red box of Figure 2-14 (A) resembles hHR23a UBA2 bound K48-Ub₂ and does seem to have enough space for the hHR23a UBA2 to bind it in sandwich-mode (Figure 3-1(B)). Additionally, it has also been shown that K6-linked polyubiquitin chains are recognized and deubiquitinated at the proteasome³¹. Thus, it is hypothesized that they play a role in proteasomal degradation. These interesting findings led us to delve further into the interaction between hHR23a UBA2 and K6-Ub₂.

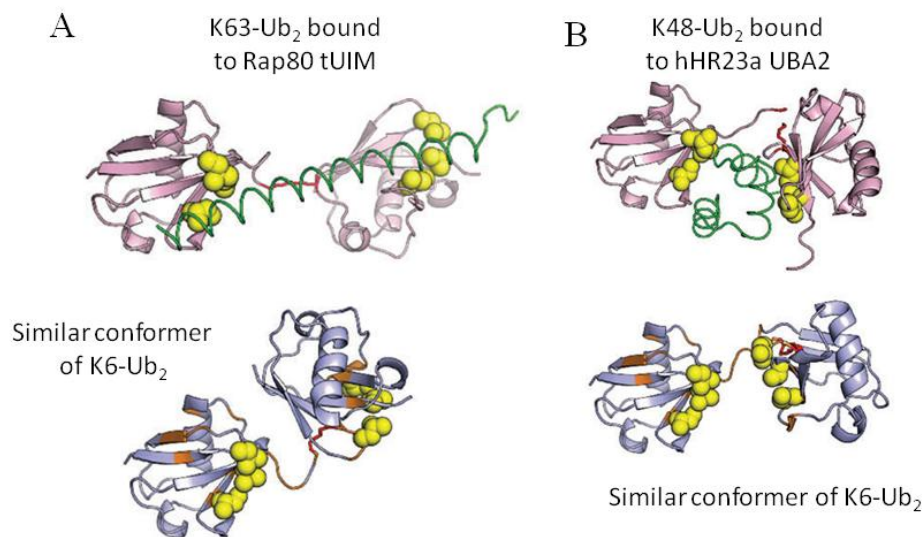


Figure 3-1. K6-Ub₂ has conformers that illustrate its potential to bind to both Rap80 tUIM and hHR23a UBA2. (A) Comparison of K6-Ub₂ conformer with the K63-Ub₂ structures from PDB IDs 2JF5 (top) and 3A1Q (bottom). (B) Comparison of the UBA2-bound structure of K48-Ub₂ (PDB ID 1ZO6) with structurally similar conformer from K6-Ub₂ ensemble. The bound ligands (UBA2 in A and tandem-UIM of Rap80 tUIM in B) are shown as green ribbon⁴².

3.2 Synthesis of K6-linked chains by enzymatic method

Since the binding studies require large quantities of K6-Ub₂ and Lin *et al.*⁵⁵ showed that NleL, an E3 ubiquitin ligase along with Ubch7 (E2) catalyzes formation of K6- and K48-linked polyubiquitin chains; we decided to design a method that would help us synthesize all-natural K6-Ub₂ using an enzymatic method. Our method is similar to a published method by Hospenthal *et al.*⁵⁶ but unlike their method, ours synthesizes a completely natural chain. They utilize K to R mutations to block chain extension from the Lysine-6 of the distal domain while we use the genetically incorporated unnatural amino acid Lys(Boc) at that position. By utilizing Lys(Boc), which can be easily removed in the end, we obtain a K6-linked diubiquitin that is

completely natural. The method is illustrated in Figure 3-2 and we were able to assemble and purify K6-Ub₂ with individual domains isotopically labeled with ¹⁵N.

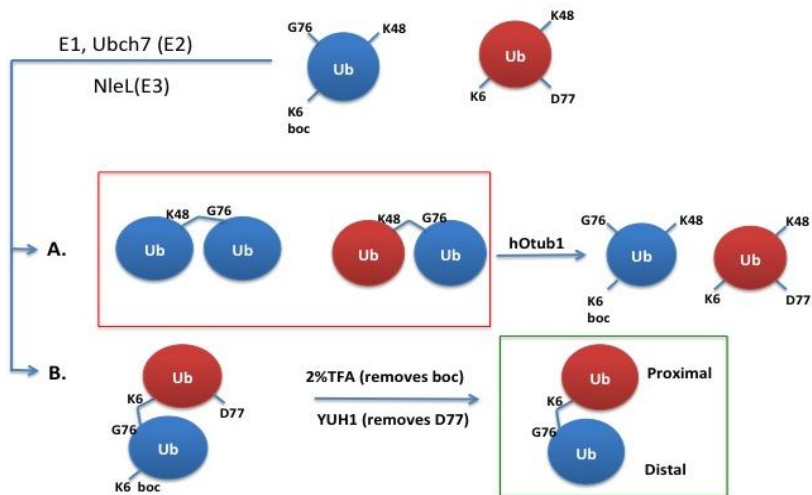


Figure 3-2. Enzymatic method to synthesize all-natural K6-Ub₂. The different shades of the monomers represent selective isotopic labeling.

The ubiquitin unit that is to be the proximal domain has its C-terminus blocked from E1 activation by aspartic acid while the distal ubiquitin has the lysine-6 position blocked by unnatural amino acid Lys(Boc). In the presence of the enzymes E1, Ubch7 (E2) and NleL (E3) along with TCEP, ATP and ATP recycling mix, we obtain K48-linked polyubiquitin chains, K48-Ub₂ with D77 on the proximal domain, K-6, 48 mixed chains and K6-Ub₂ with D77 on the proximal domain. To remove all the K48 chains, we utilize the deubiquinating enzyme specific for K48-linked chains, hOtub1. Since the synthesis of K6 chains is not hampered by the presence of hOtub1, it is added along with the ubiquitinating enzymes in the beginning. To verify that there are no residual K48-linked chains, more hOtub1 was added and incubated for 2 hours, as shown in Figure 3-3.

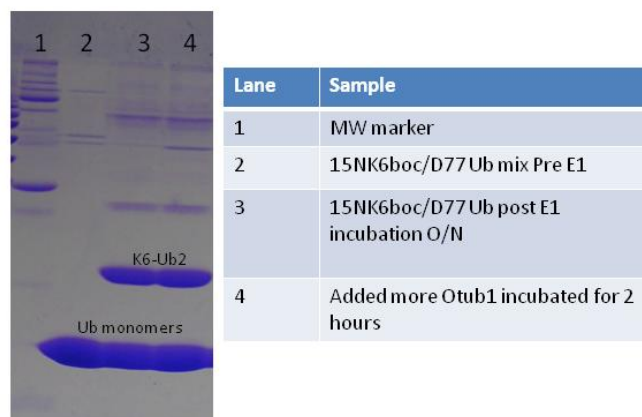


Figure 3-3. Coomassie-stained 15% SDS PAGE gel of the enzymatic reaction of K6-linked Ub₂ ¹⁵N labeled on the distal Ub. Ub: ubiquitin, K6-Ub₂: K6-linked diubiquitin, MW marker- molecular weight marker.

Once K6-Ub₂ with D77 on the proximal ubiquitin unit and Lys(Boc) on the 6th position of the distal Ub was purified, it is treated with 2% TFA to remove the Boc group from lysine-6 and C-terminal hydrolase (YUH1) to cleave D77 from the proximal domain of the C-terminus. At the end of this process, we obtained an all-natural K6-linked diubiquitin with a much better yield than the previously described non-enzymatic method.

3.3 Interaction of K6-Ub₂ with Rap80 tUIM

Rap80 is a 719 amino acid protein. Its domain structure is shown in Figure 3-4(A). It plays a central role in the BRCA1-A complex by specifically binding K63-linked ubiquitinated histones H2A and H2AX at DNA lesions sites, leading to target the BRCA1-BARD1 heterodimer to sites of DNA damage at double-strand breaks (DSBs)^{39,57}. It binds specifically to the K63-linked chains through the two ubiquitin interacting motifs (UIMs). The UIM helices are connected by a random coil linker and together they are called Rap80 tandem UIM (Rap80 tUIM, amino acids 79-124)

(Figure 3-4 (D)). The specificity of Rap80 tUIM binding tightly to K63-linked polyubiquitin chains is through avid binding⁵⁸. Avid binding means that each ubiquitin unit of K63-Ub₂ is bound to a UIM of Rap80 tUIM. Rap80 tUIM binds in a directional manner to K63-Ub₂ such that UIM1 binds the proximal domain and UIM2 binds to the distal domain (Figure 3-4 (E)). Furthermore, Rap80 tUIM forms one continuous helix upon binding to K63-Ub₂, since its linker turns from random coil to a helical structure (Figure 3-4 (E)). It is also known that a DNA damage-induced phosphorylation event occurs at position S101 of Rap80 *in vivo*³⁹. Studies performed *in vitro* by Sims and Cohen show slight impairment of binding affinity to K63-Ub₂⁵⁸.

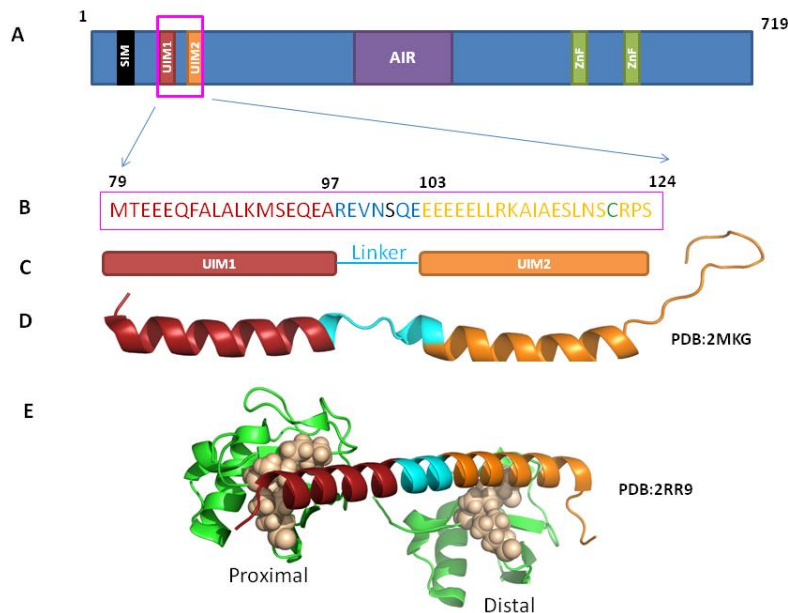


Figure 3-4. Overview of Rap80 tUIM structure. A. Domain representation of Rap80 showing small ubiquitin-like modifier (SUMO) interacting motif (SIM), ubiquitin interacting motifs 1 and 2 (UIM1 and UIM2), Abraxas-interacting region (AIR), and two zinc finger motifs (ZnF). B. Sequence of tUIM. Serine that gets phosphorylated upon DNA damage is colored black, cysteine that is modified by tyrosine for easy quantification in the construct used in binding studies is colored green. C. Domain representation of Rap80 tUIM showing UIM1 and 2 connected by a linker. D. Cartoon representation of Rap80 tUIM structure (PDB: 2MKG). E. Cartoon representation of the structure of Rap80 tUIM bound to K63-Ub₂ (PDB: 2RR9). K63-Ub₂ is shown in green with hydrophobic patch residues shown as spheres. Rap80 tUIM is color coded throughout the figure as follows: UIM1 is dark red, linker is cyan and UIM 2 is orange.

All our binding studies are performed with his-tagged Rap80 tUIM that has its cysteine mutated to tyrosine (C121Y) for easy quantification by Abs₂₈₀. The PRE studies are performed with the wild type Rap80 tUIM since the MTSL is attached at C121.

3.3.1 Binding affinity of Rap80 tUIM to K6-Ub₂

As shown in Figure 3-5, there are different possible modes of binding for K6-Ub₂ with Rap80 tUIM. To help distinguish these, we set out to determine the residues involved in the binding, binding affinity, stoichiometry and the directionality of the interaction.

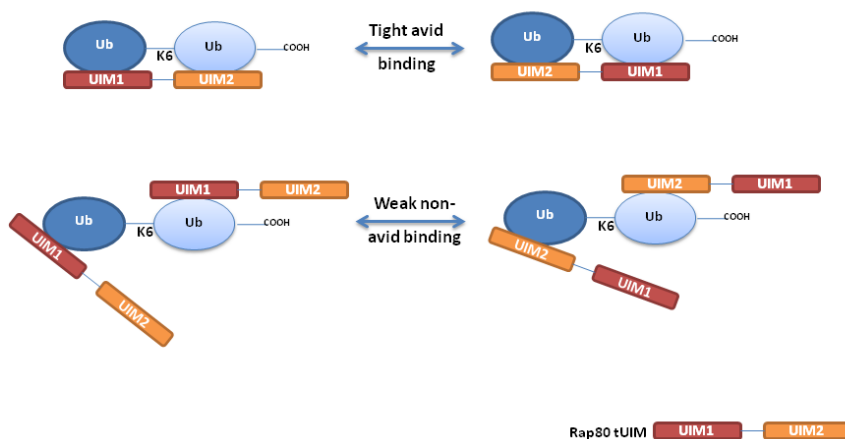


Figure 3-5. Possible modes of Rap80 tUIM binding to K6-Ub₂. Avid binding mode (top) means each ubiquitin unit of K6-Ub₂ is bound to a UIM of Rap80 tUIM that leads to tighter binding than monoubiquitin. While non-avid binding mode means only one UIM of the tUIM is involved in the binding to K6-Ub₂ and the binding is similar to monoubiquitin (below).

By titrating unlabeled Rap80 tUIM into K6-Ub₂ ¹⁵N labeled on the proximal or distal Ub, we were able to deduce the K6-Ub₂ residues involved in the binding on

each domain of K6-Ub₂. Chemical Shift Perturbations (CSPs) at saturation were plotted for both domains to visualize the areas affected by binding (Figure 3-6).

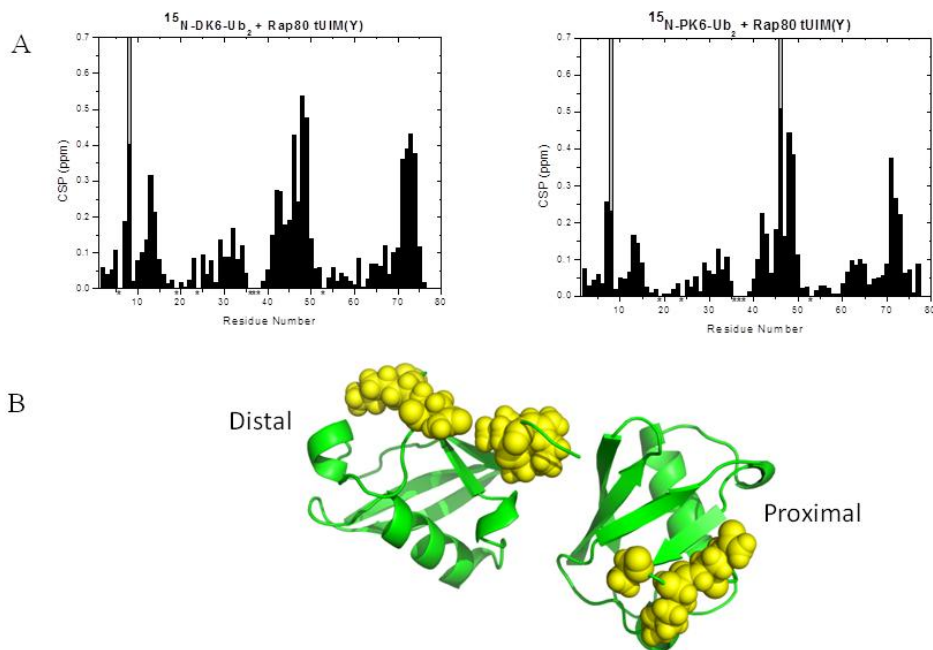


Figure 3-6. Interaction of K6-Ub₂ with Rap80 tUIM A. CSP plot of K6-Ub₂, ¹⁵N labeled on the proximal domain upon addition of his-tagged Rap80 tUIM (Y) at saturation (left) and distal domain upon addition of his-tagged Rap80 tUIM (Y) at saturation (right). Grey bars denote signal attenuation. Asterisks denote residues whose signals are not detectable or the signals overlap. B. Residues that showed CSPs from binding of over 0.38 ppm were mapped (yellow spheres) on the conformer of K6-Ub₂ predicted to bind Rap80 tUIM.

We used the in-house program KDFIT⁵⁹ to estimate the binding affinity. The data fit well to single site binding site model. Using the residues that show CSPs above 0.1 ppm, average K_d s of $20.2 \pm 3.8 \mu\text{M}$ (from 9 residues) for the proximal domain and $23.9 \pm 3.6 \mu\text{M}$ (from 8 residues) for the distal domain were determined (Figure 3-7). The average K_d values reported throughout this dissertation were calculated as mean \pm standard deviation of the individual K_d values obtained by fitting the data for residues with the CSP values at the titration endpoint above a selected threshold.

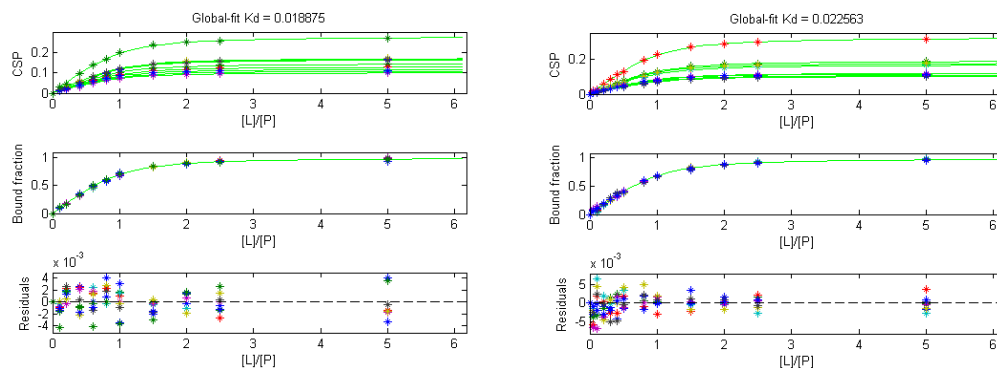


Figure 3-7. Titration fit of K6-Ub₂ labeled on the proximal (left) and distal (right) domain upon addition of his-tagged Rap80 tUIM (Y) using KDFIT global. The curves represent the results of global fit of the titration data for the residues having the titration endpoint CSP above a selected threshold, the resulting global-fit K_d values (in mM) are shown on the top. Top panel shows the global fit of CSPs from individual residues as a function of the ligand/protein molar ratio. Middle panel shows the global fit of the bound fraction of the protein as a function of the ligand/protein molar ratio. Bottom panel indicates the residuals from the fit.

The binding affinity is comparable to the K_d estimated for K63-Ub₂ from Isothermal titration calorimetry (ITC) data (22 μM) as reported by Sims and Cohen⁵⁸. The similarity to K63-Ub₂ that binds avidly to Rap80 tUIM makes the case stronger for avid binding happening in the interaction of K6-Ub₂ with Rap80 tUIM. As a control of non-avid binding, we also performed a titration where Rap80 tUIM was added into ¹⁵N labeled monoubiquitin. The CSPs were plotted at saturation and predictably show the involvement of the traditional hydrophobic surface. There are no attenuations seen unlike with K6-Ub₂ but significant CSPs are present in the similar region as K6-Ub₂. We used KDFIT to estimate the binding affinity. The expected stoichiometry is that Rap80 tUIM has two ubiquitin binding motifs, which means each ubiquitin unit of K6-Ub₂ can bind a UIM of the Rap80 tUIM (Figure 3-8(C)). That increases the effective ligand concentration by 2, so we multiplied the ligand concentration by 2 and fit the data to single site binding model. Using 8 residues that show CSPs above 0.15 ppm, we estimated an average K_d of 189.8 ± 16.1 μM (Figure 3-8(B)).

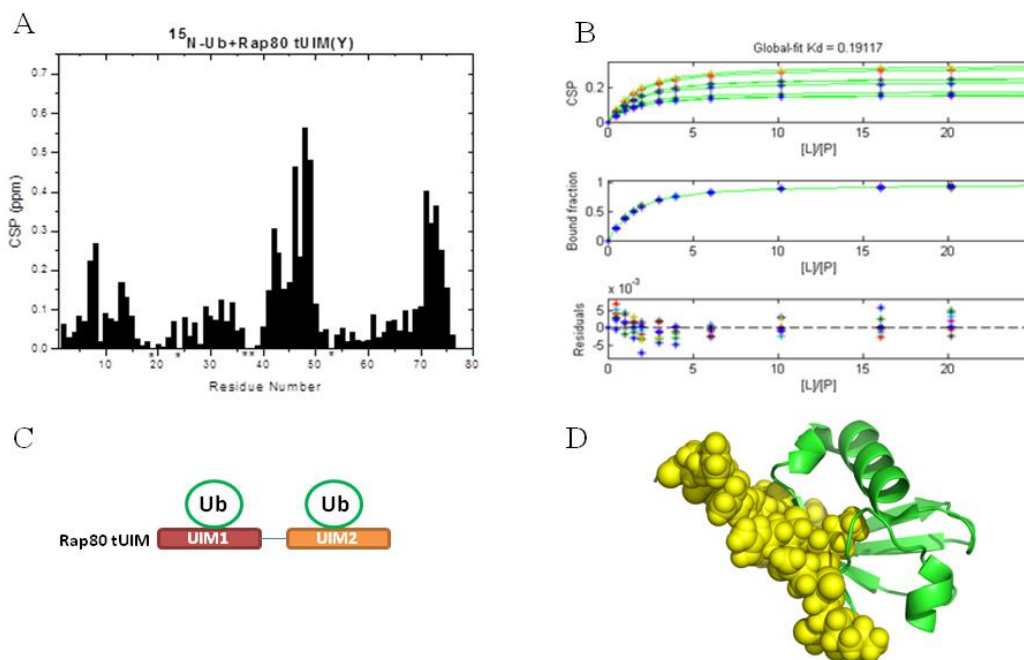


Figure 3-8. A. CSP plot of ^{15}N labeled ubiquitin upon addition of his-tagged Rap80 tUIM (Y) at saturation. Asterisks denote residues whose signals are not detectable or the signals overlap. B. Titration fit of ^{15}N labeled ubiquitin upon addition of his-tagged Rap80 tUIM (Y) using KDFIT global (top right). The curves represent the results of global fit of the titration data for the residues having the titration endpoint CSP above a selected threshold, the resulting global-fit Kd values (in mM) are shown on the top. Top panel shows the global fit of CSPs from individual residues as a function of the ligand/protein molar ratio. Middle panel shows the global fit of the bound fraction of the protein as a function of the ligand/protein molar ratio. Bottom panel indicates the residuals from the fit. C. Expected stoichiometry of the binding showing 2 ubiquitin moieties binding to each Rap80 tUIM. D. Residues that showed CSPs from binding of over 0.2 ppm were mapped (yellow spheres) on ubiquitin structure (PDB: 1D3Z)

To further confirm the avidity, we deleted UIM2 from the construct by putting a stop codon after the linker. We also added a tyrosine before the stop codon to aid with estimating the concentration of the protein as was done with the original construct. We titrated in Rap80 UIM1 into K6-Ub₂ labeled on the proximal domain. The CSPs at saturation were plotted against residue number and upon comparing them with titration using Rap80 tUIM (Figure 3-9), we determined that similar residues in the proximal domain of K6-Ub₂ are involved but the CSPs are smaller. Signal attenuations of similar signals are also observed.

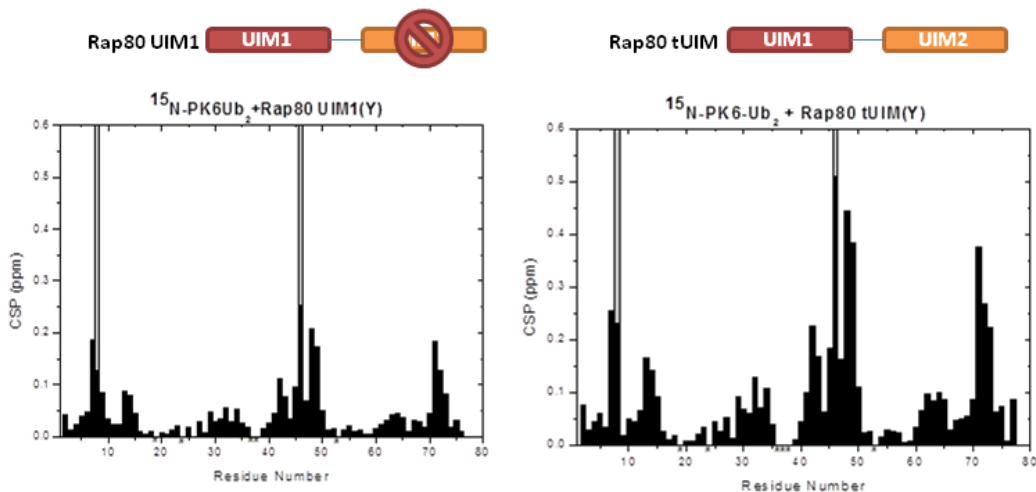


Figure 3-9. Comparison of CSP plots of K6-Ub₂, ¹⁵N labeled on the proximal domain upon addition of his-tagged Rap80 UIM1 (Y) at saturation (left) and upon addition of his-tagged Rap80 tUIM (Y) at saturation (right). Grey bars denote signal attenuation. Asterisks denote residues whose signals are not detectable or the signals overlap. Cartoons on top indicate the difference in the two Rap80 constructs.

Since K6-Ub₂ has two units that can bind to two Rap80 UIM1s, the data was fit to model with two binding sites on diubiquitin. The average K_d using 6 residues was estimated to be 207 ± 5 μM from the fit (Figure 3-10), which is similar to the non-avid binding of monoubiquitin to Rap80 tUIM. These non-avid binding controls give us more confidence that the K6-Ub₂ binding to Rap80 tUIM might be avid in nature.

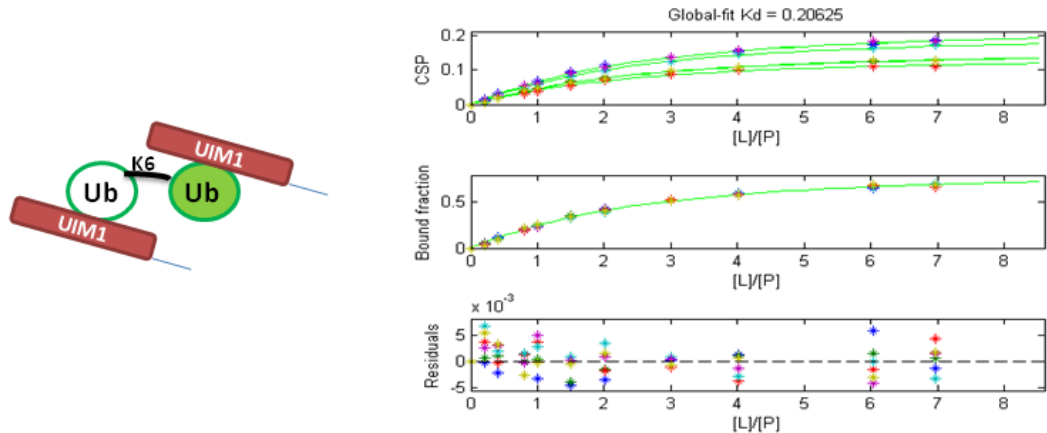


Figure 3-10. Expected stoichiometry of the binding showing 2 UIM1 binding to each domain of K6-Ub₂ (Left). Titration fit of K6-Ub₂ labeled on the proximal domain upon addition of his-tagged Rap80 UIM1 (Y) using KDFIT global (Right). The curves represent the results of global fit of the titration data for the residues having the titration endpoint CSP above a selected threshold, the resulting global-fit K_d values (in mM) are shown on the top. Top panel shows the global fit of CSPs from individual residues as a function of the ligand/protein molar ratio. Middle panel shows the global fit of the bound fraction of the protein as a function of the ligand/protein molar ratio. Bottom panel indicates the residuals from the fit.

To determine the residues on Rap80 tUIM involved in the binding, we titrated unlabeled K6-Ub₂ into ¹⁵N labeled Rap80 tUIM. The construct we used consists of 66 amino acids with a molecular weight of 7570 Da. The 3D structure of Rap80 tUIM is known but ¹⁵N-¹H signals were not assigned for Rap80 tUIM construct in the conditions used for the binding. Thus before the titration could be analyzed, we assigned the peaks for ¹⁵N labeled Rap80 tUIM construct. ¹³C, ¹⁵N labeled Rap80 tUIM was purified and we ran triple resonance experiments, namely HNCA, HN(CO)CA, HNC(O), HN(CA)CO along with NOESY and TOCSY on ¹⁵N labeled Rap80 tUIM to aid in assigning the peaks. The assignment was done by me with help from Dr. Urszula Nowicka.

Once we had the assignment, unlabeled K6-Ub₂ was titrated into ¹⁵N labeled Rap80 tUIM. From the CSPs, we determined that residues on both UIMs are involved in the binding (Figure 3-11). Interestingly, the residues in the linker region do not

show attenuation like the residues in the two UIMs. CSPs observed in this region could be from a shift in secondary structure from random coil to alpha helix or they might be involved in binding.

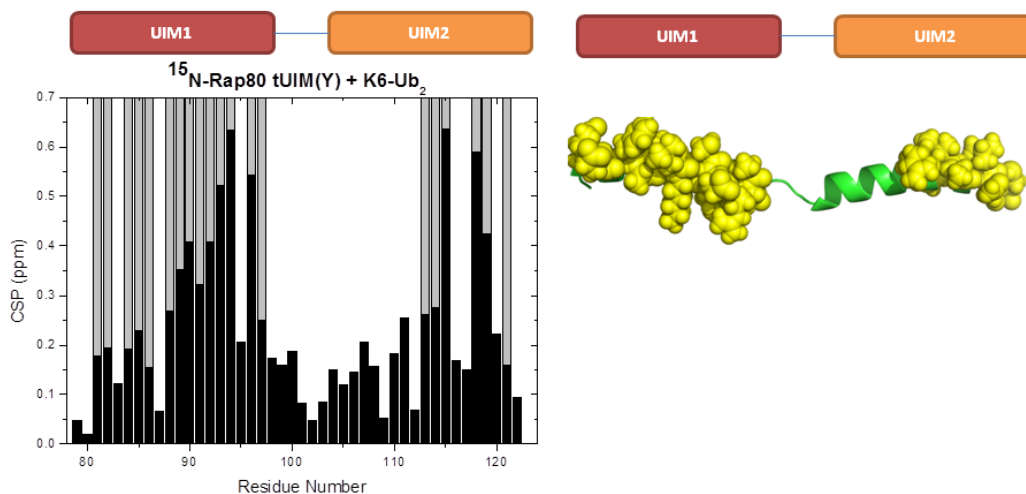


Figure 3-11. A. CSP plot of ^{15}N labeled his-tagged Rap80 tUIM(Y) upon addition of K6-Ub₂ at saturation. Grey bars denote signal attenuation. Cartoon representations show which amino acids are part of UIM1, UIM2 and the linker in between. B. Residues that showed CSPs from binding of over 0.25 ppm and signal attenuation were mapped (yellow spheres) on Rap80 tUIM structure (PDB: 2MKG).

Using the residues with CSPs over 0.15 ppm, we used KDFIT to estimate the average K_d to be $3.7 \pm 3.5 \mu\text{M}$ (6 residues). The residuals show systematic deviations that are substantial (Figure 3-12). Moreover, since we cannot confirm if the CSPs used for fitting the data are directly from binding or due to a structural change, the K_d estimated is unreliable.

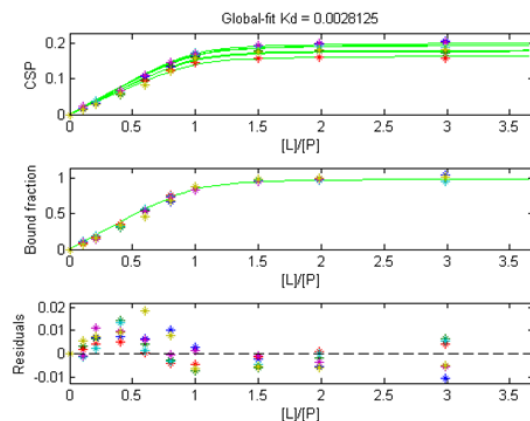


Figure 3-12. Titration fit of ^{15}N labeled his-tagged Rap80 tUIM(Y) upon addition of K6-Ub₂ using KDFIT global. The curves represent the results of global fit of the titration data for the residues having the titration endpoint CSP above a selected threshold, the resulting global-fit K_d values (in mM) are shown on the top. Top panel shows the global fit of CSPs from individual residues as a function of the ligand/protein molar ratio. Middle panel shows the global fit of the bound fraction of the protein as a function of the ligand/protein molar ratio. Bottom panel indicates the residuals from the fit.

Since we could not estimate the K_d from the above titration with confidence, Isothermal Titration Calorimetry measurement was performed and a K_d of 18.92 μM was determined (Figure 3-13). The data fit best to the single site model with n= 0.82, which gives even more credence to our hypothesis of avid binding. The change in enthalpy upon binding, ΔH was estimated to be -8.4 kcal/mol and change in entropy upon binding, ΔS was estimated to be -6.5 cal/mol.K. The ITC data was collected on nano-ITC while the department had it for demo purposes from GE.

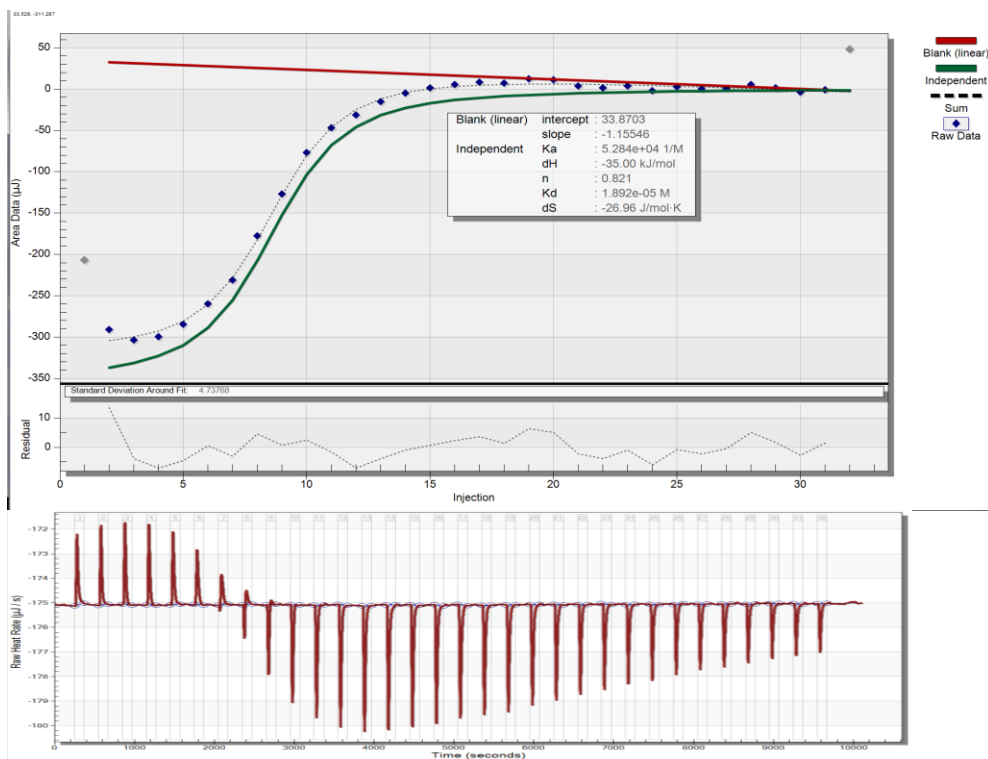


Figure 3-13. ITC titration analysis of K6-Ub₂ binding to Rap80tUIM. Top panel shows the integrated fit data plots, middle panel depicts the residuals of the fit and the raw data traces are shown in the bottom panel.

To have direct proof of avid binding and stoichiometry, small-angle neutrons scattering (SANS) experiments were performed. The data was collected by Dr. Carlos Castañeda, Dr. Jo Anna Capp and Dr. Susan Krueger at NIST and analyzed by Prof. David Fushman and Dr. Susan Krueger. Upon comparing the reduced data for the complex with the predictions, we observed that extrapolated scattering intensity $I(0)$ from experimental data (0.0807) is closer to the predicted $I(0)$ based on 1:1 stoichiometry (0.0794) than based on 2:1 (2 Rap80 tUIMs:1 K6-Ub₂) stoichiometry (~0.1). These results confirm that Rap80 tUIM binds to K6-Ub₂ with 1:1 stoichiometry.

3.3.2 Directionality of binding

Sekiyama *et al.* have shown that there is directionality in Rap80 tUIM binding to K63-Ub₂, where UIM1 of Rap80 tUIM binds the distal domain of K63-Ub₂ and the UIM2 binds the proximal domain. While Zhang N *et al.* have observed that S5a tUIM binds K48-linked diubiquitin in either direction⁵⁸. To determine if there is a specific direction in which Rap80 tUIM binds K6-Ub₂, a nitroxide spin-label, MTSL (methyl methanesulfonylthioate) was attached to C121 position on Rap80 tUIM, which is present after UIM2. As shown in Figure 3-14, if each UIM prefers a specific ubiquitin unit, we expect a more pronounced paramagnetic relaxation enhancement (PRE) effect on one of the units compared to the other. We should also be able to fit the PRE data using our in-house program SLFIT and coordinates from the PDB of the crystal structure to a single position of MTSL.

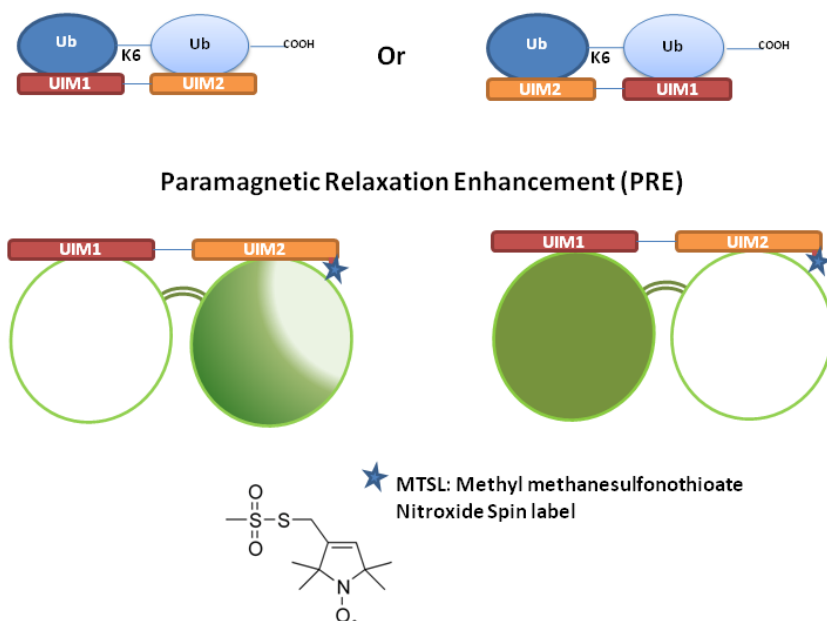


Figure 3-14. Determined directionality of Rap80 tUIM binding to K6-Ub₂. Paramagnetic Relaxation Enhancement (PRE) measurements were used. Blue star denotes nitroxide spin-label MTSL, effective distance range of 25 Å for PRE effect of MTSL. Circle denotes ubiquitin unit and bars labeled UIM denote Rap80 tUIM.

Figure 3-15 clearly shows that PRE effect is observed on both domains. The data fit reasonably well using the coordinates from the RDC optimized PDB structure of monoubiquitin (1D3Z), as shown in Figure 3-15, but we were unable to get a good fit for the data using the PDB coordinates from K6-Ub₂ crystal structure 2XK5. From the data, Rap80 tUIM seems to bind K6-linked diubiquitin in either orientation as illustrated in Figure 3-15.

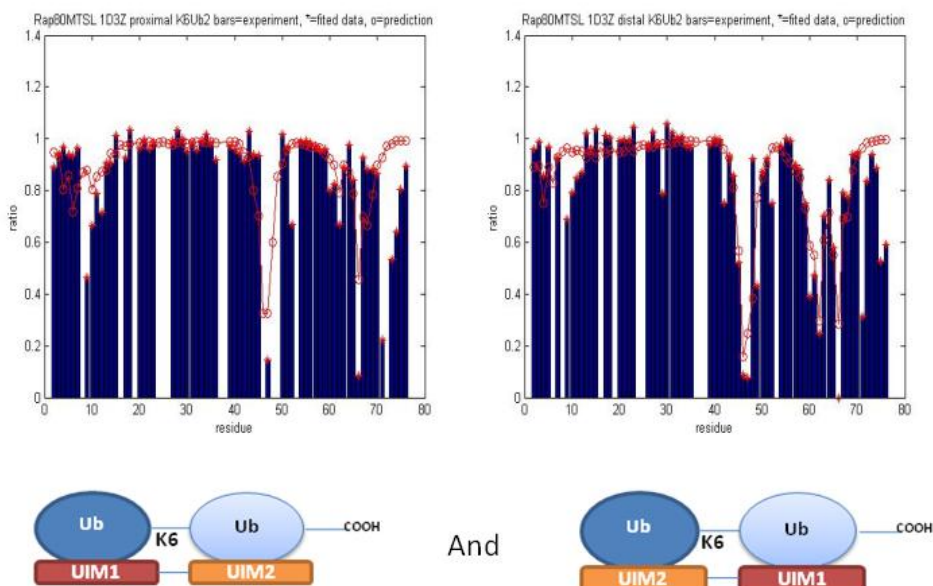


Figure 3-15. PRE effect measured on ¹⁵N labeled K6-Ub₂ on proximal domain (left) and distal domain (right) upon addition of Rap80 tUIM with MTSL attached at position C121. PRE data fitted using the coordinates from the RDC optimized PDB structure of monoubiquitin (1D3Z) Blue bars and red asterisks depict experimental PREs for each ubiquitin; red circles connected by lines are back-calculated PREs from the reconstructed position of the spin label.

To confirm this, we synthesized a mutant K6-linked diubiquitin, in which lysine at the 6th position of the distal domain was mutated to cysteine (K6C). We attached an MTSL at the position K6C on the distal domain. If there is directionality, we would expect to observe PRE effect predominantly on one of the UIMs but we

observed that signals from residues of both UIMs showed attenuation as seen in Figure 3-16. This confirms that Rap80 tUIM binds K6-Ub₂ in both orientations.

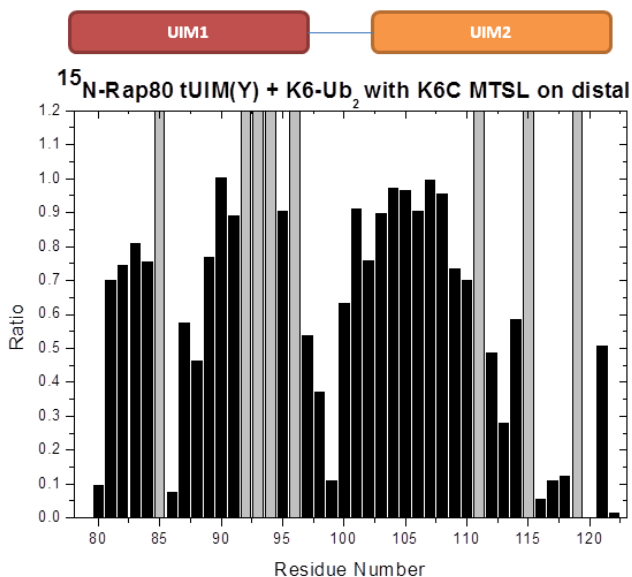


Figure 3-16. PRE effect measured on ¹⁵N labeled Rap80 tUIM upon addition of K6-Ub₂ with MTSL attached on K6C of distal domain. Grey bars denote residues that could not be picked with confidence. The cartoon representation on top indicates which amino acids are part of UIM1, UIM2 and the linker.

3.3.3 Mimicking the effect of Rap80 tUIM Phosphorylation

Rap80 is phosphorylated at position S101 *in vivo*³⁹. Sims and Cohen⁵⁸ observed that phosphorylation of this serine slightly impairs the selectivity for K63-Ub₂. We asked the question, does phosphorylation at position S101 affect binding of Rap80 to K6-linked diubiquitin in the same manner? Since we did not have a method to phosphorylate Rap80 at that specific position, we used a previously reported⁵⁸ phosphorylation mimic mutation S101E Rap80 tUIM for the titrations.

We titrated in the unlabeled S101E Rap80 tUIM into K6-Ub₂, ¹⁵N labeled on proximal or distal domain. We were able to deduce the K6-Ub₂ residues involved in the binding on each domain of K6-Ub₂. As shown in Figure 3-17, the CSP plots of

^{15}N labeled distal Ub in K6-Ub₂ with Rap80 tUIM (left) and S101E Rap80 tUIM (right) are almost alike. Thus, similar region on the distal domain of K6-Ub₂ is affected by the binding of the phosphorylation mimic as with the wild type Rap80 tUIM.

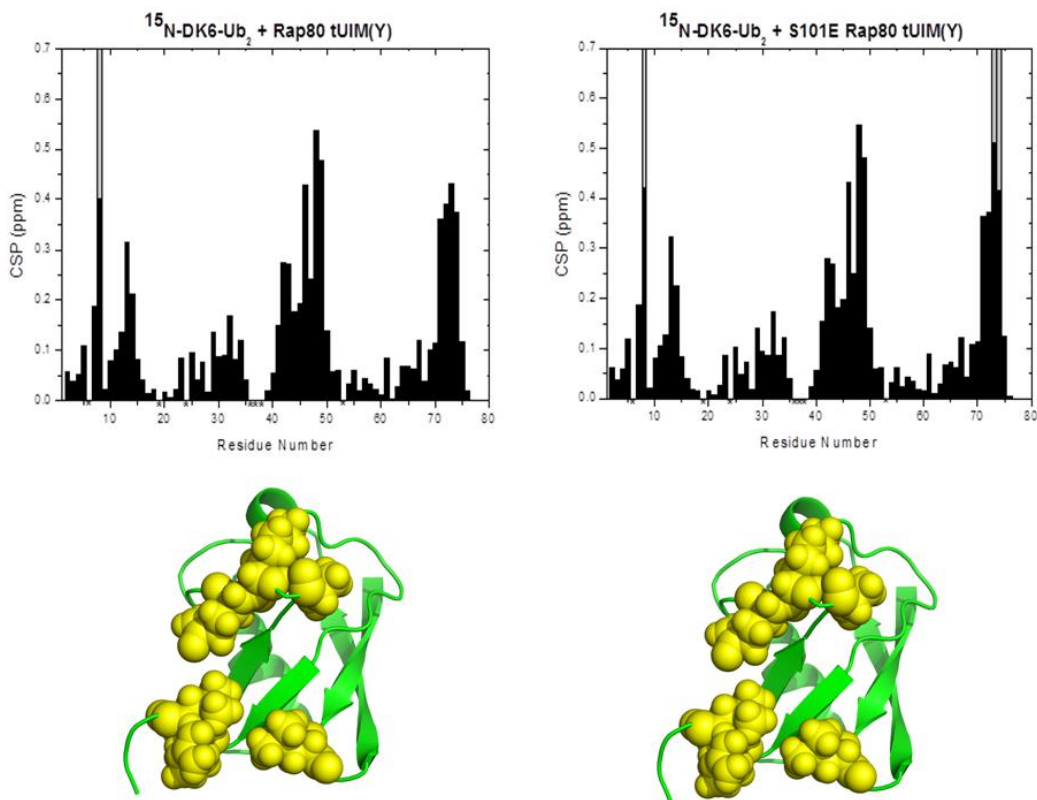


Figure 3-17. Comparison of CSP plots of K6-Ub₂, ^{15}N labeled on the distal domain upon addition of his-tagged Rap80 tUIM (Y) at saturation (left) and upon addition of his-tagged S101E Rap80 tUIM (Y) at saturation (right). Grey bars denote signal attenuation. Asterisks denote residues whose signals are not detectable or the signals overlap. Residues that showed CSPs from binding to Rap80 tUIM (bottom left) and S101E Rap80 tUIM (bottom right) of over 0.38 ppm were mapped (yellow spheres) on the distal domain of conformer of K6-Ub₂ predicted to bind Rap80 tUIM.

The CSP plots of ^{15}N labeled proximal Ub in K6-Ub₂ with Rap80 tUIM (Figure 3-18, left) and S101E Rap80 tUIM (Figure 3-18, right) are also similar. Thus, like distal domain, proximal domain of K6-Ub₂ is also affected by the binding of the phosphorylation mimic in a similar manner as by binding of wild type Rap80 tUIM.

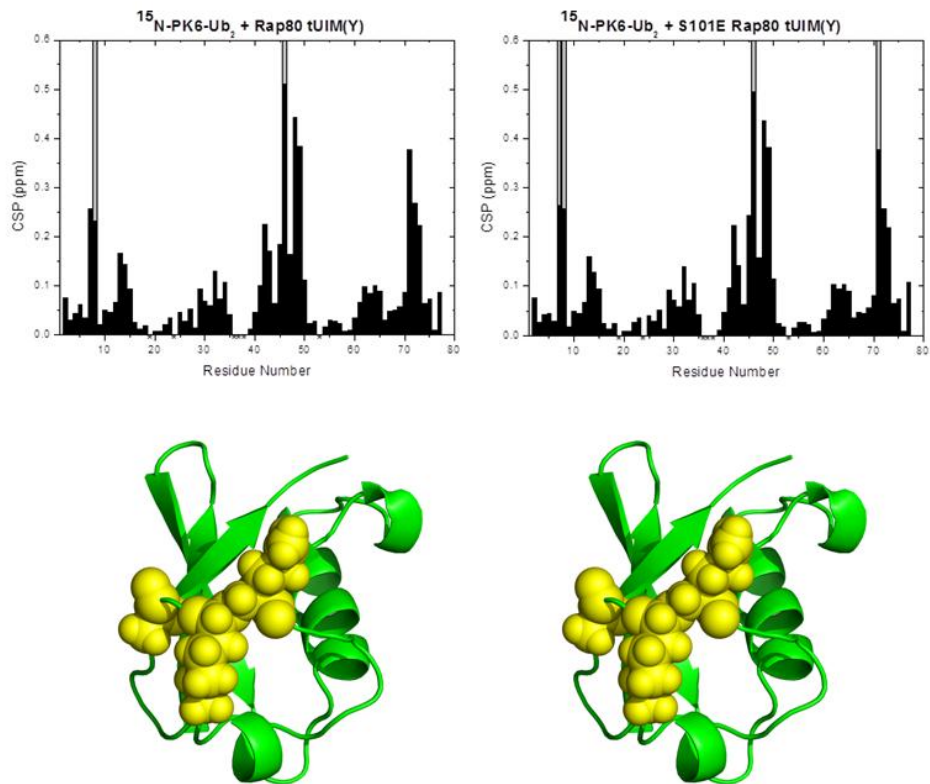


Figure 3-18. Comparison of CSP plots of K6-Ub₂, ¹⁵N labeled on the proximal domain upon addition of his-tagged Rap80 tUIM (Y) at saturation (top left) and upon addition of his-tagged S101E Rap80 tUIM (Y) at saturation (top right). Grey bars denote signal attenuation. Asterisks denote residues whose signals are not detectable or the signals overlap. Residues that showed CSPs from binding to Rap80 tUIM(Y) (bottom left) and S101E Rap80 tUIM(Y) (bottom right) of over 0.38 ppm were mapped (yellow spheres) on the proximal domain of conformer of K6-Ub₂ predicted to bind Rap80 tUIM.

We used residues from both domains with CSPs over 0.15 ppm to estimate K_d using KDFIT. The data fit best to the 1:1 binding model. Since the residuals showed significant systematic deviations, we wanted to confirm if these deviations are because of error in estimating the concentration. We determined that multiplying the ligands in both cases by 1.15 reduced the systematic deviation of the residuals. The average K_d of the interaction for proximal domain is $7.8 \pm 1.4 \mu\text{M}$ (from 4 residues) and for distal domain, it is $9.5 \pm 1.3 \mu\text{M}$ (from 8 residues) (Figure 3-19).

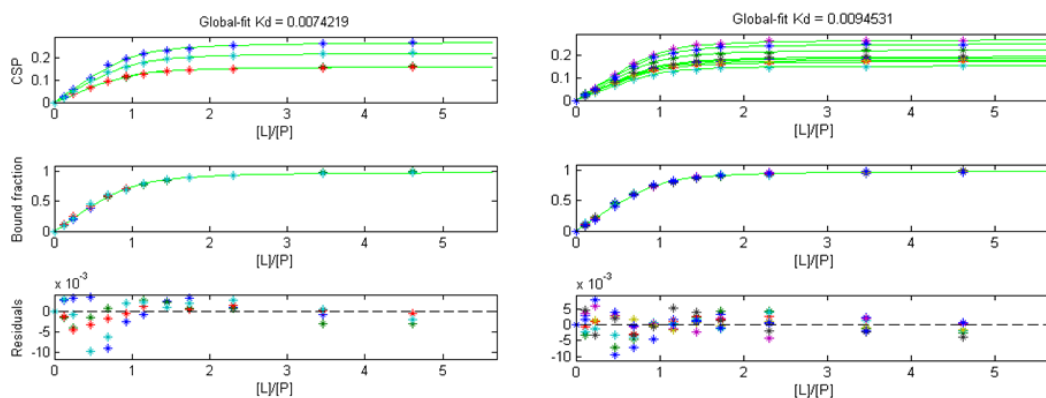


Figure 3-19. Titration fit of K6-Ub₂ labeled on the proximal (left) and distal (right) domain upon addition of his tagged S101E Rap80 tUIM (Y) using KDFIT global. The curves represent the results of global fit of the titration data for the residues having the titration endpoint CSP above a selected threshold, the resulting global-fit K_d values (in mM) are shown on the top. Top panel shows the global fit of CSPs from individual residues as a function of the ligand/protein molar ratio. Middle panel shows the global fit of the bound fraction of the protein as a function of the ligand/protein molar ratio. Bottom panel indicates the residuals from the fit.

Compared to the K_ds observed looking at the proximal and distal domains of K6-Ub₂ when Rap80 tUIM was titrated in, the binding affinity of both domains to S101E Rap80 tUIM seems to be a bit tighter. We cannot say how relevant this slight difference is but since it was reported by Sims and Cohen⁵⁸ that with this construct, K63-Ub₂ binding is slightly impaired, it leads us to speculate that phosphorylation of Rap80 tUIM at position S101 might be a way for the cell to choose K6-Ub₂ over K63-Ub₂ to bind to Rap80 tUIM.

3.3.4 Salt effect

In order to determine if the K6 Ub₂: Rap80 tUIM interaction is preserved in physiological conditions and to understand the role of electrostatic interactions in binding to K6-Ub₂, we performed titrations in Phosphate-buffered saline (PBS) with 150 mM NaCl at pH 7.4, which are more physiologically relevant conditions compared to 20 mM sodium phosphate buffer with no salt. CSPs observed in the

absence of NaCl indicate that the glutamates of Rap80 UIM1 are affected upon binding to K6-Ub₂. Furthermore, the solution structure of the Rap80:K63 Ub₂ complex shows involvement of the glutamates from UIM1 (PDB: 2RR9)⁶⁰. Unlabeled Rap80 tUIM was titrated into K6-Ub₂, ¹⁵N labeled on proximal or distal domain. From Figure 3-20, we can see that similar pattern of CSPs is there in the presence or absence of salt for both wild-type Rap80 as well as the phosphorylation mimic Rap80. Thus the shielding effect of salt does not change the residues involved in the interaction.

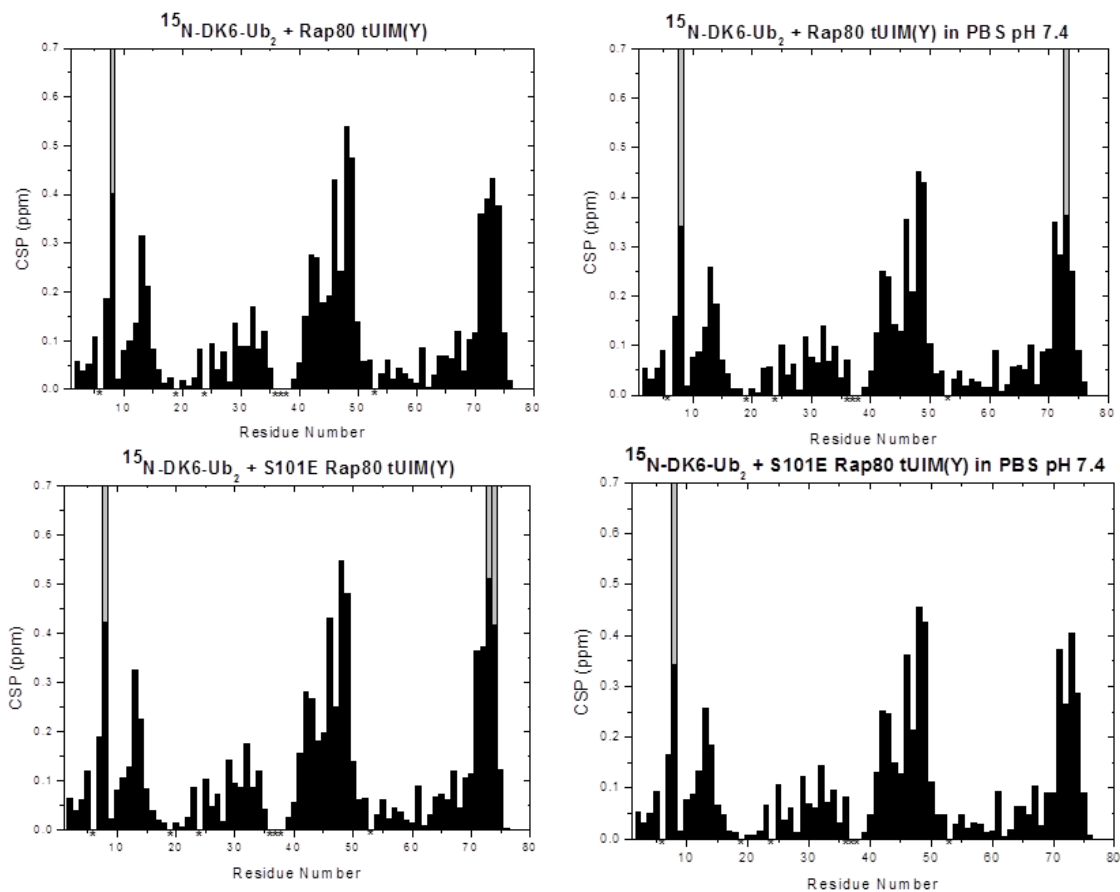


Figure 3-20. CSP plot of K6-Ub₂, ¹⁵N labeled on the distal domain upon addition of his-tagged Rap80 tUIM (Y) at saturation in presence (top left) or absence of salt (top right) and upon addition of his-tagged S101E Rap80 tUIM (Y) at saturation in the presence (bottom left) or absence of salt (bottom right). Grey bars denote signal attenuation. Asterisks denote residues whose signals are not detectable or the signals overlap.

Next, we wanted to know if the binding affinity is different in the presence of salt. For that, we determined K_d using residues that had CSPs higher than 0.15 ppm for distal and 0.12 ppm for proximal domain. The data fit best to 1:1 binding model. The average K_d from 7 residues for proximal domain is $44.9 \pm 5 \mu\text{M}$ and for distal domain, it is $40.5 \pm 5 \mu\text{M}$ (Figure 3-21). We also titrated in phosphorylation mimic mutant S101E into K6-Ub₂ labeled on the distal domain. The K_d was estimated using residues with CSP more than 0.15 ppm and estimated to be $27.1 \pm 2.3 \mu\text{M}$. These results show that electrostatic interactions do play a role in the interaction of Rap80 tUIM with K6-Ub₂, which is not surprising considering the number of glutamates on Rap80 tUIM that are involved in the binding to ubiquitin.

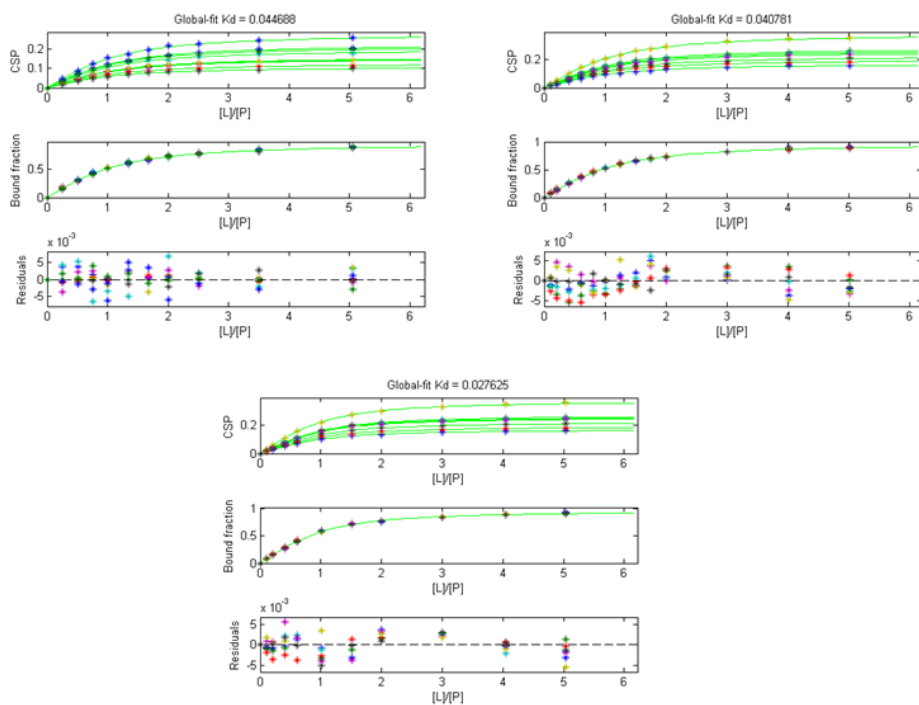


Figure 3-21. Titration fit of K6-Ub₂ labeled on the proximal (top left) upon addition of his-tagged Rap80 tUIM(Y) in PBS pH 7.4 buffer, distal domain upon addition of his-tagged Rap80 tUIM (Y) (top right) and his-tagged S101E Rap80 tUIM (Y) (bottom) in PBS pH 7.4 buffer using the in-house program Kdfit global. The curves represent the results of global fit of the titration data for the residues having the titration endpoint CSP above a selected threshold, the resulting global-fit K_d values (in mM) are shown on the top. Top panel shows the global fit of CSPs from individual residues as a function of the ligand/protein molar ratio. Middle panel shows the global fit of the bound fraction of the protein as a function of the ligand/protein molar ratio. Bottom panel indicates the residuals from the fit.

The K_d s from all the titrations mentioned above are summarized in Table 3-1.

¹⁵ N Labeled (observed)	Ligand	Buffer	Global-fit Kd (uM)	Individual fit Kds (uM) (mean ± std dev)
Ubiquitin	Rap80 tUIM	pH6.8, no NaCl	191	190 ± 16
Proximal Ub in K6-Ub2	Rap80 UIM1	pH6.8, no NaCl	206	207 ± 5
Distal Ub in K6-Ub2	Rap80	pH6.8, no NaCl	22.6	23.9 ± 3.6
Proximal Ub in K6-Ub2	Rap80	pH6.8, no NaCl	18.9	20.2 ± 3.8
Distal Ub in K6-Ub2	S101E Rap80	pH6.8, no NaCl	9.5	9.5 ± 1.3
Proximal Ub in K6-Ub2	S101E Rap80	pH6.8, no NaCl	7.4	7.8 ± 1.4
Distal Ub in K6-Ub2	Rap80	PBS	40.8	40.5 ± 5
Proximal Ub in K6-Ub2	Rap80	PBS	44.7	44.9 ± 5
Distal Ub in K6-Ub2	S101E Rap80	PBS	27.6	27.1 ± 2.3

Using **isothermal titration calorimetry**

Observed Kd of K6Ub2 binding to Rap80 tUIM(Y) in Nap pH 6.8 buffer= **18.92 uM**

Table 3-1. Summary of K_d s from all titrations of K6-Ub₂ and Rap80 tUIM.

From the studies above, we determined that K6-Ub₂ interacts with Rap80 tUIM tightly. It binds Rap80 tUIM in an avid manner that might be similar to K63-linked diubiquitin. Unlike with K63-linked diubiquitin, Rap80 tUIM does not have a specific orientation in which it binds to K6-linked diubiquitin. We demonstrated that phosphorylation mimic mutant S101E Rap80 tUIM binds tighter to K6-Ub₂, which might be used by the cell to differentiate it from K63-Ub₂. Finally, by performing studies in PBS, we showed that K6-Ub₂:Rap80 tUIM interaction is preserved in physiological conditions and that electrostatic interactions play a role in the interaction.

Section 3.4 Interaction of K6-Ub₂ with hHR23a UBA2

hHR23a (human homologue of yeast Rad23) is a member of the UBL-UBA family of shuttle proteins. It contains 363 amino acids and its molecular weight is 39.6 kDa. It is implicated in the modulation of polyUb:proteasome interactions by binding selectively to K48-linked polyubiquitin²⁵. It has two ubiquitin-associated domains that bind ubiquitin, one of which, UBA2 (amino acids 318-358) is known to bind K48-Ub₂ selectively in a “sandwich-mode”. It means that one domain of the diubiquitin binds the side of hHR23a UBA2 that monoubiquitin binds and the other domain binds on the “back-side”, thus making the binding stronger²⁰.

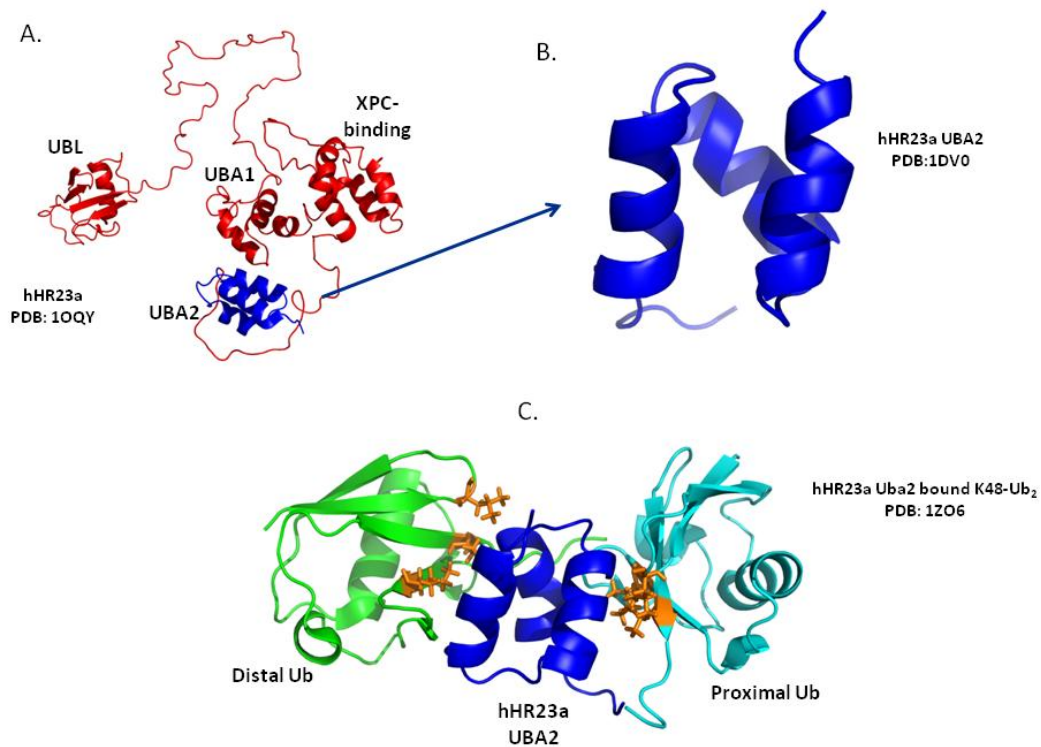


Figure 3-22. Structure and function of hHR23a UBA2. A. Structural cartoon representation of hHR23a showing ubiquitin-like domain (UBL), Ubiquitin-associated domain 1 (UBA1), xeroderma pigmentosum group C protein-binding domain (XPC-binding domain), Ubiquitin-associated domain 2 (PDB: 1OQY). B. Structural cartoon representation of hHR23a UBA2 (PDB: 1DV0). C. Structural cartoon representation of K48-Ub₂ bound to hHR23a UBA2 (PDB: 1ZO6) showing distal domain of K48-Ub₂ (green), proximal domain of K48-Ub₂ (cyan), hHR23a UBA2 (blue) and hydrophobic patch amino acids on both domains (orange sticks).

Castañeda *et al.* demonstrated that hHR23a UBA2 binds with a similar K_d to K27-Ub₂ as it does to K48-Ub₂⁴¹. Structurally, one of the conformers of K6-Ub₂ in solution is similar to hHR23a UBA2 bound K48-linked diubiquitin. It also seems like there is sufficient space between the two domains of this K6-Ub₂ conformer for hHR23a UBA2 to fit between them and bind in a sandwich-mode⁴². Functionally, it has been shown that there is a possibility that they play a role in proteasomal degradation³¹. These findings motivated us to do a detailed study of the interaction between K6-Ub₂ and hHR23a UBA2.

3.4.1 Binding affinity of hHR23a UBA2 to K6-Ub₂

Unlabeled hHR23a UBA2 was titrated into K6-Ub₂ ¹⁵N labeled on the proximal or distal domain. By analyzing the CSP plot, we were able to determine the residues involved in the interaction. Interestingly, the CSPs in the distal domain are different from the proximal domain (Figure 3-23).

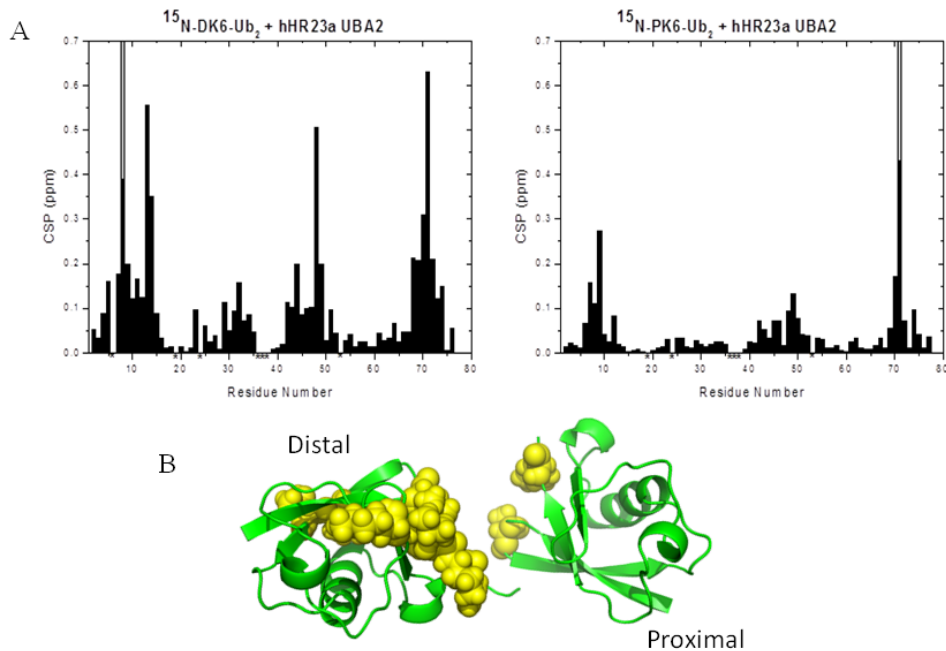


Figure 3-23. Studying the interaction of K6-Ub₂ with hHR23a UBA2, observing K6-Ub₂. A. CSP plot of K6-Ub₂, ¹⁵N labeled on the distal domain upon addition of hHR23a UBA2 at saturation (left) and proximal domain upon addition of hHR23a UBA2 at saturation (right). Grey bars denote signal attenuation. Asterisks denote residues whose signals are not detectable or the signals overlap. B. Residues that showed CSPs from binding of over 0.25 ppm were mapped (yellow spheres) on the conformer of K6-Ub₂ predicted to bind hHR23a UBA2.

When the CSP plots were compared with the ones obtained from the interaction of hHR23a with K48-Ub₂, an interesting pattern was noticed. The proximal domain of K6-Ub₂ shows very similar CSPs as distal domain of K48-Ub₂ when hHR23a UBA2 is added. Correspondingly, distal domain of K6-Ub₂ shows very similar CSPs to proximal domain of K48-Ub₂ when hHR23a UBA2 is added (Figure 3-24). But residues in both domains of K48-Ub₂ show a lot more attenuations upon binding to hHR23a UBA2.

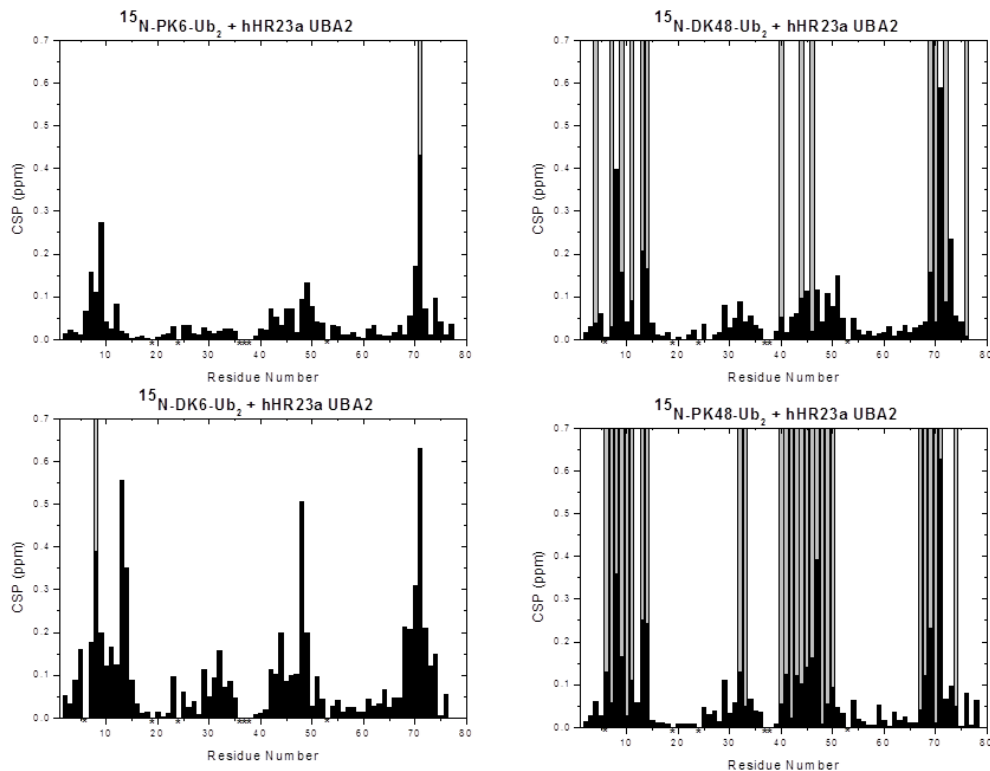


Figure 3-24. CSP plot of K6-Ub₂, ¹⁵N labeled on the proximal domain upon addition of hHR23a UBA2 at saturation (top left) and distal domain upon addition of hHR23a UBA2 at saturation (bottom left) compared with CSP plot of K48-Ub₂, ¹⁵N labeled on the distal domain upon addition of hHR23a UBA2 at saturation (top right) and proximal domain upon addition of hHR23a UBA2 at saturation (bottom right). Grey bars denote signal attenuation. Asterisks denote residues whose signals are not detectable or the signals overlap.

Using KDFIT, dissociation constant of binding between K6-Ub₂ and hHR23a UBA2 was determined. The data looking at either domain fit best with single site binding model. For proximal domain, we determined an average K_d 5.9 ± 2.4 μ M (from 5 residues) and looking at distal domain, we estimated the K_d to be 41.3 ± 2.4 μ M (from 5 residues) (Figure 3-25).

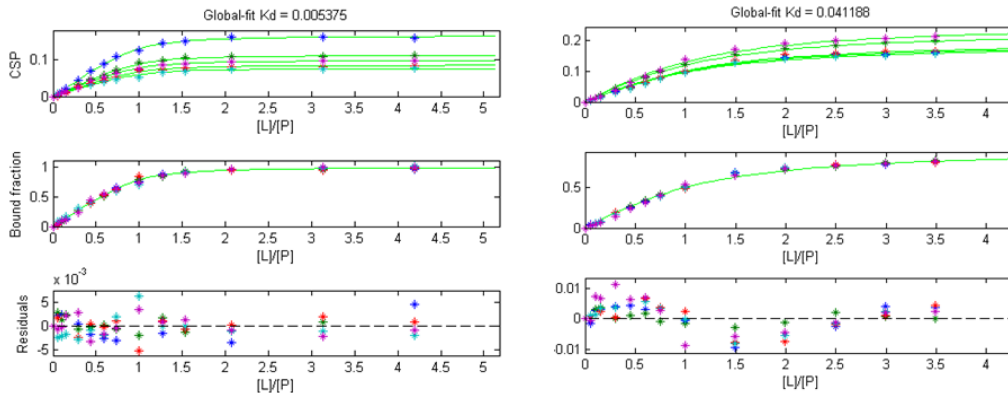


Figure 3-25. Titration fit of K6-Ub₂ labeled on the proximal domain (left) upon addition of hHR23a UBA2 and distal domain upon addition of hHR23a UBA2 using KDFIT global. The curves represent the results of global fit of the titration data for the residues having the titration endpoint CSP above a selected threshold, the resulting global-fit K_d values (in mM) are shown on the top. Top panel shows the global fit of CSPs from individual residues as a function of the ligand/protein molar ratio. Middle panel shows the global fit of the bound fraction of the protein as a function of the ligand/protein molar ratio. Bottom panel indicates the residuals from the fit.

Since there were significant systematic deviations in the residuals of the fit for distal domain, we adjusted the concentration of the ligand to reduce the deviation. Upon multiplying the ligand concentration by 0.75, the deviation of the residuals is reduced and the estimated K_d is $10.6 \pm 1.3 \mu\text{M}$ (Figure 3-26).

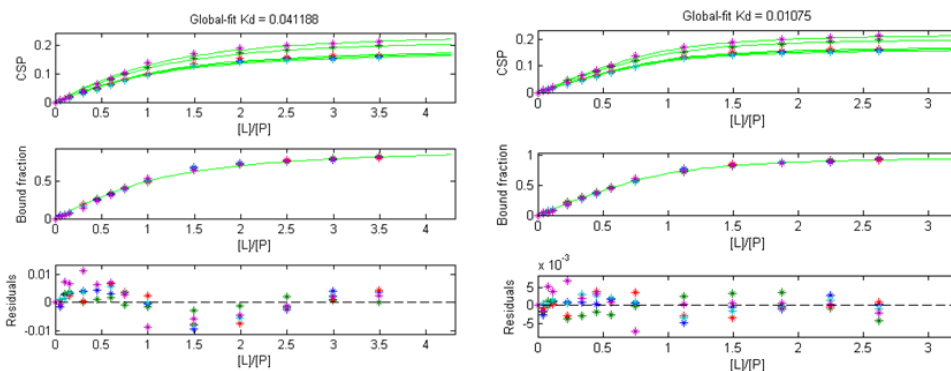


Figure 3-26. Titration fit of K6-Ub₂ labeled on the distal domain upon addition of hHR23a UBA2, original fit (left) and adjusted (multiply ligand by 0.75) fit (right) using KDFIT global. The curves represent the results of global fit of the titration data for the residues having the titration endpoint CSP above a selected threshold, the resulting global-fit K_d values (in mM) are shown on the top. Top panel shows the global fit of CSPs from individual residues as a function of the ligand/protein molar ratio. Middle panel shows the global fit of the bound fraction of the protein as a function of the ligand/protein molar ratio. Bottom panel indicates the residuals from the fit.

To determine which residues on hHR23a UBA2 are involved in the interaction with K6-Ub₂, we titrated unlabeled K6-Ub₂ into labeled ¹⁵N hHR23a

UBA2. There are residues on the “back side” on helix 2 that seem to be affected by interaction with K6-Ub₂ and not with monoUb. This is similar to what was reported by Varadan *et al.*²⁰ for K48-Ub₂ interaction with hHR23a UBA2. Looking at how similar CSPs are for ¹⁵N hHR23a with K6-Ub₂ and with K48-Ub₂ gives more weight to the idea that K6-Ub₂ binds hHR23a UBA2 in sandwich mode similar to K48-Ub₂ (Figure 3-27). The CSPs for hHR23a UBA2 interaction with mono Ub and K48-Ub₂ were calculated by former lab member Dr. Ranjani Varadan and are re-plotted here.

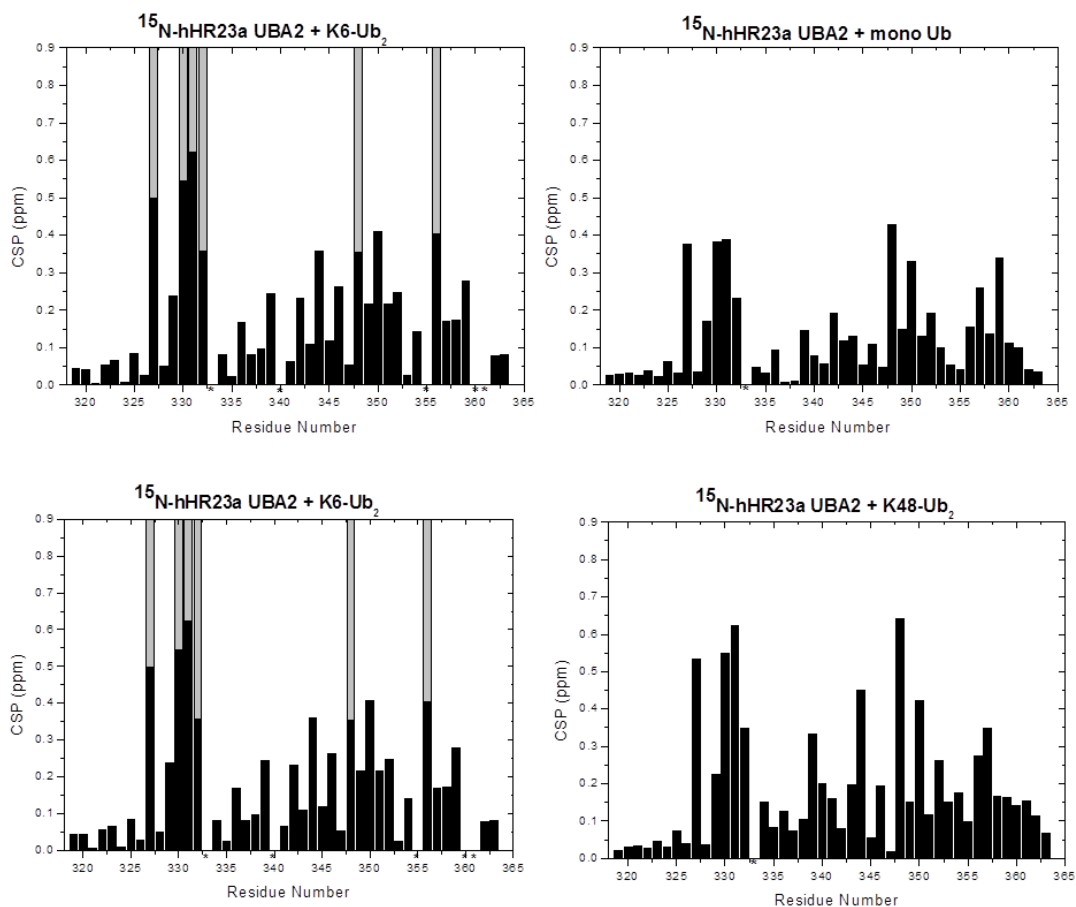


Figure 3-27. CSP plot of ¹⁵N labeled hHR23a UBA2 upon addition of K6-Ub₂ (top left and bottom left) and of mono ubiquitin (top right) and K48-Ub₂ (bottom right) at saturation. Grey bars denote signal attenuation. Asterisks denote residues whose signals are not detectable or the signals overlap.

In order to visualize the interaction on the back-side of UBA2 upon addition of K6-Ub₂, we mapped the residues showing CSPs greater than 0.15 ppm on the surface of UBA2, using the PDB 1DV0. From the Figure 3-28, we observed that residues on the “back-side” of hHR23a UBA2 are involved in the binding to K6-Ub₂ just like they were for K48-Ub₂.

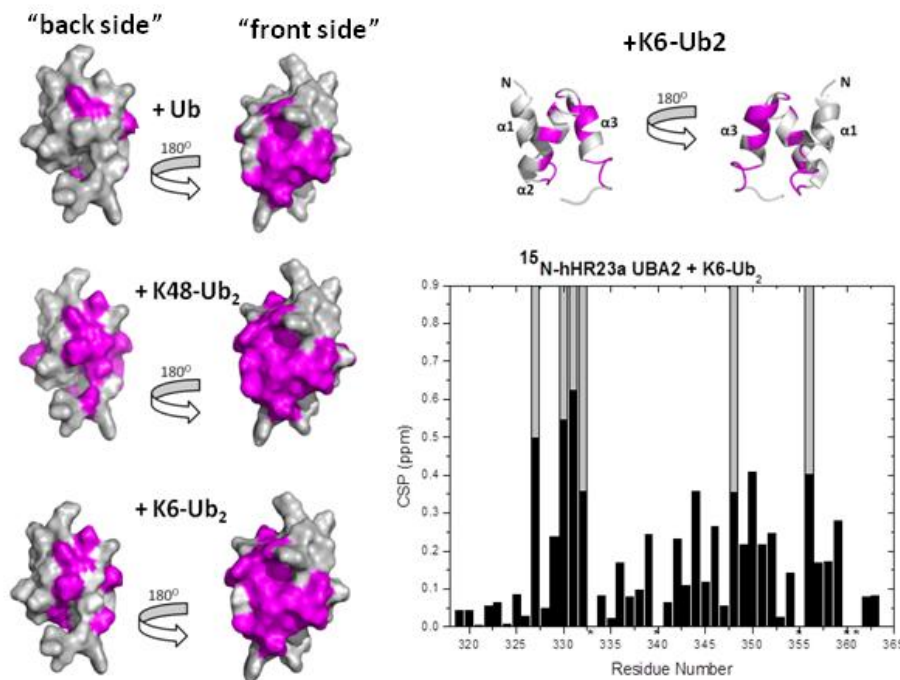


Figure 3-28. CSPs more than 0.15 ppm on ¹⁵N labeled hHR23a UBA2 upon addition of Ub, K48-Ub₂ or K6-Ub₂ mapped on the surface representation of the structure of hHR23a UBA2 (PDB 1DV0) (left). CSPs more than 0.15 ppm on ¹⁵N labeled hHR23a UBA2 upon addition of K6-Ub₂ mapped on the cartoon representation of the structure of hHR23a UBA2 (PDB 1DV0) (top right). CSP plot of ¹⁵N labeled hHR23a UBA2 upon addition of K6-Ub₂ at saturation. Grey bars denote signal attenuation. Asterisks denote residues whose signals are not detectable or the signals overlap.

3.4.2 Directionality of hHR23a UBA2 with K6-Ub₂ interaction

From the above results, we inferred that K6-Ub₂ binds hHR23a UBA2 in a sandwich-like manner similar to K48-Ub₂. It has been shown by Varadan *et al.* that K48-Ub₂ binds in a directional manner to hHR23a UBA2²⁰. The proximal domain binds the “front-side” while distal domain binds the “back-side”. To check if K6-Ub₂

also binds hHR23a UBA2 with the same directionality, we performed some PRE experiments.

In order to perform PRE studies, a mutant K6-linked diubiquitin was synthesized enzymatically and purified, in which lysine at the 6th position of the distal domain is changed to cysteine. We attached an MTSL at this K6C on the distal domain. hHR23a UBA2 was added to bring the ratio of Ub₂:UBA2 to 1:1. HSQC spectra were collected before and after adding the reducing agent (ascorbate). The ratio of intensities of the signals before and after adding ascorbate was plotted against the residue number. The data was fit using the in-house program SLFIT and coordinates from PDB structure 1DV0. As can be seen in Figure 3-29, the fit is generally good except for the backside residues.

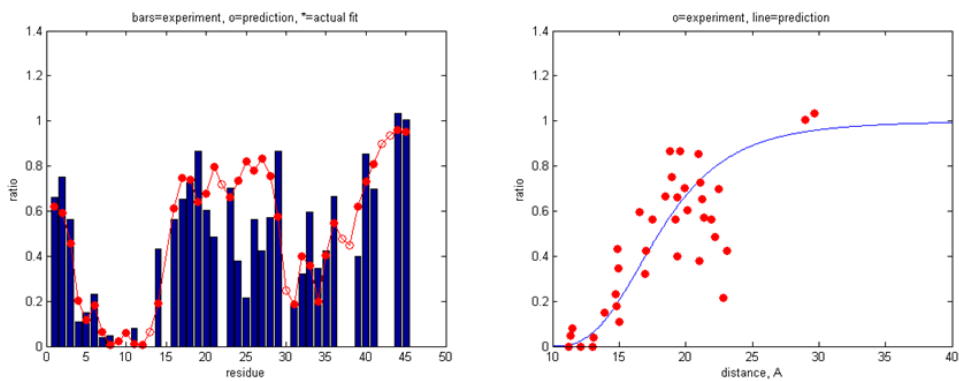


Figure 3-29. PRE effect measured on ¹⁵N labeled hHR23a UBA2 upon addition of K6-Ub₂ with MTSL attached at position Cys6 of the distal domain. Position of the spin label fitted using the coordinates from the PDB structure of hHR23a UBA2 (1DV0). Left panel: Blue bars depict experimental PREs for hHR23a UBA2; red circles connected by lines are back-calculated PREs from the reconstructed position of the spin label. Right panel: Red circles indicate experimental PRE data as a function of the calculated distance of the residues from the spin label's unpaired electron, while the blue curve represents the calculated distance dependence of the PREs

The coordinates for the spin label that were generated from SLFIT were added onto the PDB 1DV0 (Figure 3-30).

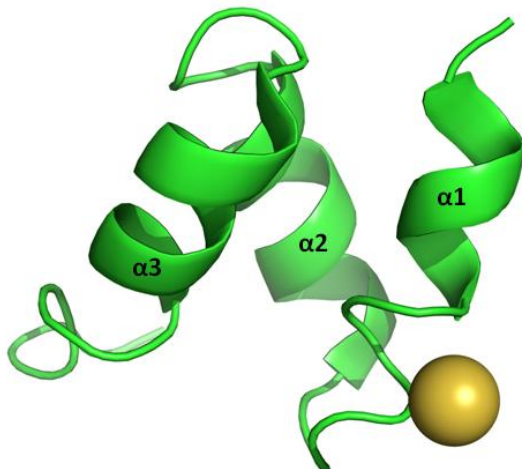


Figure 3-30. Reconstructed position of the spin label on Cys6 of the distal domain of K6-Ub₂ with respect to the hHR23a UBA2 domain generated from SLFIT added onto the PDB structure of hHR23a UBA2 (1DV0). Yellow sphere represents MTSL position estimated from the fit.

To confirm that we have the best fit, the data was also fit assuming 2 spin labels are present using the program SLFIT_2s. The fit got better indicated by the lower χ^2 (χ^2) but one of the coordinates generated from this fit is not spatially possible (Figure 3-31, red sphere), thus it was disregarded. Interestingly, the coordinates of the label that had more weight of the two (Figure 3-31, yellow sphere) and is spatially possible is very similar to the single label coordinate (Figure 3-30).

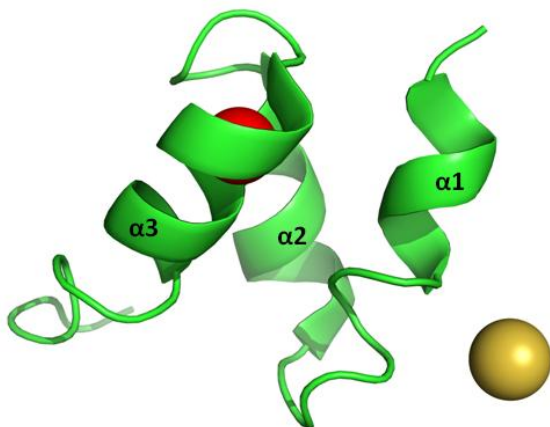


Figure 3-31. Reconstructed position of the spin label on Cys6 of the distal domain of K6-Ub₂ with respect to the hHR23a UBA2 domain generated from SLFIT assuming two positions for the spin label added onto the PDB structure of hHR23a UBA2 (1DV0). Yellow sphere represents MTSL position that has more weight and the red sphere represents MTSL position that has less weight.

Since the more weighted position of spin label with the 2 spin label SLFIT was similar to the position of the spin label from the more poorly fitted single label SLFIT, we wanted to check if the reconstructed position will be significantly different or not after removing the outliers. We removed the residues 24-28 that were the outliers. From figure 3-32 (right), we can see that it improves the fit while keeping a very similar position for the spin label as before. So, most likely the K6 on the distal domain of K6-Ub₂ is positioned in the manner shown in figure 3-30.

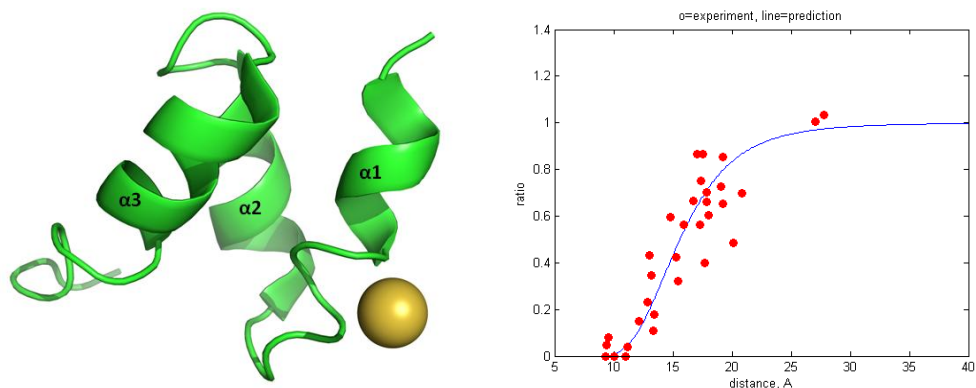


Figure 3-32. Reconstructed position of the spin label on Cys6 of the distal domain of K6-Ub₂ with respect to the hHR23a UBA2 domain after removing residues 24-28 of the UBA2 domain, generated from SLFIT added onto the PDB 1DV0 (left). Yellow sphere represents MTSL position estimated from the fit. Red circles indicate experimental PRE data as a function of the calculated distance of the residues from the spin label's unpaired electron, while the blue curve represents the calculated distance dependence of the PREs (right).

We also attached MTSL to hHR23a UBA2 at the C334 position and performed PRE experiments looking at each of the domains of K6-Ub₂. The ratio of intensities of the signals before and after adding ascorbate was plotted against the residue number. The data from each domain was fit individually using the in-house program SLFIT and coordinates from ubiquitin structure (1D3Z) (Figure 3-33).

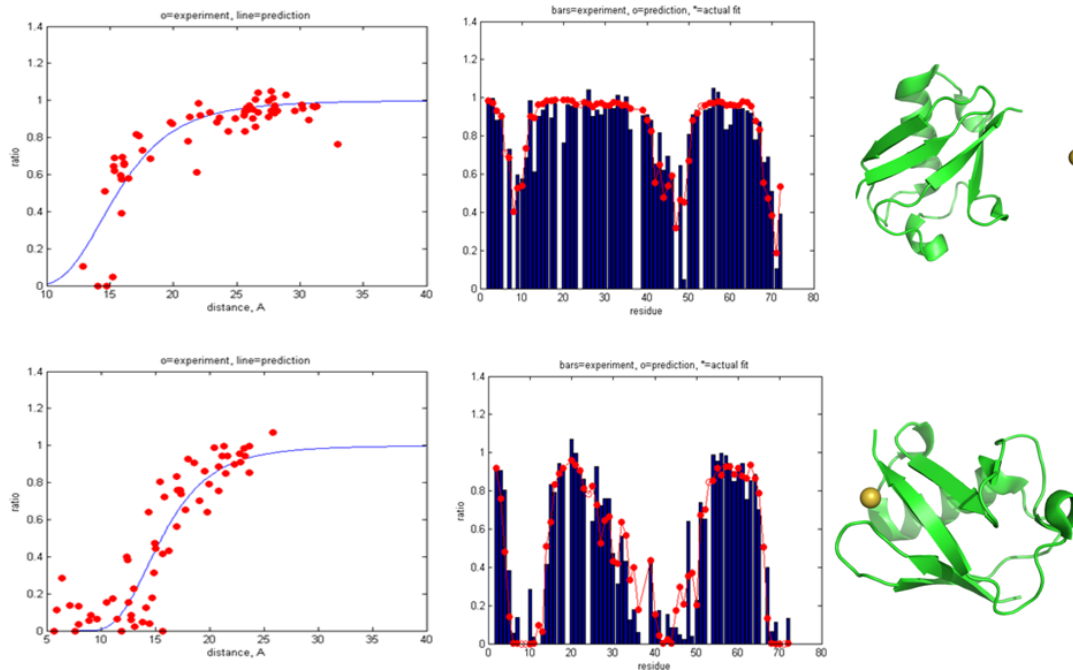


Figure 3-33. PRE effect measured on K6-Ub₂ labeled on distal domain (top) and proximal domain (bottom) upon addition of hHR23a UBA2 with MTSL attached at position C334. Position of the spin label fitted using the coordinates from the PDB structure of ubiquitin (1D3Z). Left: Red circles indicate experimental PRE data as a function of the calculated distance of the residues from the spin label's unpaired electron, while the blue curve represents the calculated distance dependence of the PREs. Middle: Blue bars depict experimental PREs for hHR23a UBA2; red circles connected by lines are back-calculated PREs from the reconstructed position of the spin label. Right: Reconstructed position of the spin label on C334 of hHR23a UBA2 with respect to the distal (top) and proximal (bottom) domain generated from SLFIT and added onto the PDB structure of ubiquitin (1D3Z). Yellow sphere represents MTSL position estimated from the fit.

The fit with individual domains was good but when SLFIT was run using the coordinates from K6-Ub₂ crystal structure, we did not obtain a good fit. Since we know that different conformers of K6-Ub₂ are possibly present in solution, we used the coordinates from SASSIE generated *in silico* ensemble (over 20,000 conformers) that has been superimposed by RDC-optimized PDB 1D3Z⁴². A modified version of SLFIT was used such that the experimental data is fit to coordinates of each conformer. The best fitting conformer based on the lowest χ^2 (χ^2) (conformer number 11921) was chosen. Interestingly, this conformer seems to have enough space

between the two ubiquitin units for hHR23a UBA2 to fit in (Figure 3-34). Also, the canonical hydrophobic patches are facing where hHR23a UBA2 would bind.

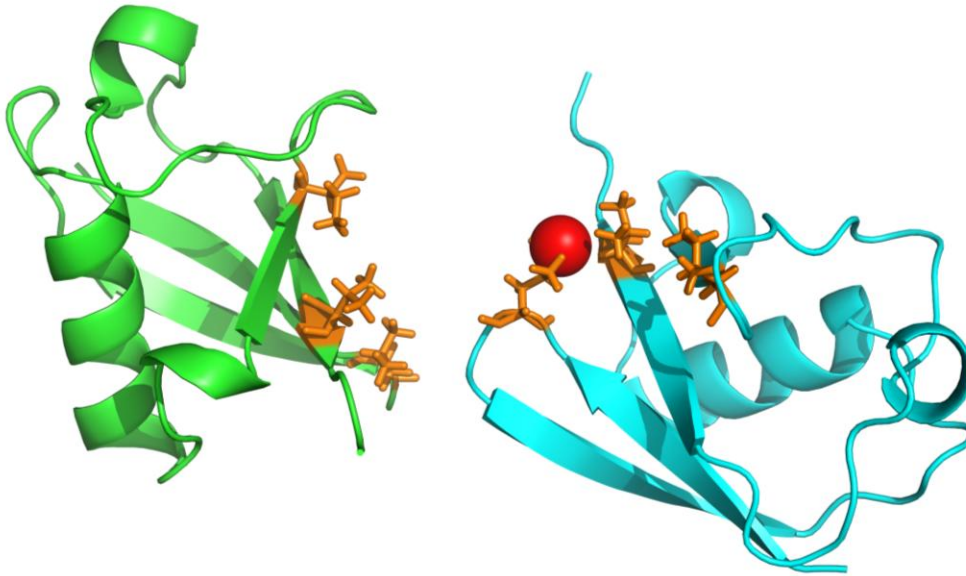


Figure 3-34. Conformer from SASSIE generated ensemble whose coordinates gave the best fit of the PRE data on K6-Ub₂ labeled on distal domain (green) and proximal domain (blue) upon addition of hHR23a UBA2 with MTSL attached at position C334. The PRE data for both domains was fit together. Red sphere represents MTSL position reconstructed from the fit. Orange sticks represent L8, I44 and V70 hydrophobic patch.

Chapter 4: Studying K27-Ub₂

4.1 Introduction

As mentioned before, K27-linked polyubiquitin chains have been shown to exist *in-vivo*³¹ and play a role in non-proteolytic processes. Mitochondrial trafficking protein Miro1 ubiquitinated with K27-linked chains is a marker of mitochondrial damage since it reduces its degradation by the proteasome⁴³. K27-linked chains are also involved in the regulation of innate immunity⁴³⁻⁴⁶. Gatti *et al.* claim that K27-linked polyubiquitin chains are a marker for DNA damage⁴⁷.

As with K6-linked diubiquitin structure, Castañeda *et al.* ran SES analysis against SASSIE generated ensemble and found that two-conformer ensemble give a much better fit between experimental and predicted RDCs and ¹⁵N relaxation data compared to a single conformer⁴¹. The two-conformer ensembles that gave the best fit between experimental and predicted RDCs are shown in Figure 4-1.

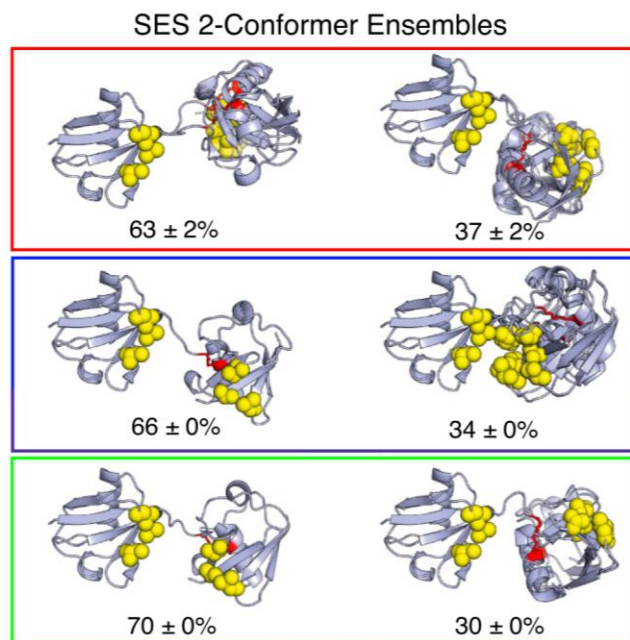


Figure 4-1. Three sets of two-conformer ensembles of K27-Ub₂. Hydrophobic patch residues on each ubiquitin unit is represented by yellow spheres. Numbers below the structure indicate the population weight of each conformer.

Castañeda *et al.* demonstrated that the major conformer of all the sets resembles bound form of K48-Ub₂ to hHR23a UBA2 and that K27-Ub₂ interacts strongly with hHR23a UBA2. Interestingly, the other conformer of a couple of sets (red and green) shows a resemblance to K63-Ub₂ bound Rap80 structure in the way the ubiquitin units are arranged with hydrophobic patches exposed on the same side as shown in Figure 4-2⁴¹.

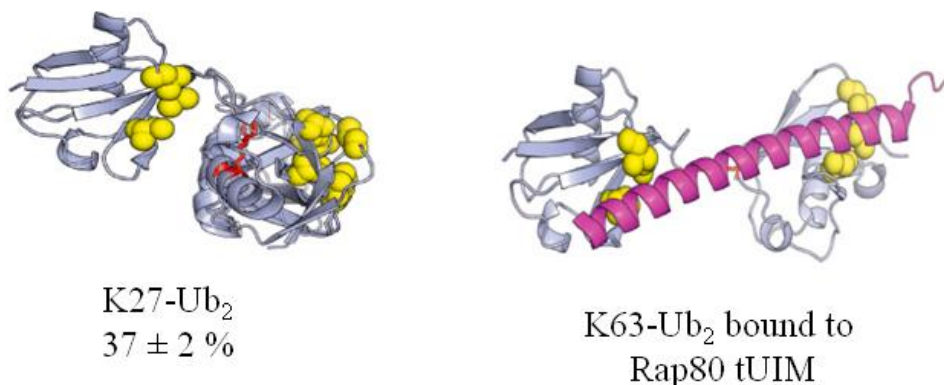


Figure 4-2. Conformer of K27-Ub₂ (left) with similar Ub/Ub orientation as Rap80 tUIM bound K63-Ub₂ (right). Yellow balls represent hydrophobic patch residues. The number below K27-Ub₂ is the percentage population of the conformer in the two-conformer ensemble.

Gatti *et al.* have shown by performing a pull-down assay that K27-Ub₂ interacts with Rap80 tUIM⁴⁷. These interesting structural and functional findings made us look at this interaction in more detail.

4.2 Interaction of K27-Ub₂ with Rap80 tUIM

4.2.1 Binding affinity of K27-Ub₂ to Rap80

The information mentioned above led us to check if K27-Ub₂ binds tightly to Rap80 tUIM and if there is any avidity involved. Unlabelled Rap80 tUIM was titrated into K27-Ub₂, ¹⁵N labeled on the proximal domain and separately into K27-Ub₂ ¹⁵N labeled on the distal domain. CSPs in the proximal domain of K27-Ub₂ are different from what we observed in the distal domain. Although similar residues on both domains of Ub₂ are involved in the binding, the proximal domain shows higher CSPs than the distal domain. This leads us to believe that there might be avid binding involved, since if it was UIM binding to each domain individually, it would provide a similar CSP pattern.

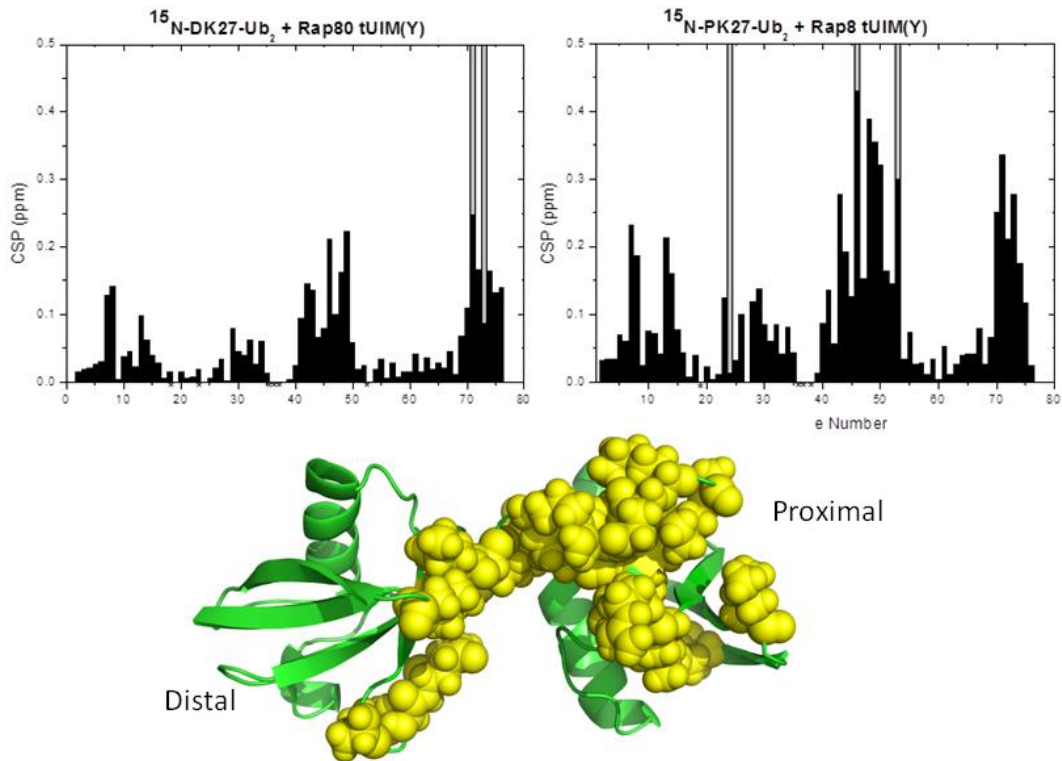


Figure 4-3. CSP plot of K27-Ub₂, ¹⁵N labeled on the distal domain upon addition of his-tagged Rap80 tUIM(Y) at saturation (top left) and proximal domain upon addition of his-tagged Rap80 tUIM(Y) at saturation (top right). Grey bars denote signal attenuation. Asterisks denote residues whose signals are not detectable or the signals overlap. Residues that showed CSPs from binding of over 0.13 ppm were mapped (yellow spheres) on the conformer of K27-Ub₂ predicted to bind Rap80 tUIM.

After analyzing the data using KDFIT, the average K_d of 5 residues for distal domain was estimated to be $18.6 \pm 8.3 \mu\text{M}$ and for proximal domain it was found to be $16.1 \pm 3.7 \mu\text{M}$ (from 7 residues) (Figure 4-4). This is much lower than the K_d for Rap80 tUIM binding to monoUb ($191 \mu\text{M}$) and similar to the K_d for K63-Ub₂ with Rap80 tUIM reported by Sims and Cohen ($22 \mu\text{M}$)⁵⁸, which is known to bind avidly. Thus we can conclude that most likely there is avidity involved in the binding of K27-Ub₂ to Rap80 tUIM.

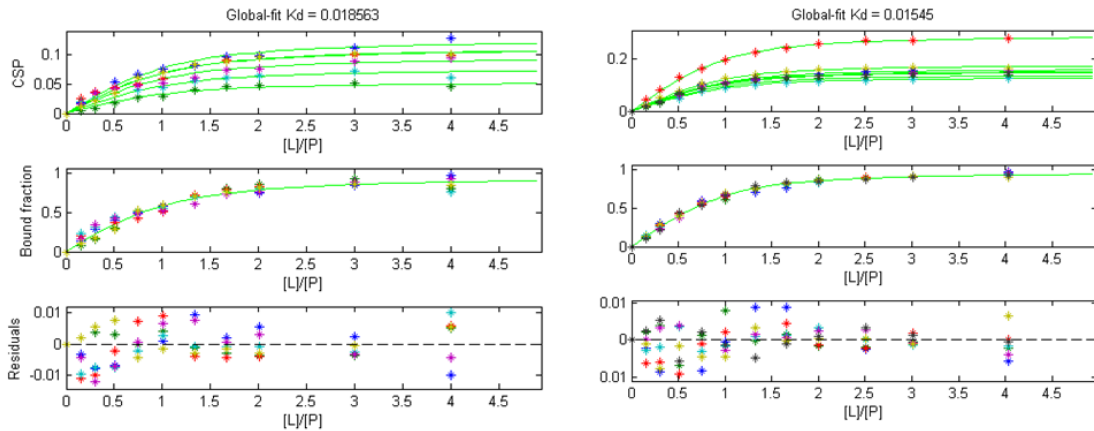


Figure 4-4. Titration fit of K27-Ub₂ labeled on the distal domain (left) and proximal domain (right) upon addition of his-tagged Rap80 UIM1 (Y) using KDFIT global. The curves represent the results of global fit of the titration data for the residues having the titration endpoint CSP above a selected threshold, the resulting global-fit K_d values (in mM) are shown on the top. Top panel shows the global fit of CSPs from individual residues as a function of the ligand/protein molar ratio. Middle panel shows the global fit of the bound fraction of the protein as a function of the ligand/protein molar ratio. Bottom panel indicates the residuals from the fit.

4.2.2 Directionality of binding of K27-Ub₂ to Rap80

The next question we asked was if K27-Ub₂ binds in directional manner to Rap80 tUIM, i.e. does the proximal domain of K27-Ub₂ prefer UIM1 or UIM2? We were able to answer this question by attaching an MTSL to Rap80 C-terminus at position C121 and monitor the PRE effect on both proximal and distal domain of K27 Ub₂. If there is directionality in binding we would see PRE effect on one domain and not the other (Figure 4-5).

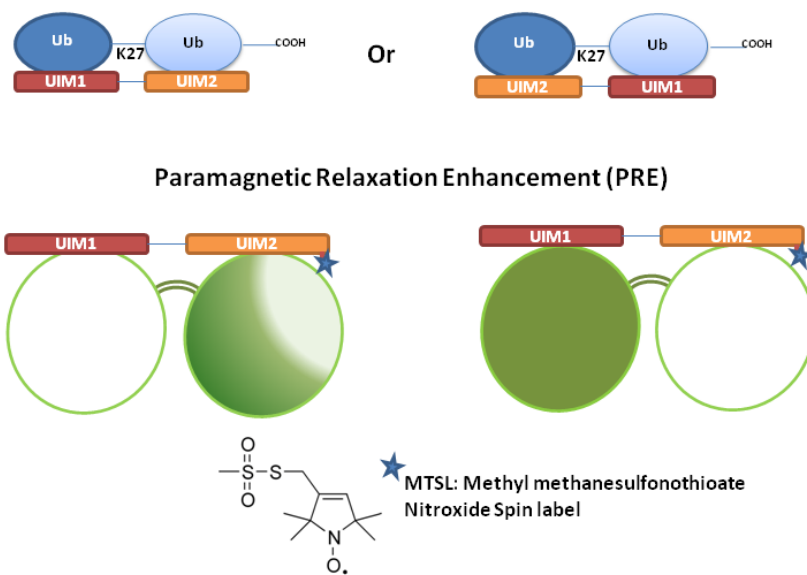


Figure 4-5. Determine directionality of Rap80 tUIM binding to K27-Ub₂ using Paramagnetic Relaxation Enhancement (PRE) measurements. Blue star denotes nitroxide spin-label MTSL, effective distance range of 25 Å for PRE effect of MTSL. Circle denotes ubiquitin unit and bars labeled UIM denote Rap80 tUIM.

Rap80 tUIM with the MTSL attached was added to K27-Ub₂ in a 1:1 molar ratio. HSQC spectra were collected before and after adding reducing agent. The ratio of intensities of the residues before and after adding ascorbate was plotted against the residue number. A clear PRE effect highlights that the pattern is similar between the domains. Thus most likely, there is no directionality in binding of K27-Ub₂ to Rap80 tUIM. Interestingly, upon fitting the PRE data to 1D3Z coordinates, proximal domain gave a lower χ^2 than the distal domain indicating the PRE data of proximal domain fits much better than the PRE data of the distal domain. (Figure 4-6).

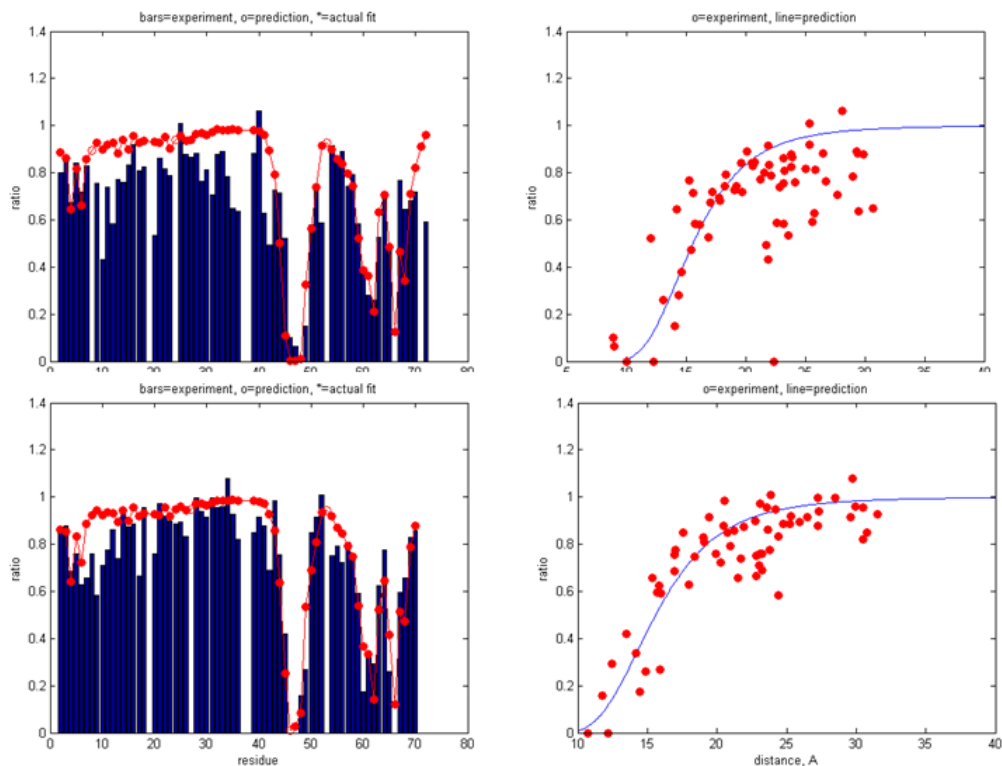


Figure 4-6. PRE effect on K27-Ub₂ labeled on distal domain (top) and proximal domain (bottom) upon addition of his-tagged Rap80 tUIM with MTSL attached at position C121. PRE data fitted using the coordinates from the PDB structure of ubiquitin (PDB:1D3Z). Left: Blue bars depict experimental PREs for each ubiquitin; red circles connected by lines are back-calculated PREs from the reconstructed position of the spin label. Right: Red circles indicate experimental PRE data as a function of the calculated distance of the residues from the spin label's unpaired electron, while the blue curve represents the calculated distance dependence of the PREs.

4.3 DUB inhibition by K27-Ub₂

As mentioned before, former lab member and co-author Emma Dixon showed that K27-Ub₂ is resistant to cleavage by most deubiquitinating enzymes (DUBs)⁴¹. Taking this study forward, we performed experiments to see if this resistance to cleavage by DUBs is due to inability to bind to K27-Ub₂ or some other reason. For that purpose, we ran DUB inhibition assays by K27-Ub₂ of K48-Ub₂ and K63-Ub₂ cleavage. As our model DUB, we used USP5/IsoT that has been shown to cleave all polyUb chains with a free C-terminus except K27-Ub₂. In the presence of K27-Ub₂, IsoT cleaved K48- and K63-Ub₂ with significantly reduced activity as shown in

Figure 4-7. The results showed that K27-Ub₂ inhibits IsoT DUB activity towards both K48-Ub₂ and K63-Ub₂, which means that resistance to IsoT DUB activity by K27-Ub₂ is not due to its inability to bind the DUB but some other reason. This suggests that due to its resistance to cleavage by DUBs and its ability to bind them, K27-Ub₂ can act as a competitive inhibitor of DUB activity toward other linkages.

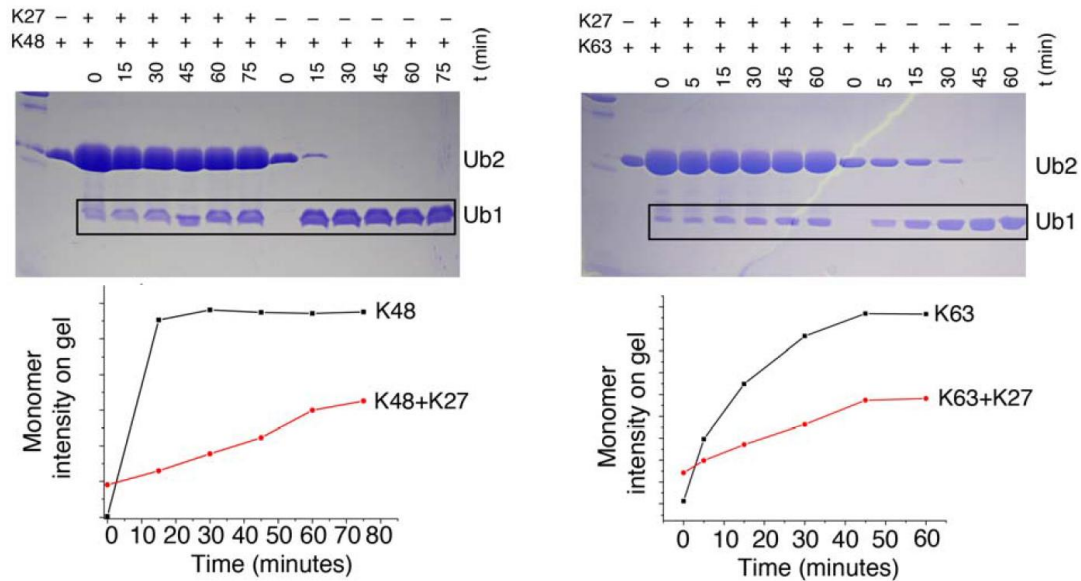


Figure 4-7. K27-Ub₂ inhibits IsoT/USP5 DUB activity towards K48-Ub₂ (left) and K63-Ub₂ (right). 15% SDS-PAGE gels stained with Coomassie blue monitoring the disassembly of the respective chains in the absence or presence of K27-Ub₂. The graphs on the bottom quantify the buildup of monoubiquitin as K48-Ub₂ or K63-Ub₂ is disassembled by IsoT. Note that in contrast with K48- and K63-Ub₂, K27-Ub₂ is not disassembled by IsoT. The reactions were run in PBS, pH 7.4, at room temperature. The initial concentration of K48-Ub₂ or K63-Ub₂ was 20 μ M, K27-Ub₂ was at 100 μ M, and IsoT was at 20 nM. The monoubiquitin bands were integrated using the software ImageJ.

In summary, K27-Ub₂ interacts with Rap80 tUIM with a similar binding affinity as K6-Ub₂ most likely due to avidity effect. There is no directionality in binding of K27-Ub₂ as well. Interestingly, K27-Ub₂ inhibits DUB activity of IsoT against K48 and K63-Ub₂s and might be used to inhibit DUB activity toward other linkages.

Chapter 5: Binding studies of yeast Ddi1UBL

5.1 Charge Dependency of Yeast Ddi1UBL Binding to Ubiquitin

DNA Damage Inducible 1 (Ddi1) is believed to be a shuttle protein that targets polyubiquitinated substrates for proteasomal degradation. In yeast, it consists of a ubiquitin-associated domain (UBA) that is believed to bind polyubiquitin chains attached to the substrate, a ubiquitin-like domain (UBL) that is recognized by receptors on proteasome and a conserved retroviral protease fold domain (RVP) between the two whose function is still unknown (Figure 5-1).

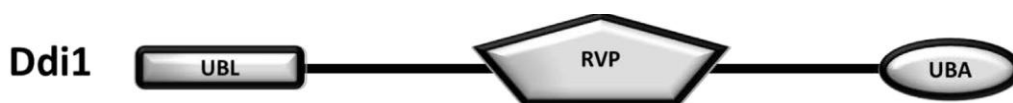


Figure 5-1. Cartoon representation of domain composition of Ddi1 in yeast²⁸. UBL stands for ubiquitin-like domain, RVP for retroviral protease fold domain and UBA for ubiquitin-associated domain.

It was shown by Nowicka *et al.*²⁸ that yeast Ddi1UBL (yDdi1UBL) has an unexpected binding property. Even though, based on the structure, it has an ubiquitin fold, instead of binding to UBL receptors, it surprisingly binds ubiquitin. As shown in Figure 1-4, Ddi1UBL has negative charges at positions around the hydrophobic patch whereas in Ub there are positive charges. The interaction with ubiquitin is mediated by surface hydrophobic residues on both proteins along with a unique interface formed by salt bridges between the oppositely charged residues of yDdi1UBL and ubiquitin (Figure 1-4).

To test the effect of charges we used site-directed mutagenesis to remove the positively charged amino-acids in ubiquitin near the binding interface (K6, R42 and

R72) and change them into either neutral (Alanine) amino acids or negatively charged (Glutamate) amino acids. From the studies with these mutants, we have shown that when we remove all three positive charges (K6, R42 and R72) to either negative or neutral charge we lose the binding. To try and find which of these charges are more important, we made further mutations and it appears that R42 is the most important charge (Figure 5-2)

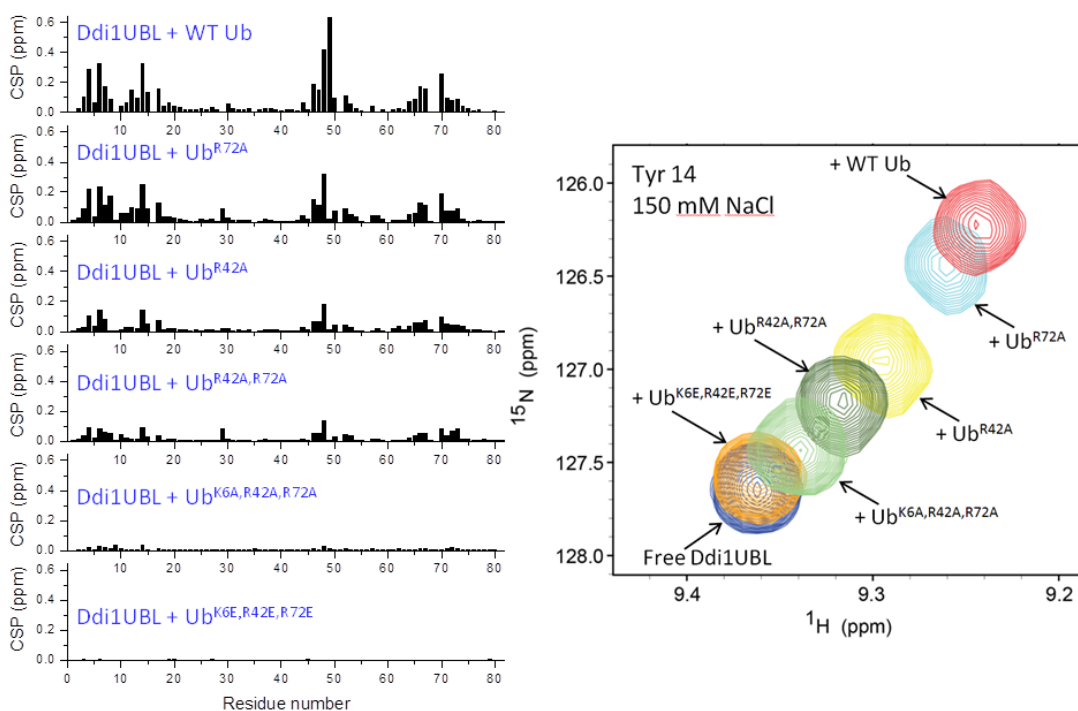


Figure 5-2. Charge-charge interactions are critical for interaction between ubiquitin and γ Ddi1UBL. Left, comparison of binding of ubiquitin mutants to Ddi1UBL through comparison of the CSPs in Ddi1UBL upon addition of different ubiquitin mutants. Right, overlay of peak representing Y14 in ¹⁵N Ddi1UBL upon addition of ubiquitin and different ubiquitin mutants²⁸.

5.2 Yeast Ddi1UBL Binding to Different Diubiquitin Chains

Furthermore, my former labmate and collaborator on this project Dr. Urszula Nowicka observed that γ Ddi1UBL has two binding surfaces; one is the expected β -

sheet side of binding and another on the α -helix (residues 26-33) on the opposite side of the structure. We believed it might lead to a characteristic binding with specific diubiquitin chains. In the preliminary studies, it was observed that K48-Ub₂ interacts with the second binding surface on yDdi1UBL, while both monoubiquitin and K63-Ub₂ do not. Upon analyzing the chemical shift perturbations in ¹⁵N labeled yDdi1UBL upon addition of K48-Ub₂, it was observed that along with the residues on the β -sheet side, the residues in the α -helix on the opposite side were also affected (CSPs > 0.07) while significant CSPs were not observed upon titrating K63-Ub₂ into yDdi1UBL (Figure 5-3). Also, compared to titrations of ¹⁵N yDdi1UBL with K63-Ub₂ and monoubiquitin²⁸, the one with K48-Ub₂ showed more signal attenuation, which usually indicates tighter binding.

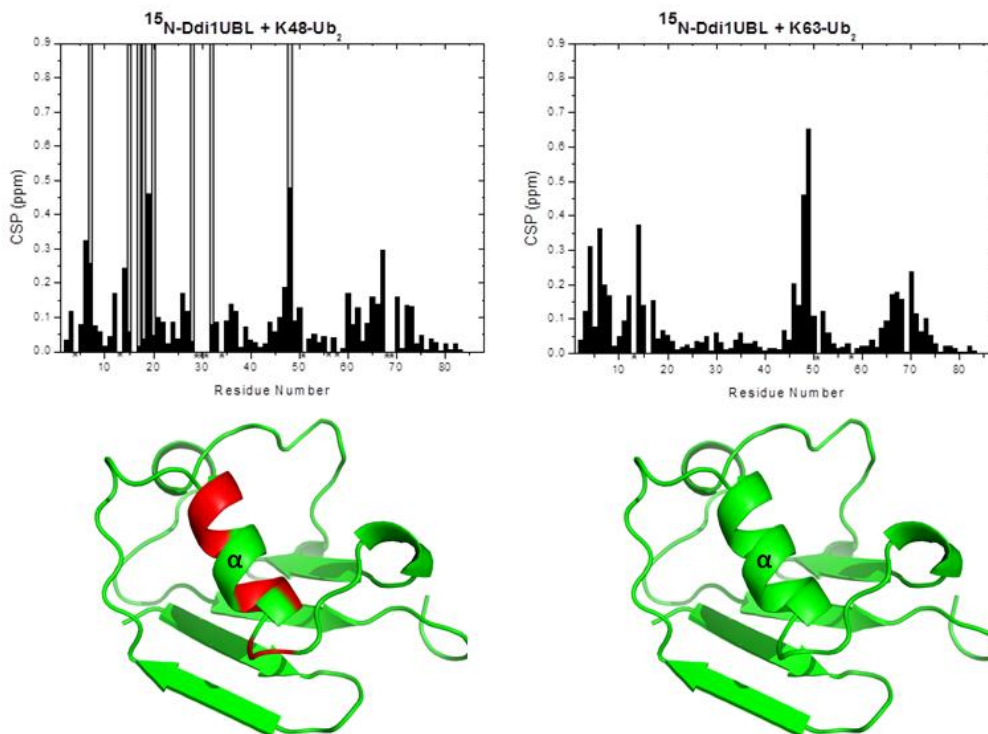


Figure 5-3. CSP plot of ¹⁵N labeled yDdi1UBL upon addition of K48-Ub₂ (top left) and of K63-Ub₂ (top right) at saturation. Grey bars denote signal attenuation. Asterisks denote residues whose signals are not detectable or the signals overlap. CSPs greater than 0.07 from binding of ¹⁵N labeled yDdi1UBL upon addition of K48-Ub₂ (bottom left) and of K63-Ub₂ (bottom right) mapped (red) on the alpha helix (“back side”, residues 26-33) of yDdi1UBL structure 2MRP. α indicates the alpha helix.

To determine the amino-acids on yDdi1UBL that are important in binding to the secondary site, sequence analysis of Ddi1UBL α -helix with corresponding α -helices of Rad23UBL, Dsk2UBL and ubiquitin was performed by Dr. Urszula Nowicka. The analysis revealed that there is a unique stretch of hydrophobic amino-acids in Ddi1UBL compared to the others (Figure 5-4, black box) This sequence is similar to an ubiquitin interacting motif (UIM) leading us to consider its significance in the secondary binding site. Looking closer at the putative UIM sequence, it was determined that the sequence AL in the proposed UIM in yDdi1UBL is not conserved in any of the UBLs or Ub (Figure 5-4, red box). We hypothesized that by mutating this stretch of amino-acids (AL) in yDdi1UBL to the corresponding amino-acids in ubiquitin (SK), it would abolish the secondary binding site. The mutations were performed using site-directed mutagenesis.

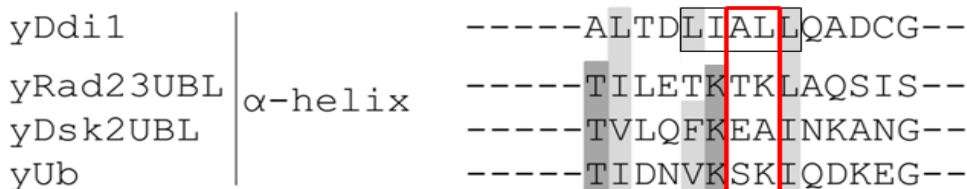


Figure 5-4. Alignment of the sequence of the α -helix in yDdi1UBL with the sequence of amino acids that compose α -helix of Ub and UBL domains of shuttle proteins: Rad23 and Dsk2. Amino acids that are similar are highlighted in light grey; amino acids that are identical are highlighted in dark grey. Black box indicates putative UIM on Ddi1UBL α -helix sequence. Red box indicates the residues in the putative UIM of yDdi1UBL that are not conserved in yUb or the other two UBLs.

Titration of K48- and K63-Ub₂ into ¹⁵N labeled A30S, L31K Ddi1UBL (referred to as Ddi1UBL_SK in the text) mutant that we hypothesized to have only one binding site, with the back side binding abolished, were performed. The CSPs demonstrate that binding of K48-Ub₂ to secondary surface on the “back side” of

yDdi1UBL is reduced (Figure 5-5, red box). Moreover, fewer signal attenuations are observed indicating weaker binding than with wild type yDdi1UBL. We can conclude that residues AL are important for the specific binding of K48-Ub₂. (Figure 5-5).

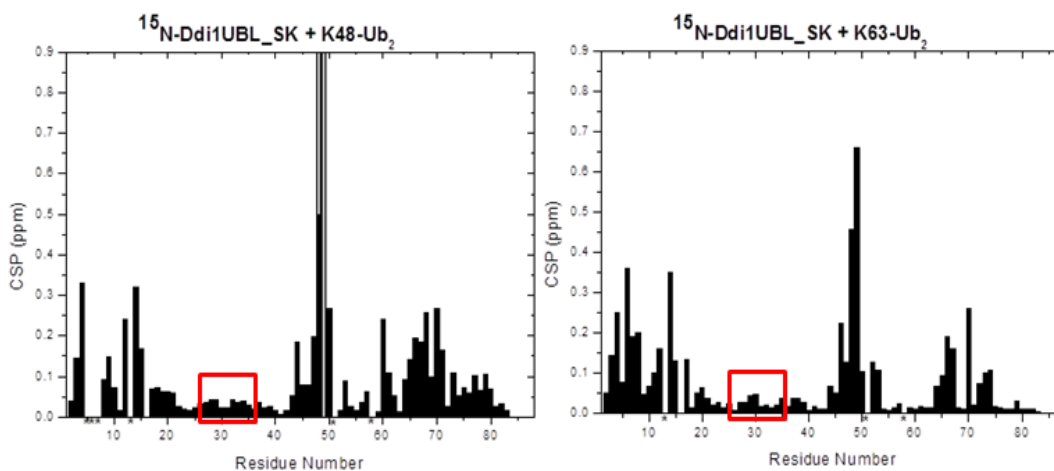


Figure 5-5. CSP plot of ¹⁵N labeled yDdi1UBL_SK upon addition of K48-Ub₂ (left) and of K63-Ub₂ (right) at saturation. Grey bars denote signal attenuation. Asterisks denote residues whose signals are not detectable or the signals overlap. Red box indicates the residues forming the alpha helix (“back side”, residues 26-33) of yDdi1UBL_SK.

We used human ubiquitin in all the studies with yDdi1UBL since ubiquitin is a highly conserved protein and there is a difference of only three residues between human ubiquitin and yeast ubiquitin. But unlike ubiquitin in yeast, based on the comparison between ubiquitin sequence in humans and yDdi1UBL, there is only one residue difference in the putative UIM on the α -helix. Therefore, we made a single amino acid mutant L31K Ddi1UBL (referred to as Ddi1UBL_K in the text) to test if that is sufficient to remove the interaction of K48-Ub₂ with binding surface to α -helix on the opposite side of the structure. From the results, we see that the “back side” binding is abrogated by mutating a single amino acid (Figure 5-6).

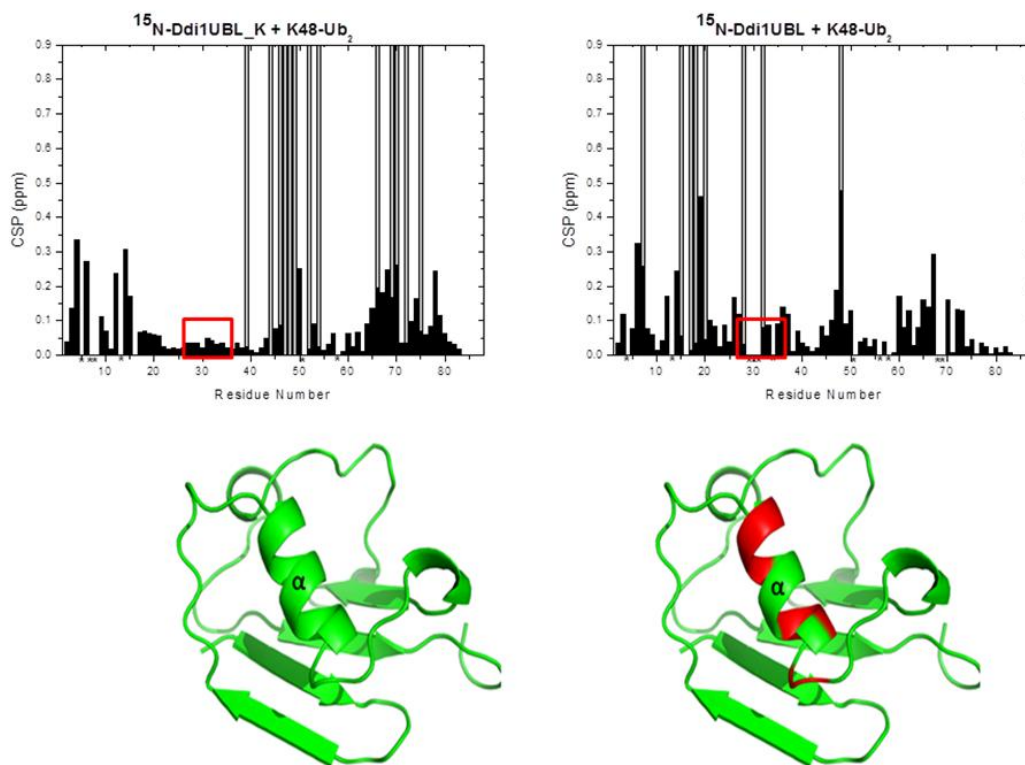


Figure 5-6. Comparison between CSP plot of ^{15}N labeled yDdi1UBL_K upon addition of K48-Ub₂ at saturation (left) and CSP plot of ^{15}N labeled yDdi1UBL upon addition of K48-Ub₂ (right). Grey bars denote signal attenuation. Asterisks denote residues whose signals are not detectable or the signals overlap. Red box indicates the residues forming the alpha helix (“back side”, residues 26-33). CSPs over 0.07 ppm from binding of ^{15}N labeled yDdi1UBL_K upon addition of K48-Ub₂ (bottom left) and of ^{15}N labeled yDdi1UBL upon addition of K48-Ub₂ (bottom right) mapped (red) on the alpha helix (“back side”, residues 26-33) of yDdi1UBL structure 2MRP. α indicates the alpha helix.

We calculated the average K_d by fitting the titration data using in house program KDFIT (Figure 5-7). The binding of yDdi1UBL is a lot tighter for K48-Ub₂ than for K63-Ub₂. Average K_d of $1.1 \pm 0.3 \mu\text{M}$ (from 5 residues) was determined for K48-Ub₂ binding while for K63-Ub₂, a K_d of $39.7 \pm 8.8 \mu\text{M}$ (from 8 residues) was determined. Due to the tight binding, there is significant deviation in the residuals of the fit for ^{15}N labeled yDdi1UBL when K48-Ub₂ is titrated in.

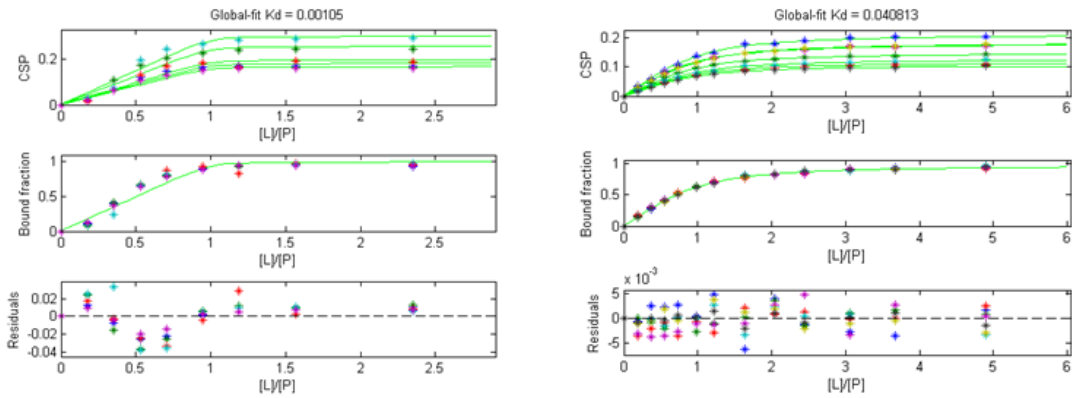


Figure 5-7. Titration fit of ^{15}N labeled yDdi1UBL upon addition of K48-Ub₂ (left) and K63-Ub₂ (right) using KDFIT global. The curves represent the results of global fit of the titration data for the residues having the titration endpoint CSP above a selected threshold, the resulting global-fit K_d values (in mM) are shown on the top. Top panel shows the global fit of CSPs from individual residues as a function of the ligand/protein molar ratio. Middle panel shows the global fit of the bound fraction of the protein as a function of the ligand/protein molar ratio. Bottom panel indicates the residuals from the fit.

Since we could not determine a reliable K_d from the above titration, isothermal titration calorimetry was performed by Dr. Robert Brinson at IBBR. K_d of 7.1 μM and stoichiometry of around 1:1 was estimated. The ΔH and ΔS were calculated to be 1.8 kcal/mol and 29.5 cal/mol.K respectively (Figure 5-8).

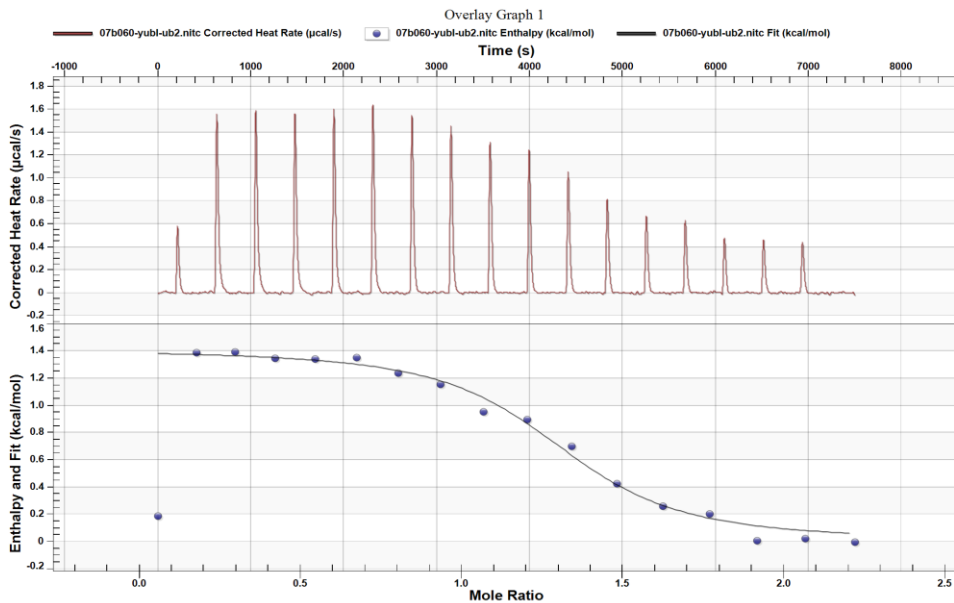


Figure 5-8. ITC titration analysis of yDdi1UBL and K48-Ub₂ binding. The raw data traces are shown in the top panel with the bottom panel illustrating the integrated fit data plots.

When the “back-side” of yDdi1UBL is mutated (Ddi1UBL_SK), average K_d for its binding to K48-Ub₂ increases to $16.9 \pm 0.7 \mu\text{M}$ (from 5 residues) but the stoichiometry is still 1:1 (Figure 5-9 (A)). The mutant yDdi1UBL_SK binds K63-Ub₂ with a stoichiometry of 2 UBL to one diubiquitin, which means each ubiquitin unit of K63-Ub₂ binds one unit of yDdi1UBL_SK (Figure 5-9 (B)). An average K_d of $67.6 \pm 18.8 \mu\text{M}$ (from 6 residues) was determined. Also, yDdi1UBL_K gave a similar K_d as yDdi1UBL_SK ($16.8 \pm 5.6 \mu\text{M}$ from 7 residues) when K48-Ub₂ was titrated in with a stoichiometry of 1:1. (Figure 5-9 (C))

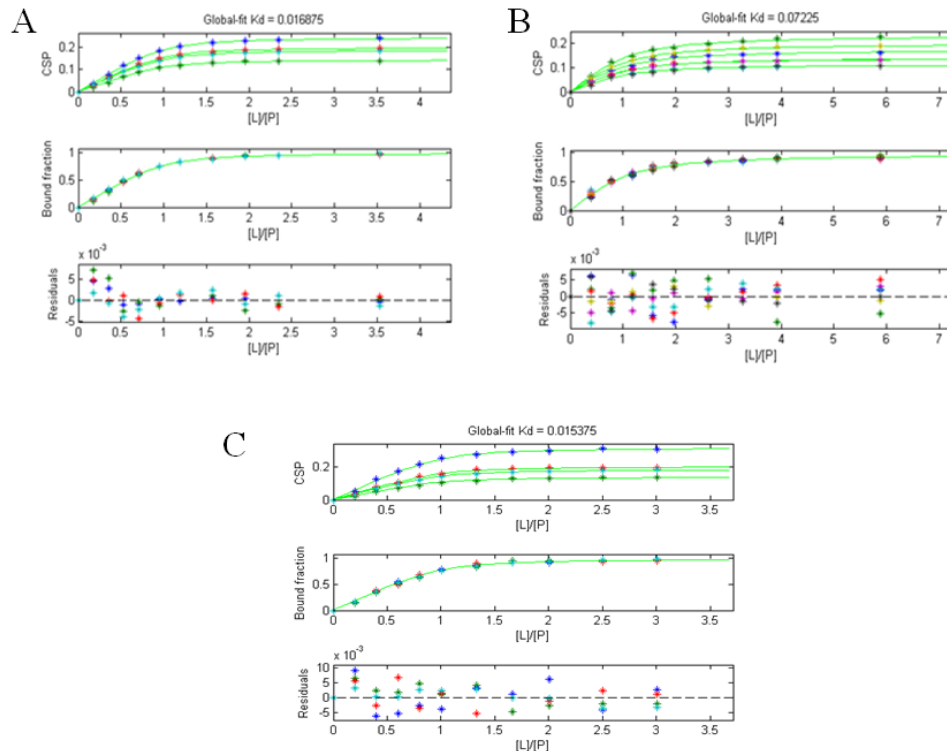


Figure 5-9. Titration fit of ¹⁵N labeled yDdi1UBL_SK upon addition of K48-Ub₂ (A) and K63-Ub₂ (B) using KDFIT global. Titration fit of ¹⁵N labeled yDdi1UBL_K upon addition of K48-Ub₂ (C) using KDFIT global. The curves represent the results of global fit of the titration data for the residues having the titration endpoint CSP above a selected threshold, the resulting global-fit K_d values (in mM) are shown on the top. Top panel shows the global fit of CSPs from individual residues as a function of the ligand/protein molar ratio. Middle panel shows the global fit of the bound fraction of the protein as a function of the ligand/protein molar ratio. Bottom panel indicates the residuals from the fit.

Solution NMR binding studies observing either the proximal or distal domain of K48-Ub₂ and titrating in unlabelled yDdi1UBL were performed to determine the residues involved in the interaction on K48-Ub₂. The CSPs of each of the two domains are different (Figure 5-10), which points to the possibility that there is directionality in the binding.

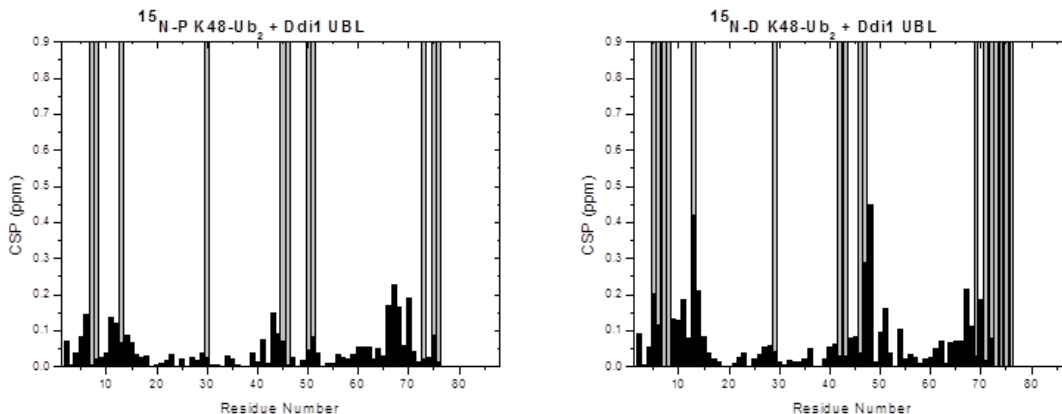


Figure 5-10. CSP plot of ¹⁵N labeled K48-Ub₂ on the proximal (left) and distal (right) domain upon addition of yDdi1UBL at saturation. Grey bars denote signal attenuation. Asterisks denote residues whose signals are not detectable or the signals overlap.

Surprisingly, we noticed that there is significant deviation in the residuals of the fit (Figure 5-11), which upon adjusting the ligand concentration seems to be reduced but still remains (Figure 5-12). The estimated K_d for distal domain of K48-Ub₂ after adjusting the ligand concentration is 1.22 ± 0.8 μM (from 7 residues) and for proximal domain the average K_d is 1.34 ± 1.1 μM (from 6 residues).

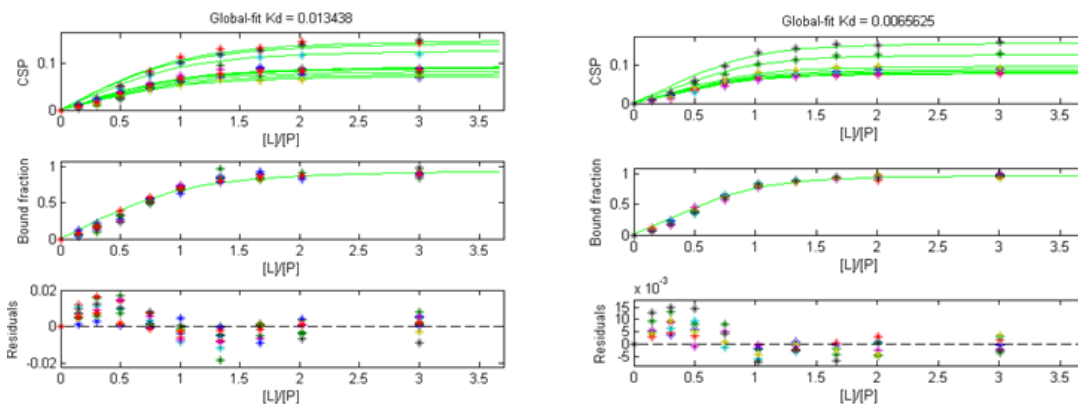


Figure 5-11. Titration fit of K48-Ub₂ ¹⁵N labeled on proximal domain (left) and distal domain (right) upon addition of yDdi1UBL using the program Kdfit global.

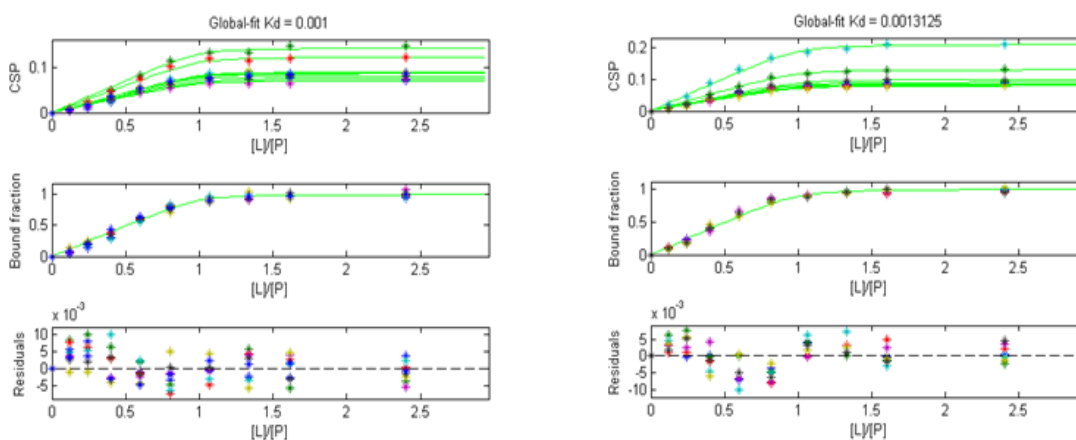


Figure 5-12. Titration fit of K48-Ub₂ ¹⁵N labeled on proximal domain (left) and distal domain (right) upon addition of yDdi1UBL using KDFIT global after multiplying the ligand concentration by 0.8. The curves represent the results of global fit of the titration data for the residues having the titration endpoint CSP above a selected threshold, the resulting global-fit Kd values (in mM) are shown on the top. Top panel shows the global fit of CSPs from individual residues as a function of the ligand/protein molar ratio. Middle panel shows the global fit of the bound fraction of the protein as a function of the ligand/protein molar ratio. Bottom panel indicates the residuals from the fit.

In order to determine if there is directionality in binding of K48-Ub₂ to yDdi1UBL, PRE studies were conducted. Two different K48-Ub₂ chains were synthesized enzymatically for the PRE measurements, one with mutation at T12C on the proximal domain and another with mutation at K48C on the distal domain. MTSL was attached at T12C position on the proximal domain and PRE measurements were performed. Similarly, MTSL was attached at K48C position on the distal domain of

the other K48-Ub₂ and PRE measurements were performed. If there is directionality in binding of K48-Ub₂ with yDdi1UBL, then PRE effect would be seen on different sides of yDdi1UBL depending on if MTSL is attached on the proximal (T12C) domain or the distal (K48C) domain of K48-Ub₂.

For both cases (MTSL attached to T12C on proximal or K48C on distal domain), the ratio of intensities of the signals before and after adding reducing agent (ascorbate) was plotted against the residue number. The data from each domain was fit individually using the in-house program SLFIT and coordinates from yDdi1UBL structure (PDB 2MRP).

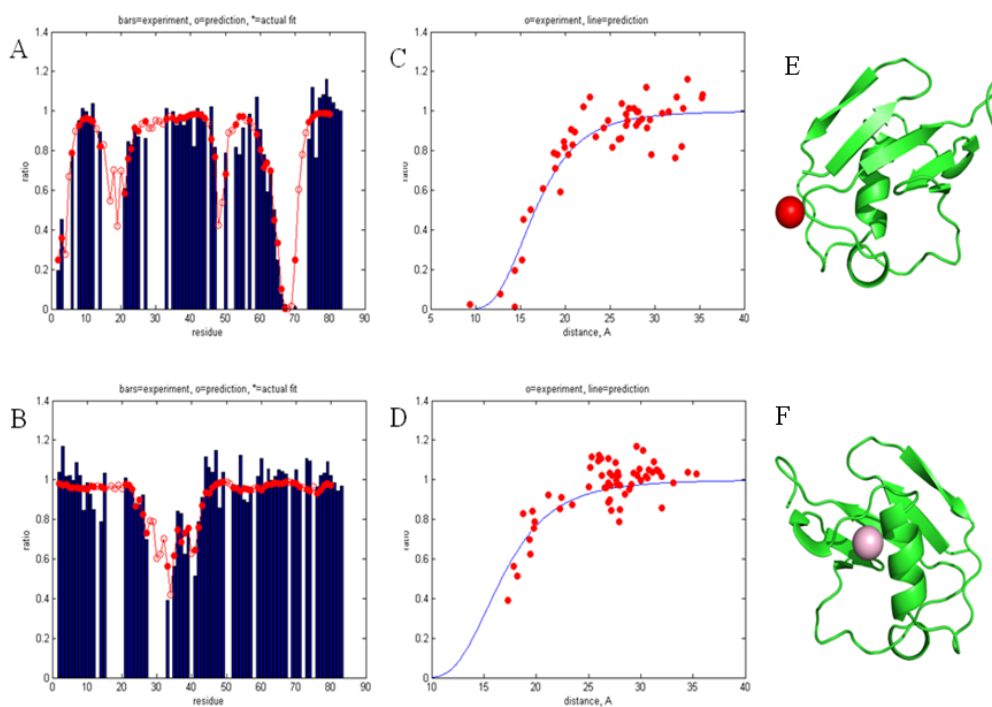


Figure 5-13. PRE effect on yDdi1UBL upon addition of K48-Ub₂ with MTSL attached at position T12C on the proximal domain (top) and K48C on the distal domain (bottom). Position of the spin label fitted using the coordinates from the PDB structure of yDdi1UBL (2MRP). A-B. Blue bars depict experimental PREs for yDdi1UBL; red circles connected by lines are back-calculated PREs from the reconstructed position of the spin label. C-D. Red circles indicate experimental PRE data as a function of the calculated distance of the residues from the spin label's unpaired electron, while the blue curve represents the calculated distance dependence of the PREs. E-F. Reconstructed position of the spin label at T12C on proximal (top) and K48C on distal (bottom) domain of K48-Ub₂ with respect to yDdi1UBL generated from SLFIT added onto the PDB structure of yDdi1UBL (2MRP).

Upon fitting the data and predicting the position of MTSL using SLFIT, it is observed that indeed there is directionality in binding. The predicted position of MTSL attached at T12C on the proximal domain is near the β -sheet surface while for MTSL attached at K48C on the distal domain, the position is predicted to be on the opposite side facing the α -helix (“back-side”) (Figure 5-13). From studies performed by Dr. Urszula Nowicka, the predicted position of MTSL attached at T12C on monoubiquitin also faces the β -sheet surface²⁸.

To determine if K48-Ub₂ binds in a similar manner to yDdi1UBL_SK, we study the PRE effect on yDdi1UBL_SK upon binding to K48-Ub₂. As in the case with yDdi1UBL, the ratio of intensities of the signals before and after adding ascorbate was plotted against the residue number. The data from each domain was fit individually using the in-house program SLFIT and coordinates from yDdi1UBL structure (PDB 2MRP). The predicted position of MTSL attached at T12C on the proximal domain is still near the β -sheet surface but the MTSL attached at K48C on the distal domain is predicted to be away from the α -helix (“back-side”) (Figure 5-14).

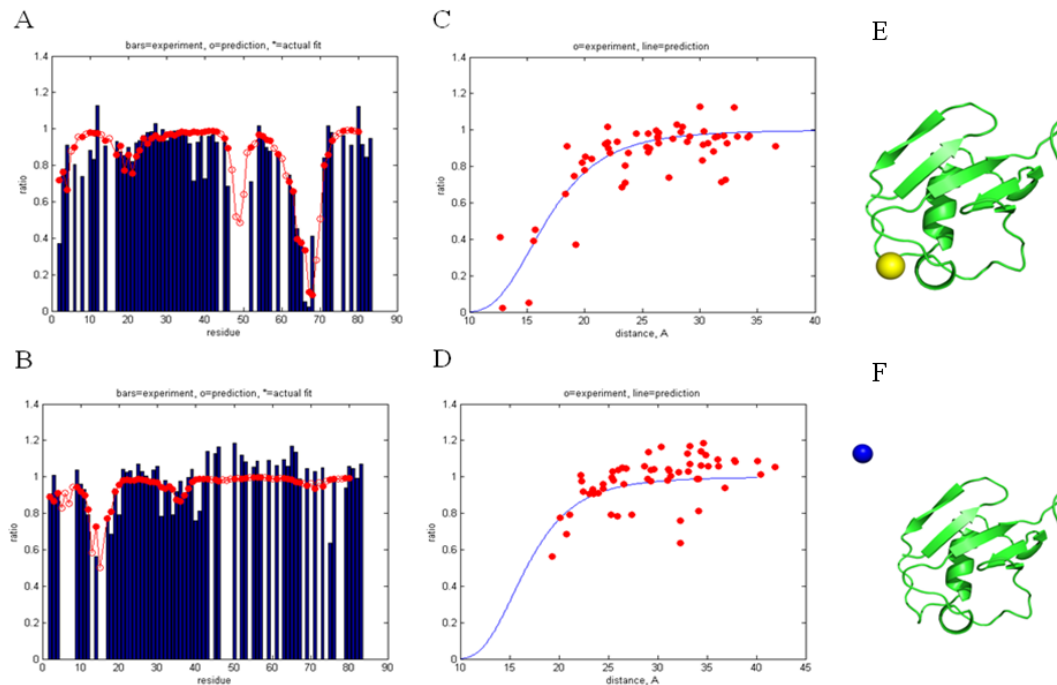


Figure 5-14. PRE effect on yDdi1UBL_SK upon addition of K48-Ub₂ with MTSL attached at position T12C on the proximal domain (top) and K48C on the distal domain (bottom). Position of the spin label fitted using the coordinates from the PDB structure of yDdi1UBL (2MRP). A-B. Blue bars depict experimental PREs for yDdi1UBL_SK; red circles connected by lines are back-calculated PREs from the reconstructed position of the spin label. C-D. Red circles indicate experimental PRE data as a function of the calculated distance of the residues from the spin label's unpaired electron, while the blue curve represents the calculated distance dependence of the PREs. E-F. Reconstructed position of the spin label at T12C on proximal (top) and K48C on distal (bottom) domain of K48-Ub₂ with respect to yDdi1UBL_SK generated from SLFIT added onto the PDB structure of yDdi1UBL (2MRP).

The positions of MTSL predicted from all the PRE measurements were consolidated and are shown in Figure 5-15. From the figure, it is apparent that proximal domain of K48-Ub₂ binds the main β -sheet surface of both yDdi1UBL and yDdi1UBL_SK similar to monoubiquitin. The distal domain of K48-Ub₂ binds yDdi1UBL on the α -helix (“back-side”) while it doesn’t bind yDdi1UBL_SK on the “back side”. Modeling of the structure of this complex is currently underway in collaboration with Dr. Olivier Walker (University of Lyon, France).

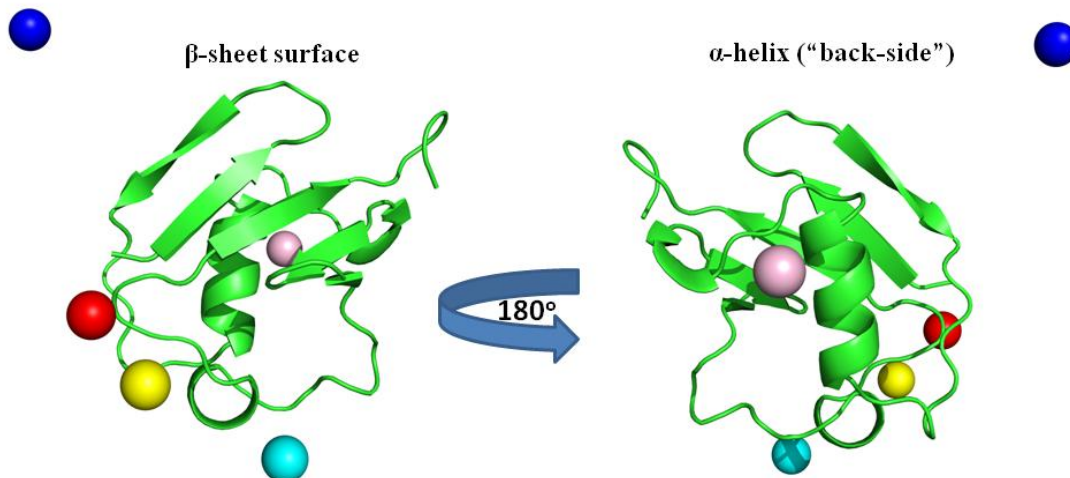


Figure 5-15. Reconstructed positions of spin labels generated using SLFIT and yDdi1UBL structure from PDB 2MRP. Pink sphere indicates position of spin label on K48C position on distal moiety of K48-Ub₂ and red sphere indicates position of spin label on T12C position on proximal moiety of K48-Ub₂ upon its addition to ¹⁵N yDdi1UBL. Blue sphere indicates position of spin label on K48C position on distal moiety of K48-Ub₂ and yellow sphere indicates position of spin label on T12C position on proximal moiety of K48-Ub₂ upon its addition to ¹⁵N yDdi1UBL_SK. Cyan sphere indicates position of spin label on T12C position of monoubiquitin upon its addition to ¹⁵N yDdi1UBL. The structure of yDdi1UBL is rotated by an angle of 180° in order to show both the β-sheet (left) and α-helix surfaces (right).

Since K6-Ub₂ forms an interface and our studies indicated that it binds hHR23a UBA₂ in a similar manner to K48-Ub₂, we performed binding study with K6-Ub₂ and yDdi1UBL as well. We observed ¹⁵N yDdi1UBL and titrated in unlabelled K6-Ub₂. From the CSPs (Figure 5-16), we detected perturbations on the “back side” that are more than what we observed with K63-Ub₂ but much less than seen with K48-Ub₂. There is only one residue that shows significant CSP on the alpha helix as shown in Figure 5-16 (right).

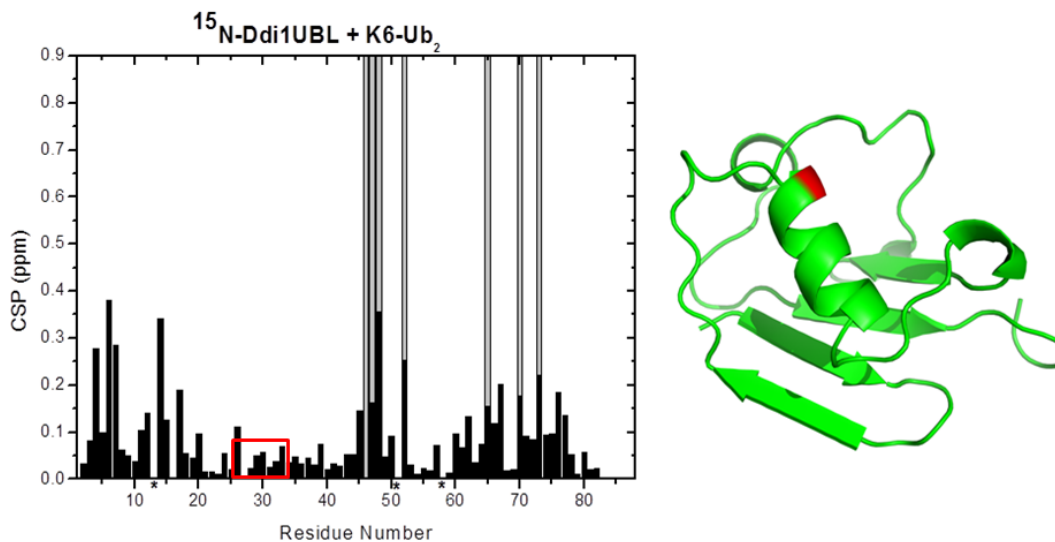


Figure 5-16. Left: CSP plot of ^{15}N labeled yDdi1UBL upon addition of K6-Ub₂ at saturation. Grey bars denote signal attenuation. Asterisks denote residues whose signals are not detectable or the signals overlap. Red box indicates the residues forming the alpha helix (“back side”, residues 26-33) of yDdi1UBL. Right: CSPs over 0.07 from binding of ^{15}N labeled yDdi1UBL upon addition of K6-Ub₂ mapped (red) on the alpha helix (“back side”, residues 26-33) of yDdi1UBL structure 2MRP.

The average K_d estimated using KDFIT is $22.3 \pm 6.2 \mu\text{M}$ (from 12 residues), which is similar to K48-Ub₂ binding to yDdi1UBL_SK (Figure 5-17). Thus we can conclude that K6-Ub₂ does not bind in a sandwich-mode.

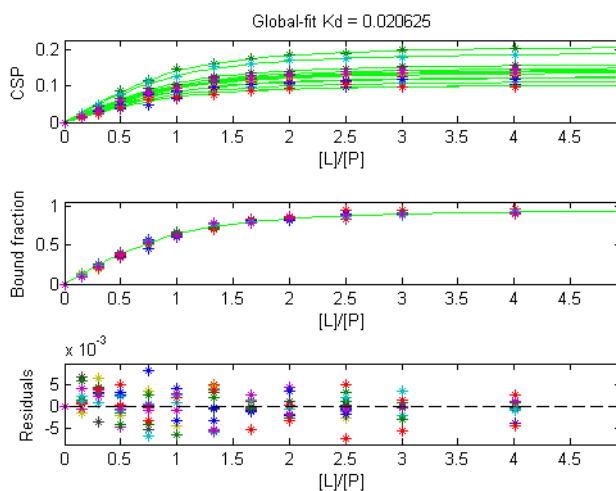


Figure 5-17. Titration fit of ^{15}N labeled yDdi1UBL upon addition of K6-Ub₂ using KDFIT global. The curves represent the results of global fit of the titration data for the residues having the titration endpoint CSP above a selected threshold, the resulting global-fit K_d values (in mM) are shown on the top. Top panel shows the global fit of CSPs from individual residues as a function of the ligand/protein molar ratio. Middle panel shows the global fit of the bound fraction of the protein as a function of the ligand/protein molar ratio. Bottom panel indicates the residuals from the fit.

Since K27-Ub₂ is also known to bind hHR23a UBA2 in a sandwich-mode fashion similar to K48-Ub₂, we performed a titration of ¹⁵N yDdi1UBL with K27-Ub₂. Since there are no significant CSPs on the alpha helix surface (Figure 5-18, red box), we can conclude that K27-Ub₂ does not bind in sandwich mode. Interestingly, the signals show no attenuations suggesting it is a weaker interaction than others. The average K_d determined using single site binding model supports that idea, since K27-Ub₂ has a high K_d of 50.7 ± 14 μM similar to K63-Ub₂ and monoubiquitin.

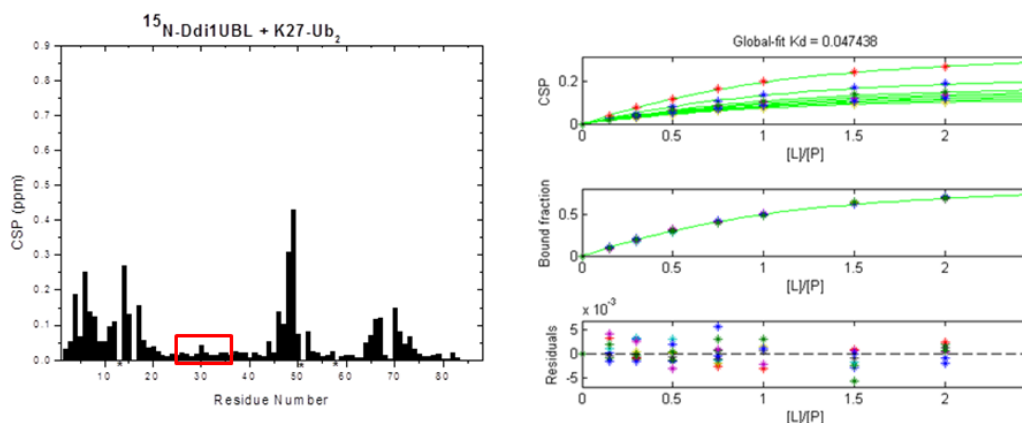


Figure 5-18. CSP plot of ¹⁵N labeled yDdi1UBL upon addition of K27-Ub₂ at saturation (left). Asterisks denote residues whose signals are not detectable or the signals overlap. Red box indicates the residues forming the alpha helix (“back side”, residues 26-33) of yDdi1UBL. Titration fit of ¹⁵N labeled yDdi1UBL upon addition of K27-Ub₂ (right) using KDFIT global. The curves represent the results of global fit of the titration data for the residues having the titration endpoint CSP above a selected threshold, the resulting global-fit K_d values (in mM) are shown on the top. Top panel shows the global fit of CSPs from individual residues as a function of the ligand/protein molar ratio. Middle panel shows the global fit of the bound fraction of the protein as a function of the ligand/protein molar ratio. Bottom panel indicates the residuals from the fit.

Similarly, K11-Ub₂ is known to have a distinct conformation and can form a compact structure as well⁶². So, we performed an NMR binding assay with ¹⁵N labeled yDdi1UBL and added in unlabeled K11-Ub₂. K11-Ub₂ chains were provided by my former labmate, Dr. Tanuja Kashyap. Only one residue in the α-helix surface showed significant CSP. K11-Ub₂ binds tighter to yDdi1UBL than K63-Ub₂ but

definitely a lot weaker than K48-Ub₂ (Figure 5-19). The average K_d was determined to be $36.4 \pm 9 \mu\text{M}$ from 11 residues using a single site model.

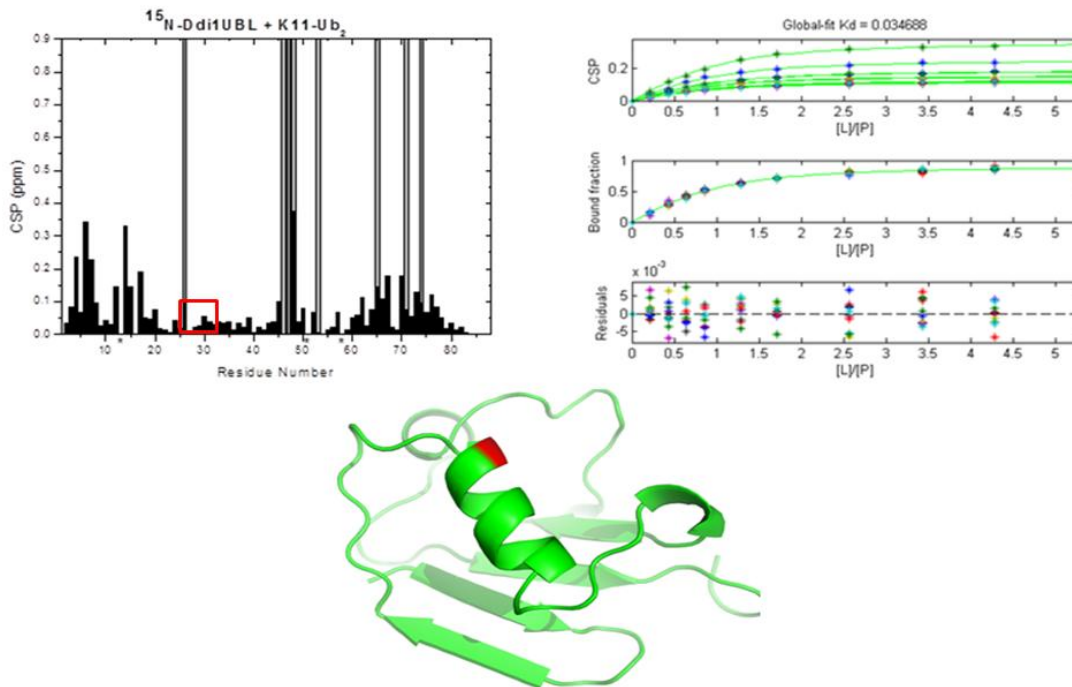


Figure 5-19. CSP plot of ¹⁵N labeled yDdi1UBL upon addition of K11-Ub₂ at saturation (top left). Grey bars denote signal attenuation. Asterisks denote residues whose signals are not detectable or the signals overlap. Red box indicates the residues forming the alpha helix (“back side”, residues 26-33) of yDdi1UBL. Titration fit of ¹⁵N labeled yDdi1UBL upon addition of K11-Ub₂ (top right) using KDFIT global. The curves represent the results of global fit of the titration data for the residues having the titration endpoint CSP above a selected threshold, the resulting global-fit K_d values (in mM) are shown on the top. Top panel shows the global fit of CSPs from individual residues as a function of the ligand/protein molar ratio. Middle panel shows the global fit of the bound fraction of the protein as a function of the ligand/protein molar ratio. Bottom panel indicates the residuals from the fit. CSPs over 0.07 from binding of ¹⁵N labeled yDdi1UBL upon addition of K6-Ub₂ mapped (red) on the alpha helix (“back side”, residues 26-33) of yDdi1UBL structure 2MRP (bottom).

All the titrations and their average K_d s are summarized in Table 5-1.

Sample	K_d (μ M)
15NyDdi1UBL vs K48-Ub ₂ (not a good fit)	1.11 ± 0.34
15NyDdi1UBL_SK vs K48-Ub ₂	15.8 ± 1.4
15NyDdi1UBL vs K63-Ub ₂	40 ± 6
15NyDdi1UBL_SK vs K63-Ub ₂ (Lt*2)	67.6 ± 18.8
15NyDdi1UBL_K vs K48-Ub ₂	18.7 ± 6.9
15NyDdi1UBL vs K6-Ub ₂	22.3 ± 6.2
15NyDdi1UBL vs K27-Ub ₂	50.7 ± 14
15NyDdi1UBL vs K11-Ub ₂	36.4 ± 9
15NDK48Ub ₂ vs yDdi1UBL (Lt*0.8)	1.22 ± 0.8
15NPK48Ub ₂ vs yDdi1UBL (Lt*0.8)	1.34 ± 1.1

Table 5-1. Summary of K_d s for yDdi1UBL and diubiquitin binding studies.

From the studies discussed here, we can conclude that yDdi1UBL interaction with ubiquitin is based on the electrostatic attraction between opposite charges surrounding the hydrophobic patch on Ub and UBL. We determined that R42 on ubiquitin might be the most important for this binding. K48-Ub₂ binds yDdi1UBL tighter than other diubiquitin chains and monoubiquitin. This specificity of K48-Ub₂ is due to the presence of a putative UIM on the “back-side” of yDdi1UBL and it can be removed by a single mutation (L31K). From the PRE studies, we determined that there is directionality in binding of K48-Ub₂ to yDdi1UBL.

Chapter 6: Binding studies of human Ddi1UBL

6.1 Introduction

From the analysis of Ddi1 domain conservation among different species by Dr. Urszula Nowicka and as presented in our paper²⁸, we know that UBL domain is conserved throughout the species (except one), while UBA domain is lost in mammals (Figure 6-1, boxed). This is unlike other UBL-UBA shuttle proteins having both UBA and UBL domains conserved among eukaryotes.



Figure 6-1. Ddi1 gene structure and domain conservation among eukaryotes. Domain composition of Ddi1 from selected organisms; UBL – ubiquitin-like domain, RVP – retroviral protease-like domain, UBA – ubiquitin-associated domain are shown as solid blocks; the dashed block indicates the potential presence of a C-terminal UBA, that was identified by the domain prediction software but did not pass the threshold criteria. The UBL and RVP domains are present in almost all species whereas the UBA domain was lost in mammals during evolution²⁸.

It was hypothesized by Dr. Nowicka that this loss of UBA domain might be due to the fact that it is not required for Ddi1 to function as a shuttle protein since

UBL might be able to bind both Ub and the proteasome. As shown in the model proposed in the paper (Figure 6-2), the conserved retroviral protease fold domain (RVP) is known to dimerize and it is possible that it dimerizes to form a functional Ddi1 proteasomal shuttle. In this scenario, one of the two UBL domains of the homodimer can bind the polyubiquitin chain attached to the substrate while the other UBL domain can bind the proteasome.

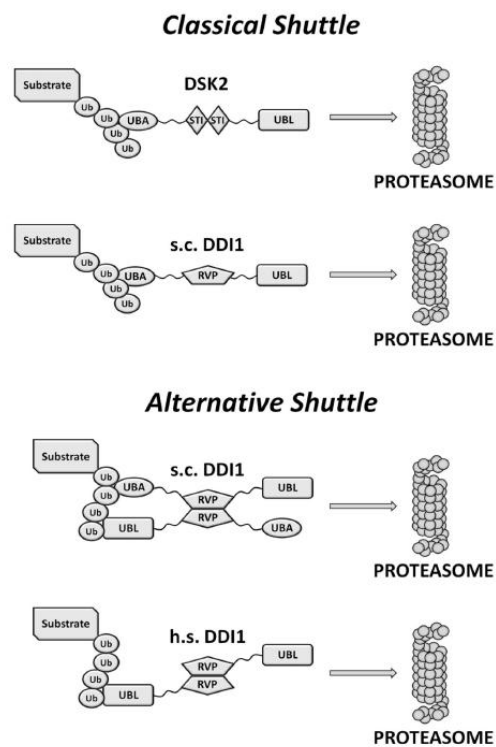


Figure 6-2. A “classical” shuttle protein (e.g. Dsk2) employs a ubiquitin-associated (UBA) domain to recognize and bind polyubiquitinated tag on a substrate protein and a ubiquitin-like (UBL) domain to target it to the proteasome. In yeast Ddi1, both the UBA and UBL domains can recognize polyubiquitinated substrates. Human Ddi1 lost its UBA domain during the evolution but still contains the UBL domain; the dual functionality of the UBL domain should allow hDdi1 to both bind polyUb tag and deliver polyubiquitinated substrates to the 26S proteasome for degradation. ²⁸.

6.2 hDdi1UBL binding to Ubiquitin

To examine if human Ddi1UBL (hDdi1UBL) binds to ubiquitin; GST-tagged hDdi1UBL was purified and titrated into ¹⁵N labeled ubiquitin. We observed shifts

upon addition of GST tagged hDdi1UBL that were concentration dependent indicating that it interacts with ubiquitin (Figure 6-3).

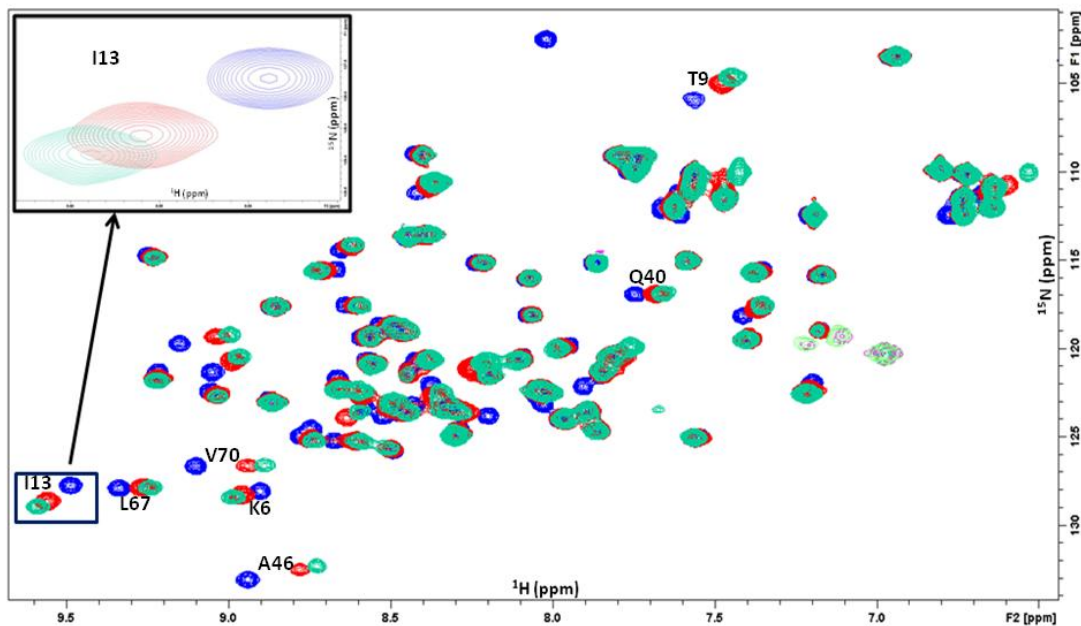


Figure 6-3. Overlay of ^{15}N WT Ub spectrum by itself (blue) and after addition of GST-tagged hDdi1UBL at 1:1 (red) and 1:2 (green) ratio.

To confirm that the interaction is indeed by hDdi1UBL and not by GST, our collaborator Dr. Michał Chojnacki cloned a construct with a PreScission protease cleavage site. This construct was also important to study interactions between hDdi1UBL and ubiquitin in more detail. The protein was successfully expressed, purified and the GST tag was cleaved to have a free hDdi1UBL for solution NMR binding studies. To demonstrate that hDdi1UBL is folded, ^{15}N labeled hDdi1UBL was purified and a ^1H - ^{15}N SOFAST HMQC spectrum collected. As can be seen from Figure 6-4, the signals are well spread over both ^1H and ^{15}N dimensions, indicating that the protein is folded.

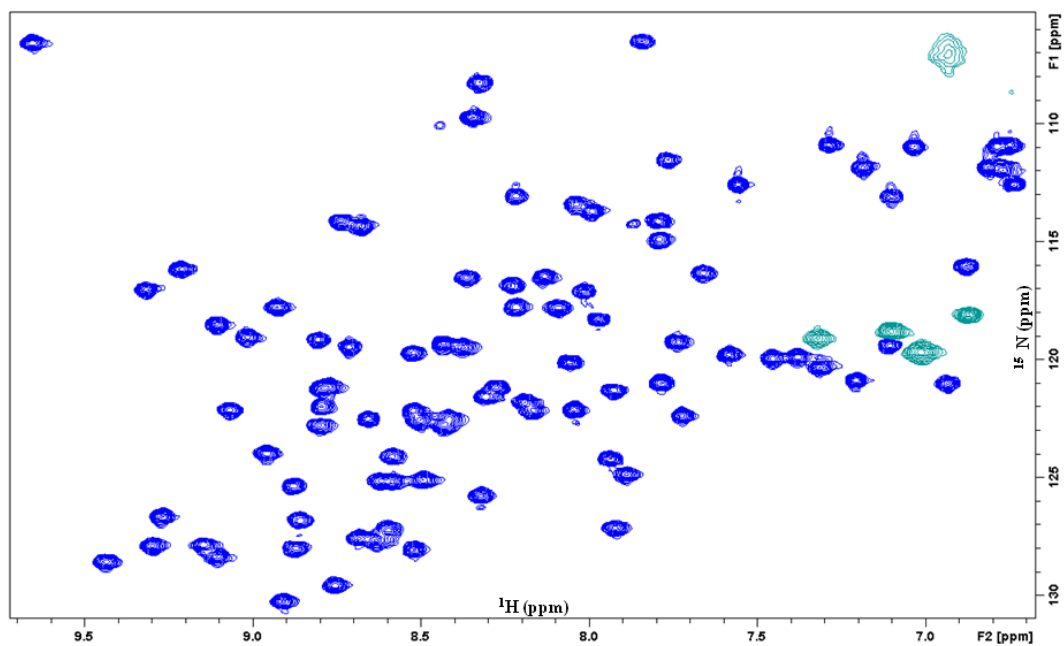


Figure 6-4. ^1H - ^{15}N SOFAST HMQC spectrum of ^{15}N labeled hDdi1UBL.

To determine the ubiquitin residues involved in the binding, we titrated in unlabeled hDdi1UBL into ^{15}N labeled ubiquitin. Unsurprisingly, the canonical hydrophobic patch is involved in the binding as noticed upon plotting the CSPs (Figure 6-5).

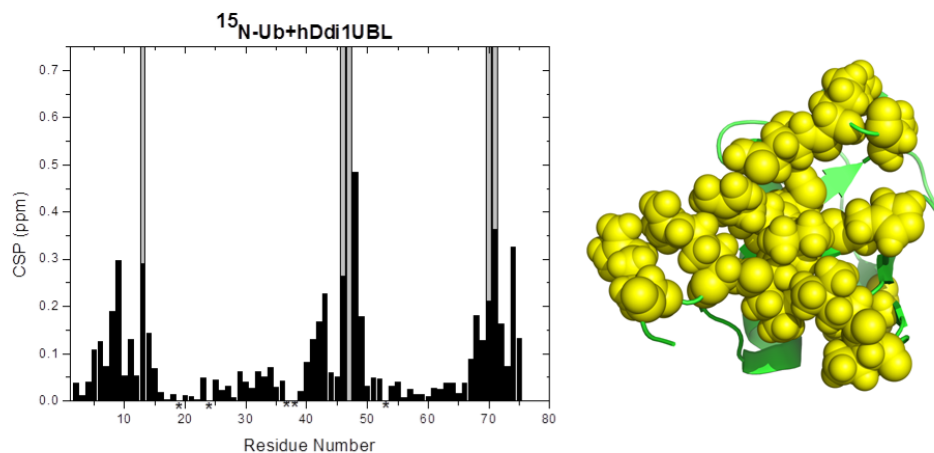


Figure 6-5. Left: CSP plot of ^{15}N labeled Ub upon addition of hDdi1UBL at saturation. Grey bars denote signal attenuation. Asterisks denote residues whose signals are not detectable or the signals overlap. Right: Residues that showed CSPs from binding of over 0.15 ppm were mapped (yellow spheres) on ubiquitin structure 1D3Z.

The amino acids involved in the binding of hDdi1UBL to ubiquitin are very similar to the ones involved in yDdi1UBL binding to ubiquitin as can be seen from the comparison in Figure 6-6.

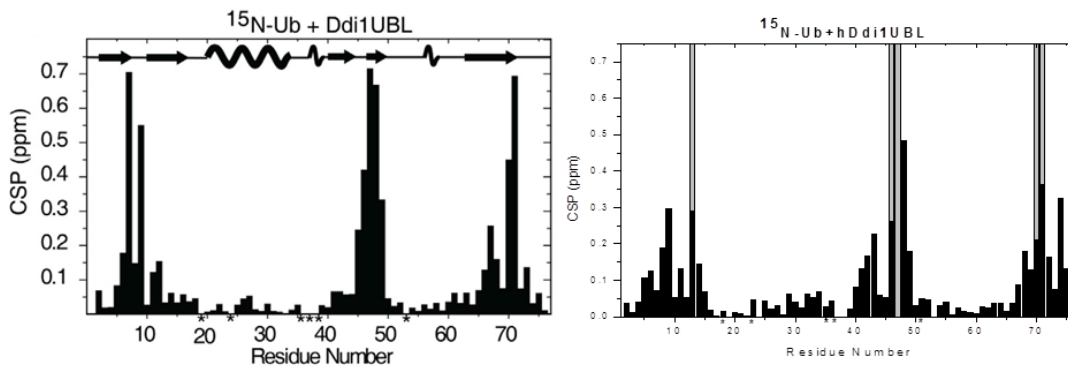


Figure 6-6. CSP plot of ^{15}N labeled Ub upon addition of yDdi1UBL²⁸ (left) and hDdi1UBL (right) at saturation. Grey bars denote signal attenuation. Asterisks denote residues whose signals are not detectable or the signals overlap.

We used KDFIT to estimate the binding affinity. The data fit well to 1:1 with one binding site model. We obtained a K_d of $39.7 \pm 2.8 \mu\text{M}$ (from 18 residues) (Figure 6-7). This is comparable to the K_d for the yDdi1UBL interaction with ubiquitin ($71 \mu\text{M}$ looking at ubiquitin and $45 \mu\text{M}$ looking at yDdi1UBL)²⁸.

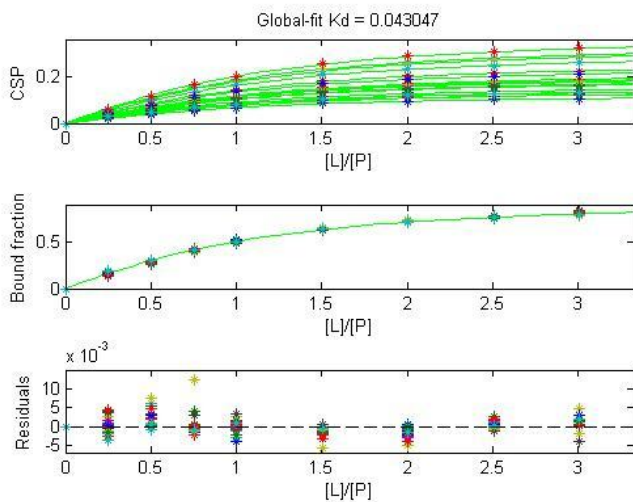


Figure 6-7. Titration fit of ^{15}N ubiquitin upon addition of hDdi1UBL using KDFIT global. The curves represent the results of global fit of the titration data for the residues having the titration endpoint CSP above a selected threshold, the resulting global-fit K_d values (in mM) are shown on the top. Top panel shows the global fit of CSPs from individual residues as a function of the ligand/protein molar ratio. Middle panel shows the global fit of the bound fraction of the protein as a function of the ligand/protein molar ratio. Bottom panel indicates the residuals from the fit.

Next, we wanted to determine the residues on hDdi1UBL involved in the binding. Since there was no assignment available for hDdi1UBL, we purified ^{13}C , ^{15}N labeled hDdi1UBL and my labmate Westley Pawloski, assigned the NMR signals corresponding to the backbone amides successfully. Once we had the signal assignments, titration of unlabeled ubiquitin into ^{15}N labeled hDdi1UBL was performed.

We used KDFIT to estimate the binding affinity. To fit the data, we had to multiply the ligand (ubiquitin) concentration by 2, which seem to suggest that two hDdi1UBL bind one ubiquitin molecule. The data fit well to a single site model. We determined an average K_d of $45.1 \pm 2.6 \mu\text{M}$ from 7 residues. The K_d agrees well with the reverse titration performed when ubiquitin was ^{15}N labeled and unlabeled hDdi1UBL was titrated but the stoichiometry of binding doesn't match. From this

titration, we determined a stoichiometry of two hDdi1UBL binding one ubiquitin while the stoichiometry for reverse titration was 1:1.

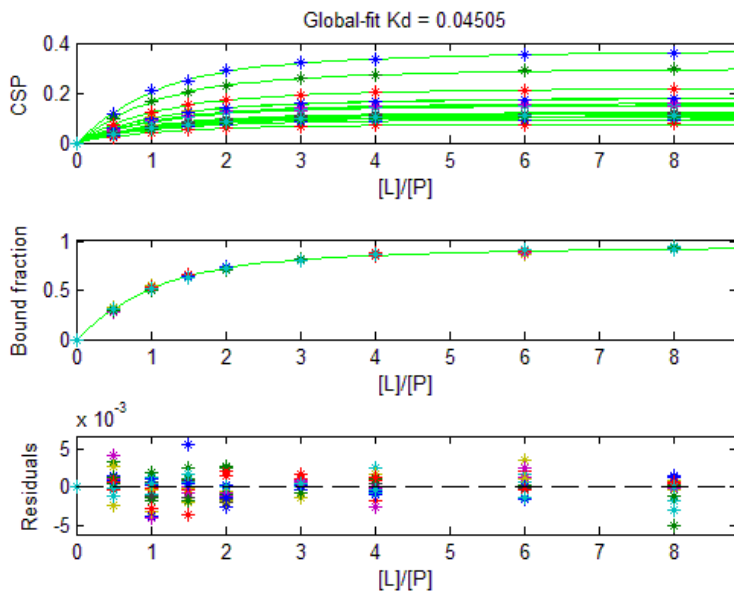


Figure 6-8. Titration fit of ^{15}N labeled hDdi1UBL upon addition of ubiquitin, using KDFIT global. The curves represent the results of global fit of the titration data for the residues having the titration endpoint CSP above a selected threshold, the resulting global-fit K_d values (in mM) are shown on the top. Top panel shows the global fit of CSPs from individual residues as a function of the ligand/protein molar ratio. Middle panel shows the global fit of the bound fraction of the protein as a function of the ligand/protein molar ratio. Bottom panel indicates the residuals from the fit.

6.3 hDdi1UBL binding to K48-Ub₂

Since hDdi1UBL binds with similar affinity to monoubiquitin as yDdi1UBL does, we wanted to test if it is selective for K48-Ub₂ like yDdi1UBL is. We performed a titration of unlabelled K48-Ub₂ into ^{15}N labeled hDdi1UBL. The binding of K48-Ub₂ to hDdi1UBL seems much tighter compared to monoubiquitin, since a lot more peaks attenuated, which is considered a sign of tighter binding. We were unable to obtain a K_d from this titration since most signals that exhibited shifts, attenuated. This data is being analyzed by an undergraduate student in our lab, Lillian Hallmark.

To find out which residues on K48-Ub₂ are involved in binding to hDdi1UBL, we performed a preliminary titration looking at individual domains of K48-Ub₂ and adding in unlabeled hDdi1UBL. Just like hDdi1UBL, a lot of the signals attenuated making it impractical to get a K_d for this interaction from solution NMR as well.

Since we were unable to fit the data from NMR binding assay due to signal attenuations, to determine a K_d for K48-Ub₂ binding to hDdi1UBL, performed ITC measurements in collaboration with Dr. Robert Brinson at IBBR (Figure 6-8). From two experiments, an average K_d of 2.1 μM and stoichiometry of 1:1 was determined. The stoichiometry was estimated to be 1:1, since n was determined to be 1.1. The deltaH and deltaS were determined to be 7.9 kcal/mol and 52.5 cal/mol.K respectively.

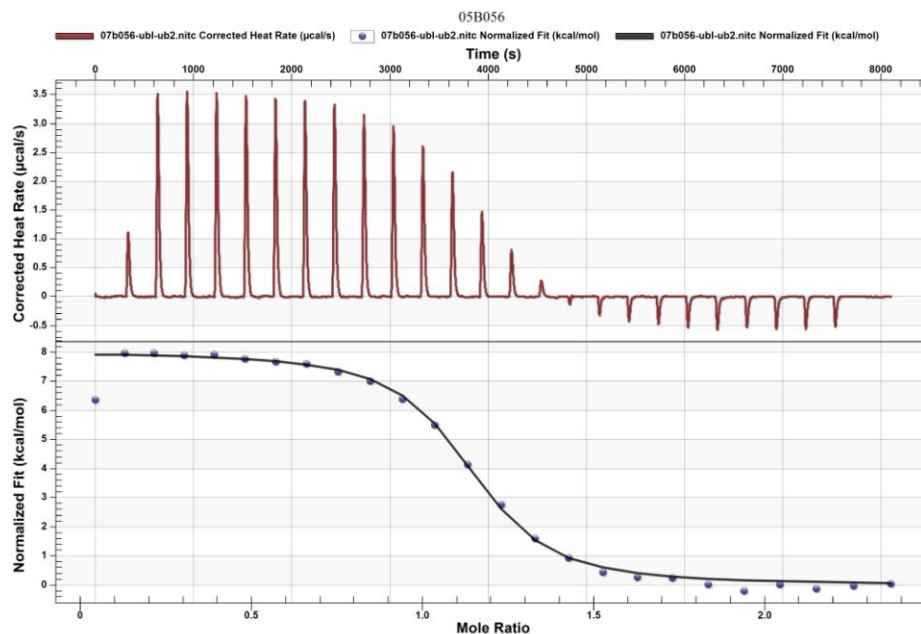


Figure 6-9. ITC titration analysis of hDdi1UBL and K48-Ub₂ binding. The raw data traces are shown in the top panel with the bottom panel illustrating the integrated fit data plots.

From our studies with hDdi1UBL, we can conclude that hDdi1UBL binds ubiquitin with a similar K_d as yDdi1UBL. The unique property of Ddi1UBL to bind ubiquitin is conserved between yeast and human. Moreover, hDdi1UBL binds tighter to K48-Ub₂ compared to monoubiquitin, which is also a property conserved between yDdi1UBL and hDdi1UBL.

Chapter 7: Materials and methods

7.1 Protein Constructs

The UBA construct used in this study contains a full-length UBA2 domain from hHR23A (human isoform A of Rad23), residues 315-363 in the protein sequence (SWS P54725).

Rap80 tUIM construct was obtained from Robert Cohen group. This construct was used for PRE studies. MTSL was attached to residue C121.

Rap80 tUIM sequence is as follows:

```
(M)PSSHHHHHHSSGLVPRGSHMTEEEQFALALKMSEQEAREVNSQEEEEEL  
LRKAI A ESLNSCRPS
```

Tyrosine was incorporated into Rap80 tUIM (C121Y) using site-directed mutagenesis by former labmate Dr. Mark Nakasone for easy quantification by Abs₂₈₀. This construct was used for all studies except when MTSL was attached to Rap80.

Rap80 tUIM (Y) sequence is as follows:

```
(M)PSSHHHHHHSSGLVPRGSHMTEEEQFALALKMSEQE  
AREVNSQEEEEELLRKAI A ESLNS YRPS
```

UIM2 was deleted to check if K6-Ub₂ binding to Rap80 tUIM is avid or not. A tyrosine followed by a stop codon was incorporated after the linker,

Rap80UIM1(Y) sequence is as follows:

```
(M)PSSHHHHHHSSGLVPRGSHMTEEEQFALALKMSEQE AREVNSQEY
```

Phosphorylation mimic was generated using site-directed mutagenesis. S101E Rap80 tUIM (Y) sequence is as follows:

(M)PSSHHHHHSSGLVPRGSHMTEEEQFALALKMSEQEAREVNEQEEEEEL
LRKAIAESLNSYRPS

The yDdi1UBL construct used in these studies contained residues 2–80 of Ddi1 from *S. cerevisiae*²⁸.

7.2 Protein purification

Ubiquitin and hHR23a UBA2 were purified as described elsewhere¹⁹. All Rap80 variants were purified as described by Sims and Cohen⁵⁸. yDdi1UBL and variants were purified as described by Nowicka *et al.*²⁸. All enzymes used for K6-polyubiquitination were purified as described elsewhere : hOtub1⁶³, Ubch7 and NleL⁵⁵. hDdi1UBL was cloned as a Prescission protease cleavable GST-tagged construct. Prescission protease was purified as a GST construct.

7.3 Polyubiquitin Chains generation and purification:

K48 and K63 diubiquitins were generated enzymatically and purified as described elsewhere⁶⁴. Poly-Ub chains were generated and purified by the chemo-enzymatic method as described by Castañeda *et al.*³⁴

All natural K6-linked polyubiquitin chains were generated enzymatically using around 15mgs each of the appropriate ¹⁵N enriched ubiquitin chain terminating mutants (for example, ¹⁵N K6(Boc) and D77Ub for generating ¹⁵N-distal labeled K6-Ub₂) in a 2ml reaction in the presence of protein breakdown mix, 2mM ATP, 3mM TCEP, 100 nM E1, 1.75μM UBCH7 (E2), 7.3μM NleL and 4.5μM hOTUB1 incubated for 5 hours at 37 °C (temperature can be 30 °C). To be confident that there is no residual K48-linked chain, the reaction mixture was vortexed to stop

ubiquitination reaction and then another 13.5 μ M final volume of hOTUB1 was added in the reaction. Reaction was incubated overnight. All enzymes were stored at -80 °C and used fresh out of the freezer. Polyubiquitin chains were separated using cation chromatography on a 5ml HiTrap SPHP column (GE LifeSciences) with a gradient of 50 mM Ammonium Acetate, 1M NaCl, pH 4.5. In case of K6-Ub₂ blocked with D77 on proximal domain & K6(Boc) on the distal domain, the diubiquitin peak was collected, concentrated down to around 1ml and buffer exchanged into 50 mM Tris pH 7.6, 1mM EDTA and 1mM fresh DTT. Removal of D77 was initiated by adding YUH1 at final concentration of 16 ug/ml and incubation for 1 hour at 37 °C⁶⁴. The reaction mix was passed through a 1ml anion exchange Q-FF column (GE LifeSciences) and flow through and 5 ml wash was collected. The flow through and wash was concentrated down to 1ml and buffer exchanged twice into 20 mM Sodium Phosphate buffer. The Boc from position K6 was removed by incubating for five hours at 37 °C after adding 2 % v/v of Trifluoro acetic acid (TFA) final concentration⁶⁵. The chains were further purified using size exclusion chromatography and finally exchanged into 20 mM sodium phosphate, pH 6.8 for NMR studies.

7.4 NMR experiments

NMR samples were prepared in 20 mM sodium phosphate buffer, pH 6.8, 5 % D₂O unless otherwise noted. In addition, if the samples had cysteine and needed to be in reduced form, so no disulfide bonds can be formed, 3 mM TCEP was added. All NMR measurements were performed at 23°C on Avance III 600 MHz and 800 MHz Bruker Biospin spectrometers equipped with cryoprobes. The data was processed

using Bruker software Topspin 3.0 and analyzed using Sparky⁶⁶. For Rap80 tUIM assignment, CARA was used⁶⁷. Relaxation and RDC studies were performed as described elsewhere⁴².

7.4.1 NMR binding assays

All binding experiments were conducted by monitoring changes in the peak positions of ¹H-¹⁵N SOFAST HMQC spectra upon titrations. The changes in peak positions were quantified as amide Chemical shift perturbation (CSP) using the following equation $\Delta\delta=[(\Delta\delta_H)^2+(\Delta\delta_N/5)^2]^{1/2}$, where $\Delta\delta_H$ is the change in the chemical shift for amide proton and $\Delta\delta_N$ is the change in chemical shift of ¹⁵N. Obtained CSP values were used to calculate the binding affinities by fitting different binding models using in-house software KDFIT¹⁹.

7.4.2 PRE Experiments

The paramagnetic spin label 1-Oxyl-2,2,5,5-tetramethyl-3-pyrroline-3-methyl methanesulfonate (MTSL) was from Toronto Research Chemicals Inc. It was attached to the cysteine side chain of the constructs studied as described elsewhere¹⁹. The paramagnetic relaxation enhancement effects were expressed for each amino acid as the ratio of signal intensities in the ¹H-¹⁵N HSQC spectra recorded with MTSL in the oxidized and reduced state. All measurements were performed at 1:1 molar ratio. The reconstruction of MTSL position and distance between spin label and particular amino acid position was determined with the in house program SLFIT⁶⁸.

7.5 DUB inhibition assays

The reactions were run in PBS, pH 7.4, at room temperature. The initial concentration of K48-Ub₂ or K63-Ub₂ was 20 μM, K27-Ub₂ was at 100 μM, and IsoT was at 20 nM. The monoUb bands were integrated using ImageJ.

Chapter 8: Discussion and Future Direction

8.1 Discussion

In the first part of this work, we presented a comprehensive characterization of the solution structure of K6-linked diubiquitin and provide information about its possible function *in vivo*. We showed using solution NMR, small angle neutron scattering and computational ensemble studies that K6-linked diubiquitin structure is most likely present in two-state solution conformers. Since we know that K6-Ub₂ chains are present on BRCA1-BARD1 complex that is part of the DNA Damage Repair (DDR) pathway and one of the solution conformers represented a structure similar to Rap80 tUIM bound K63-Ub₂, we studied how K6-Ub₂ interacts with Rap80 tUIM using NMR binding studies. We show that K6-linked diubiquitin binds Rap80 tUIM in an avid manner that might be similar to K63-linked diubiquitin. We also show that unlike K63-Ub₂ that binds in a directional manner, Rap80 tUIM does not have a specific orientation in which it binds to K6-linked diubiquitin. We also show the effect of phosphorylation of S101 in Rap80 on the interaction with K6-Ub₂ by mutating S101 to a phosphorylation mimic E101. The mutation reduces the binding to K6-linked diubiquitin but very weakly. Looking at the residues involved and effect of salt on the binding affinity we also showed that electrostatic interactions play some role in the binding of Rap80 tUIM to K6-linked diubiquitin.

As mentioned before, the major conformer from the ensemble analysis using solution NMR data and SANS data resembles the structure of hHR23a UBA2 bound K48-Ub₂ and does have enough space for the hHR23a UBA2 to bind it in sandwich-mode. We were able to show using solution NMR binding studies that K6-Ub₂ binds

to hHR23a UBA2 with similar affinity as K48-Ub₂. Looking at the CSPs on the backside of ¹⁵N labeled hHR23a UBA2 upon addition of unlabeled K6-Ub₂, it also looks like K6-Ub₂ binds UBA2 in a sandwich-like mode similar to K48-Ub₂. Using PRE analysis of the whole ensemble of K6-Ub₂ structures generated using SASSIE, we have a conformer of K6-Ub₂ that fits best to the PRE data and has enough space between it for hHR23a UBA2 to fit in (Figure 8-1).

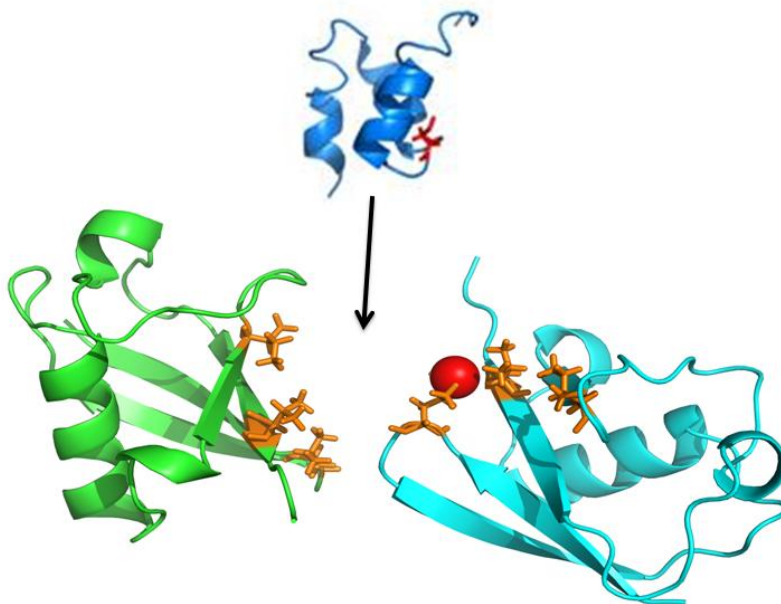


Figure 8-1. Conformer from SASSIE generated ensemble whose coordinates gave the best fit of the PRE effect on K6-Ub₂ labeled on distal domain (green) and proximal domain (cyan) upon addition of hHR23a UBA2 with MTSL attached at position C334. Red sphere represents MTSL position estimated from the fit. Orange sticks represent L8, I44 and V70 hydrophobic patch. PDB structure of Uba2 (blue) shown with C334 position represented by red sticks.

In addition to the structural and functional characterization of K6-linked diubiquitin, we also characterized possible role of K27-Ub₂ in DDR by studying its interaction with Rap80 tUIM. Similar to K6-Ub₂, K27-Ub₂ is also shown to be present in two-state solution conformers and one of the conformers is similar to Rap80 tUIM bound K63-Ub₂ structure. Moreover, Gatti *et al.*⁴⁷ have shown by

performing a pull-down assay that K27-Ub₂ interacts with Rap80 tUIM but no one had studied this interaction in solution. So, using NMR binding studies we were able to characterize the binding of K27-Ub₂ to Rap80 tUIM. K27-Ub₂ interacts with Rap80 tUIM in a similar manner to K6-Ub₂. It also shows similar binding affinity most likely due to avidity effect. Most likely, there is no directionality in binding unlike K63-Ub₂ binding to Rap80 tUIM. We also show that K27-Ub₂ inhibits DUB activity of IsoT against K48- and K63-Ub₂. This inhibition means K27-Ub₂ can be potentially utilized as a competitive inhibitor of DUBs.

From previous studies by Dr. Urszula Nowicka, we know that unlike other well-studied UBLs, yeast **DNA Damage Inducible 1 UBL** (yDdi1UBL) surprisingly binds ubiquitin²⁸. We determined that this interaction is based on the difference of charges between yDdi1UBL and ubiquitin as hypothesized by her. From analysis of the difference in binding to mutants of ubiquitin, R42 on ubiquitin seems to be most important for this binding. We also show that there is specificity in yDdi1UBL binding to K48-linked diubiquitin. K48-Ub₂ binds tightly compared to K63-Ub₂, K6-Ub₂, K11-Ub₂, K27-Ub₂ and monoUbiquitin. The binding of K48-Ub₂ is weakened upon mutating the “back-side” (A30S, L31K). We also demonstrate that L31K mutation is enough for the reduced binding. Using PRE analysis, we illustrate that there is a potential directionality in binding of K48-Ub₂ to yDdi1UBL. We are awaiting a HADDOCK generated solution model of the K48-Ub₂:yDdi1UBL complex by our collaborator Dr. Olivier Walker using CSPs and PRE data from us. The specificity of binding to K48-Ub₂ gives more weight to the hypothesis that yDdi1UBL might be involved in proteasomal system as an alternative proteasome

shuttle, where roles of both UBA and UBL can be handled by UBL alone, as hypothesized by our collaborator Dr. Urszula Nowicka. She also hypothesized this for hDdi1. This is especially interesting considering hDdi1 unlike yDdi1 lacks the UBA domain. Also, there is little sequence similarity between hDdi1UBL and yDdi1UBL, particularly the absence of the “back-side” binding sequence. So, we studied the hDdi1UBL interaction with ubiquitin using solution NMR. We found that hDdi1UBL indeed binds to ubiquitin with a similar K_d as yDdi1UBL. We also show that it binds tighter to K48-Ub₂ as compared to monoubiquitin. Since, hDdi1UBL has never been studied by solution NMR, fellow graduate student Westley Pawloski assigned the hDdi1UBL spectrum. We also setup crystallization screening trays and were able to crystallize hDdi1UBL. We collected diffraction data of the crystals but the data was not good enough to determine the structure. We have also purified hDdi1UBL with selenomethionine incorporated instead of cysteine, which we hope will help us with phasing, once better quality diffraction data is collected.

In summary, we were able to characterize structural and potential function of K6-diubiquitin. We characterized K27-Ub₂ interaction with Rap80 tUIM. Moreover, yDdi1UBL binding to different ubiquitin chains was studied in detail and it was determined that yDdi1UBL binds specifically tighter to K48-Ub₂ compared to monoubiquitin and other diubiquitins we tested. This specific binding can be removed by mutating one amino acid on yDdi1UBL (L31K). It was also established that hDdi1UBL indeed binds ubiquitin and shows tight binding to K48-Ub₂ compared to monoubiquitin.

8.2 Future directions

The research presented in this work provides insights into the structure and function of K6-Ub₂. Alongside these results, our collaborators at Colorado State University, Prof. Robert Cohen and Dr. Yun-Seok Choi also performed additional binding studies using fluorescence anisotropy by attaching a fluorescent label on Rap80 tUIM. For the K6-Ub₂ interaction with Rap80 tUIM, it mostly complements our results. We sent them K6- and K63-linked triubiquitins to test the effect of increasing the ubiquitin chain length on the binding to Rap80 tUIM. They have interestingly observed that K6-Ub₃ and K63-Ub₃ bind tighter to Rap80 tUIM than their respective diubiquitins. Currently, they are studying effect on the binding of mutants of K6-linked triubiquitin to Rap80 tUIM to deduce a model of the binding. Moreover, they have also studied the effect of the linker length and composition on binding of K6-Ub₂ and K6-Ub₃ to Rap80 tUIM. In the future, it will be useful to try and study the interaction of a few specific linker mutants of Rap80 tUIM with K6-Ub₂ by solution NMR to have more residue specific information. Furthermore, it will be particularly worthwhile to try and co-crystallize K6-Ub₃ with Rap80 tUIM, since due to its tighter affinity we might be able to co-crystallize them unlike K6-Ub₂ with Rap80 tUIM.

Also, we have sent K27-Ub₂ to our collaborators and it will be interesting to see if fluorescence anisotropy will complement our solution NMR data. Similar to K6-diubiquitin and triubiquitin studies, it will be worthwhile to test how linker composition and length of Rap80 tUIM affects binding to K27-Ub₂. In the future, it will also be interesting to test K27-Ub₃ binding to Rap80 tUIM to see if an extra Ub

unit makes a difference for K27-linked ubiquitin chains too. From our studies, it looks like both K6- and K27-linked ubiquitin chains are involved in DDR pathway and it will be interesting to study their interaction with other proteins known to be involved in the pathway.

Moreover, for K6-Ub₂ interaction with hHR23a UBA2, using the distance constraints from the PRE experiments and information from CSPs about residues that are involved in the interaction, we can generate a robust model of the complex using HADDOCK. This data should be sent to our collaborator Olivier Walker for a solution model of the complex.

For the Ddi1UBL studies, we think there is a lot of potential information that still needs to be gathered with regards to the hDdi1UBL. Firstly, it will be interesting to characterize the structure of hDdi1UBL by crystallizing it or by solution NMR and compare it with yDdi1UBL. Secondly, it will be interesting to try and co-crystallize K48-Ub₂ with hDdi1UBL to obtain a structure of the complex. To complement this crystal structure, it will be interesting to get a HADDOCK generated solution model of the complex by using CSP data and by performing PRE experiments. Moreover, like with yDdi1UBL, we can also test hDdi1UBL interaction with other diUbs to confirm if any of the other diUbs also bind as tightly as K48-Ub₂ to hDdi1UBL.

8.3 Conclusion

Structural studies that show K6-Ub₂ might exist in conformers that are similar to ligand-bound forms of both K48- and K63-Ub₂ suggest that there might be redundancy in how ubiquitin signaling works. Our study with K6- and K27-Ub₂ lead us to question the dogmatic view plaguing the ubiquitin field that proteasomal and

DNA damage repair signaling are mutually exclusive. The results demonstrating that K6- and K27-Ub₂ interact strongly with receptors from the proteasomal (hHR23a UBA2) and DNA damage repair (Rap80 tUIM) pathways, illustrate that both these chains might be involved in proteasomal signaling as well as DNA damage repair pathway. Since it is shown that yeast cells in which ubiquitin has its K63 mutated to R are still viable, might mean that K6 or K27-linked chains are able to take over its function in the DDR pathway³¹. The work presented here and results from our paper⁴¹ demonstrate that both K6- and K27-Ub₂ interact with hHR23a UBA2 with a similar binding affinity as K48-Ub₂. Moreover, it is known that ubiquitin with K48 as the single lysine cannot support yeast viability³¹, which might mean that other chains play an important role for proteasomal signaling alongside K48-linked chains. This leads us to propose that the redundancy in structure and function shown here, allows the cells to survive under stress where function of K48- or K63-linked chains is somehow hampered.

Our studies with yeast and human orthologs of Ddi1UBL question another ubiquitin field dogma that a proteasomal shuttle requires both a UBA domain and a UBL (Figure 6-2). Nowicka *et al.* demonstrated that yDdi1UBL is the first UBL shown to bind ubiquitin tightly²⁸. Our results give further support to the hypothesis proposed in that paper that an alternative proteasomal shuttling system might exist where the proteasomal shuttle does not require a UBA domain for its function (Figure 6-2). This is especially important to understand the role of Ddi1 in humans since it does not contain a UBA domain. It has been shown that yDdi1UBL plays a role in the proteasomal degradation pathway and by showing that human Ddi1UBL binds K48-

Ub₂ as tightly as yeast Ddi1UBL, we propose that even in humans, Ddi1 might be part of the proteasomal signaling system. It is still unknown whether hDdi1UBL is able to bind a receptor on proteasome or not. In the future, if we can show that hDdi1UBL interacts with a proteasomal receptor, we will be able to indisputably confirm this hypothesis and disprove the existing dogma that UBA domain is required in a proteasomal shuttle.

Appendices

Attempt to co-crystallize Rap80 with K6-Ub₂

We tried to co-crystallize K6-Ub₂ and Rap80 tUIM in an attempt to determine the structure of the complex. We obtained crystals in two conditions (0.05M Zinc acetate dihydrate +20% w/v Polyethylene glycol 3,350 and 0.2 M Sodium acetate trihydrate pH 7.0+20% w/v Polyethylene glycol 3,350) (Figure i). They were cubic in shape and were not birefringent.

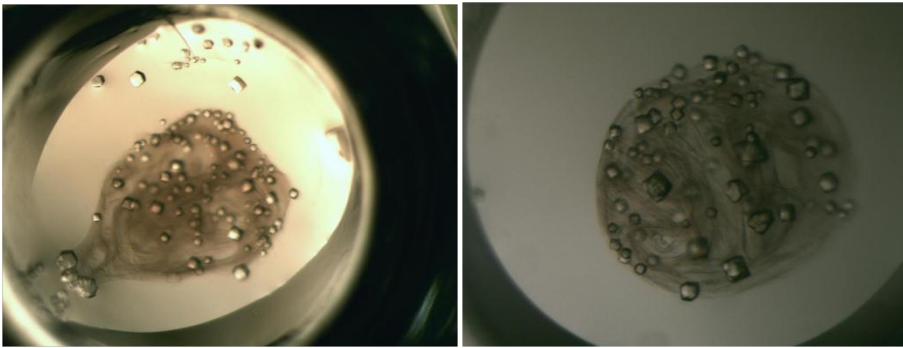


Figure i. Crystals from K6-Ub₂: Rap80 tUIM mix formed in 0.05M Zinc acetate dihydrate +20% w/v Polyethylene glycol 3,350 (left) and 0.2 M Sodium acetate trihydrate pH 7.0+20% w/v Polyethylene glycol 3,350 (right).

To confirm that the crystals were formed by protein and not by salt, 15% SDS PAGE gel was run. Upon running the gel, we realized that the crystals consisted of protein but only of K6-linked Ub₂ and not K6Ub₂:Rap80 tUIM complex (Figure ii). The Rap80 tUIM band seen in the sample from the crystal is similar in intensity to the Rap80 tUIM band seen in the wash buffer. We tried to crystallize it again after letting the mix of Rap80 tUIM and K6-linked Ub₂ incubate overnight and running size-exclusion chromatography to separate the complex from the individual proteins. No crystals were obtained.

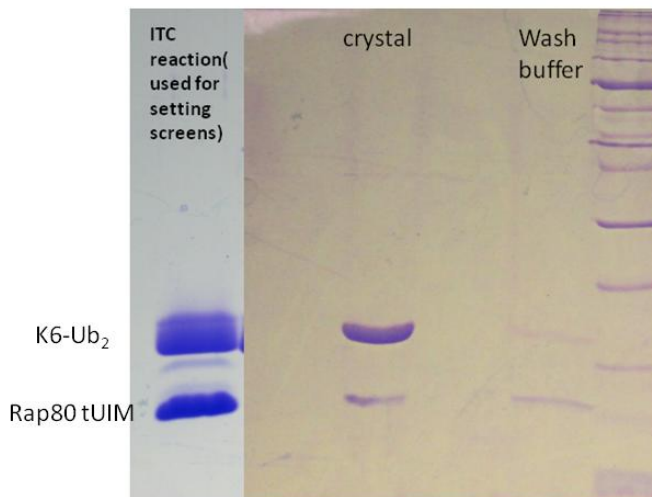


Figure ii. 15% SDS PAGE of crystals formed in 0.05M Zinc acetate dihydrate +20% w/v Polyethylene glycol 3,350.

Effect of salt on yeast Ddi1UBA binding to Ubiquitin:

Titration of ¹⁵N labeled yDdi1UBA with monoubiquitin in the presence and absence of salt to understand the effect of salt on binding was performed. Although the binding interface was conserved, the binding affinity was weakened almost two-fold in the presence of salt (150 mM NaCl) compared to no salt (Figure iii).

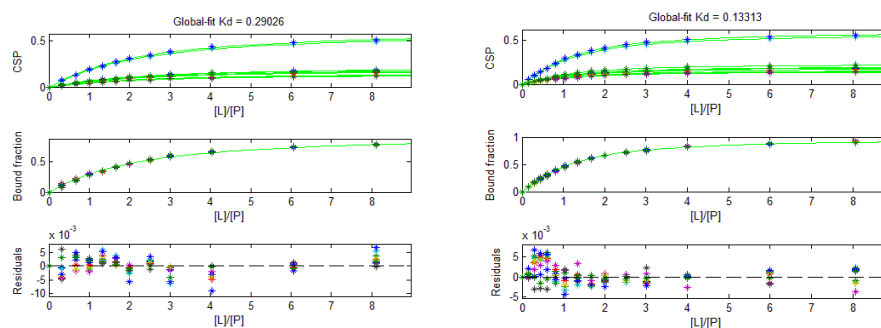


Figure iii. Titration fit of ¹⁵N labeled Ddi1UBA with ubiquitin in the presence (left) and absence (right) of salt using Kdfit global. The curves represent the results of global fit of the titration data for the residues having the titration endpoint CSP above a selected threshold, the resulting global-fit K_d values (in mM) are shown on the top. Top panel shows the global fit of CSPs from individual residues as a function of the ligand/protein molar ratio. Middle panel shows the global fit of the bound fraction of the protein as a function of the ligand/protein molar ratio. Bottom panel indicates the residuals from the fit.

Ubiquitin 62 Project:

While attempting to express K63(Boc) ubiquitin for synthesis of K63-linked diubiquitin chains using chemo-enzymatic method, we found that instead of incorporating Lys(Boc) at amber codon (TAG), the tRNA machinery recognizes it as a stop codon leading to a truncated ubiquitin. We named this protein Ub62 since it truncates after 62 amino acids. Ub62 is missing the residues K63-G76 which include a β -sheet and the highly flexible tail (Figure iv, red).

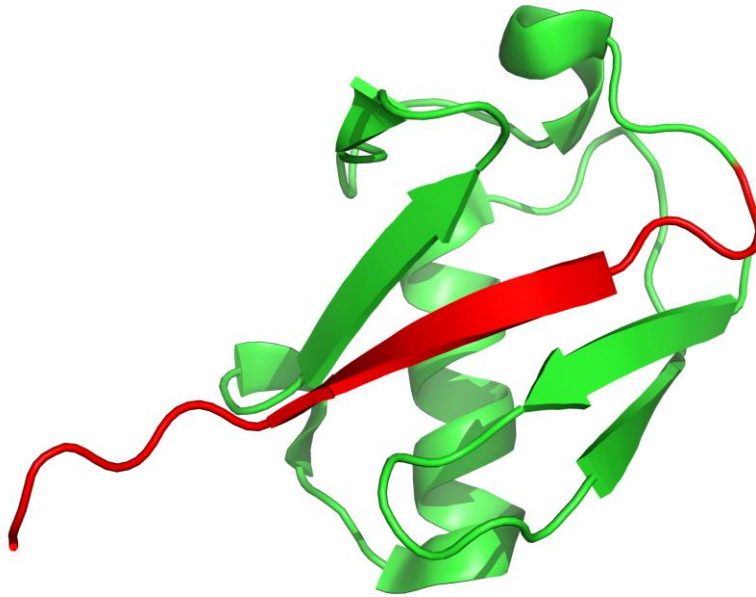


Figure iv. Cartoon structural representation of ubiquitin indicating the residues missing in Ub62 (K63-G76) in red (PDB: 1D3Z).

We purified this protein using the same method as for wild type ubiquitin, except that instead of cation-exchange we used anion-exchange chromatography. It runs as a single band on 15% SDS PAGE (Figure v).

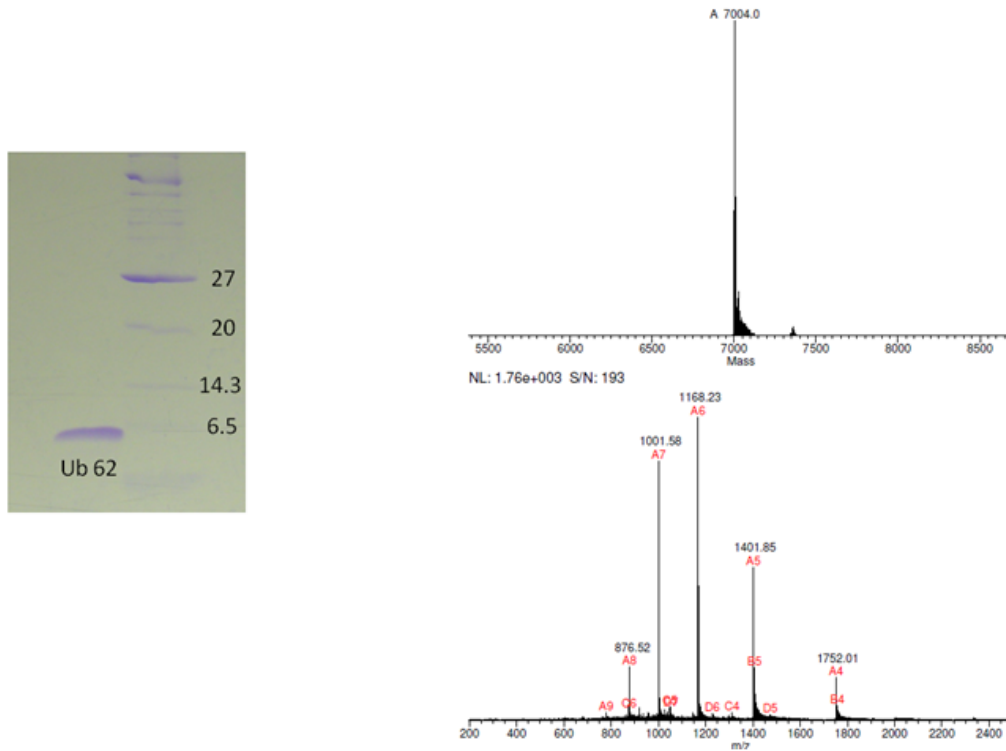


Figure v. Coomassie-stained 15% SDS PAGE gel of Ub62 (left). Deconvoluted ESI-MS of Ub62 (right). The expected mass is 7003.98 Da.

Upon purifying the protein, we collected a ^1H - ^{15}N SOFAST HMQC spectrum. From the spectrum, we determined that it is folded since the amide signals are well spread. But there are a lot more peaks compared to wild type ubiquitin (Figure vi).

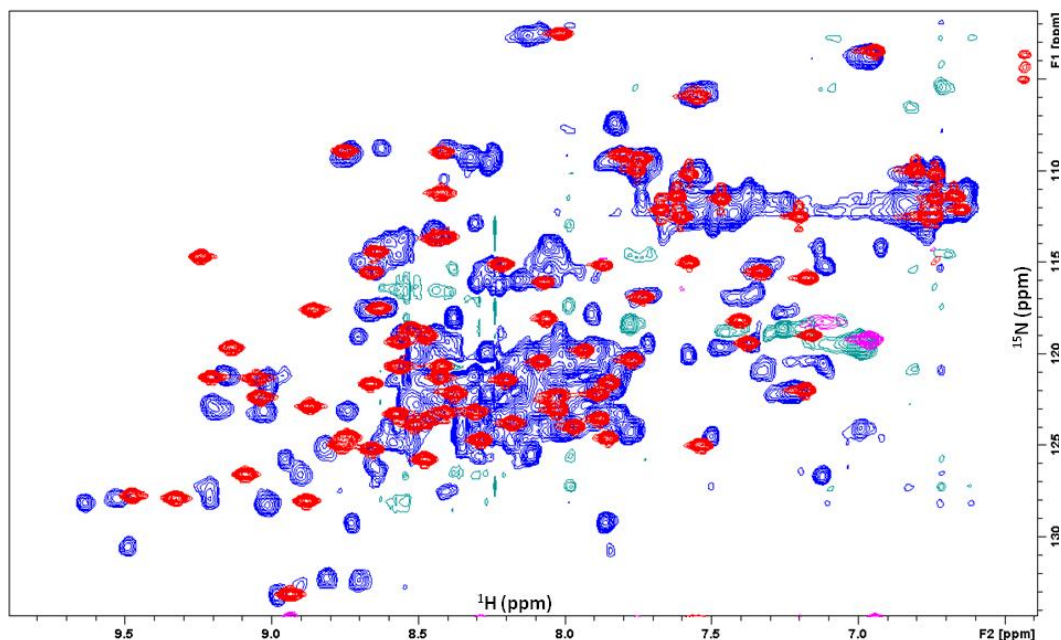


Figure vi. Comparison of ^1H - ^{15}N SOFAST HMQC spectra of wild type ubiquitin (red) and Ub62 (blue).

To confirm that this property of Ub62 was not because of its instability and the result of being exposed to harsh acidic conditions during purification, we purified it with a relatively gentler heat precipitation method. The cells were harvested and lysed in the same way as for wild type ubiquitin and the lysed cells were heated to 55 °C (lower than ubiquitin accounting for more possible instability) for 10 minutes to precipitate proteins other than Ub62. After that the sample was purified with the same protocol as wild type ubiquitin. After purifying ^{15}N labeled Ub62, another ^1H - ^{15}N SOFAST HMQC was collected and upon overlaying this spectrum with the spectrum of Ub62 purified using acid precipitation, we observed that it still behaves in a similar manner (Figure vii).

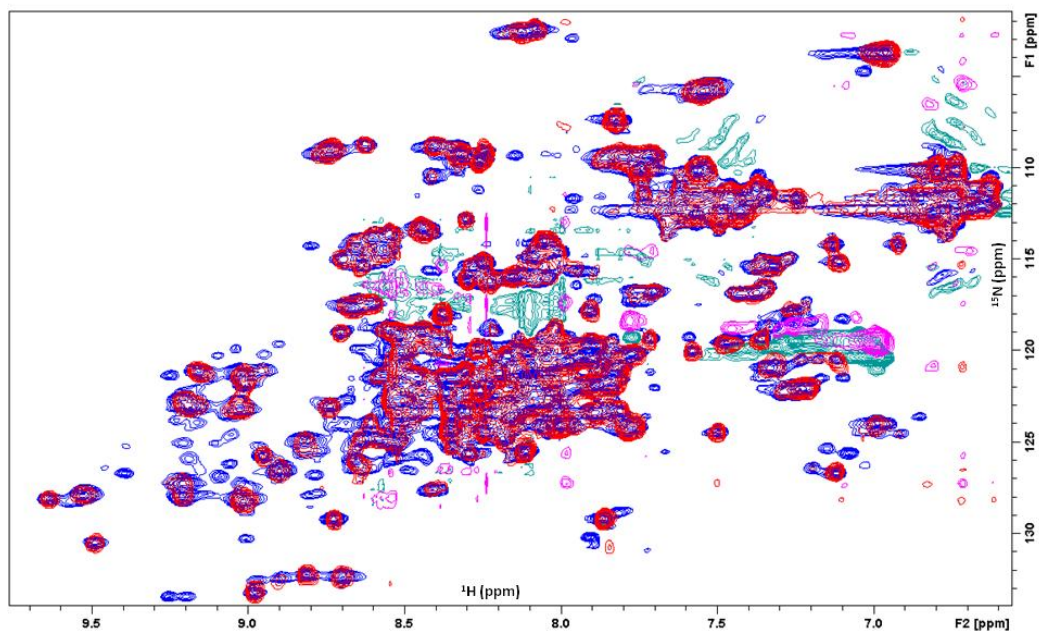


Figure vii. Comparison of ^1H - ^{15}N SOFAST HMQC spectra of Ub62 purified using acid precipitation plus anion exchange chromatography (red) and purified using heat precipitation plus cation exchange chromatography (blue).

UBA of ubiquilin-1 is one of the strongest ubiquitin binders, and we wanted to (1) examine if the ligand binding properties are preserved in Ub62 and (2) if it binds, we hoped that the binding will capture Ub62 as a single conformer. Adding the ligand to a final molar ratio of 1:1 did not have any significant effect on the signals of Ub62 (Figure viii) indicating that the removal of residues 63-76 abolished UBA binding.

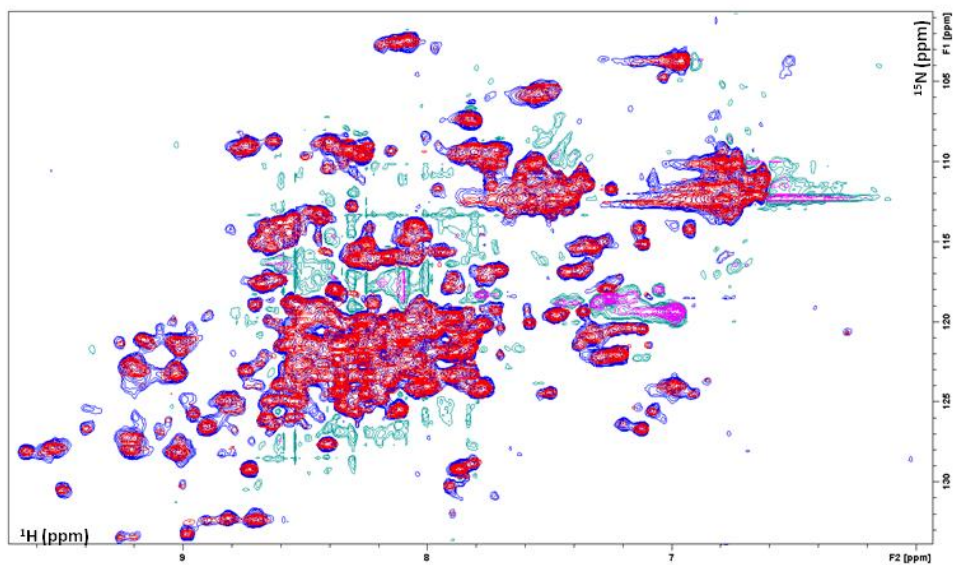


Figure viii. Comparison of ^1H - ^{15}N SOFAST HMQC spectra of Ub62 before (red) and after (blue) the addition of ubiquitin-1 UBA in a 1:1 molar ratio.

We also tested if unfolding by 8M urea and slow refolding of Ub62 by dialyzing the denaturant away in a stepwise manner will help refold Ub62 to a conformer with fewer signals. However, the multiple signals remained.

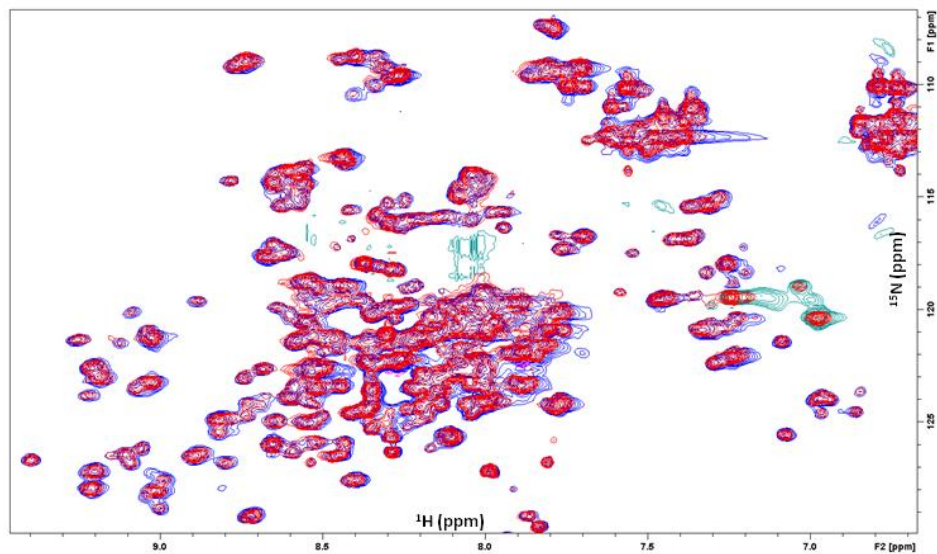


Figure ix. Comparison of ^1H - ^{15}N SOFAST HMQC spectra of Ub62 before denaturation by 8M urea (blue) and after denaturation/refolding (red).

We attempted to determine the secondary structure of this protein by circular dichroism (CD) spectroscopy. The CD spectrum (Figure x) suggests a significant β -sheet content. In the future, it will be worthwhile to compare it with circular dichroism spectrum of ubiquitin.

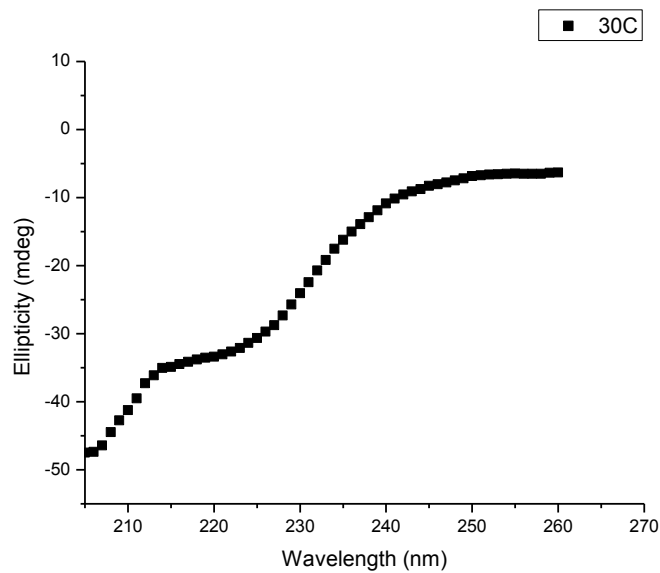


Figure x. Circular dichroism spectrum of Ub62 at 30 °C.

Furthermore, using CD spectroscopy, we performed temperature melting studies on Ub62 to test its stability. This would be good spectra to compare with wild type ubiquitin CD temperature dependence spectra. It can be seen from the spectra that as the temperature increases there is loss in secondary structure.

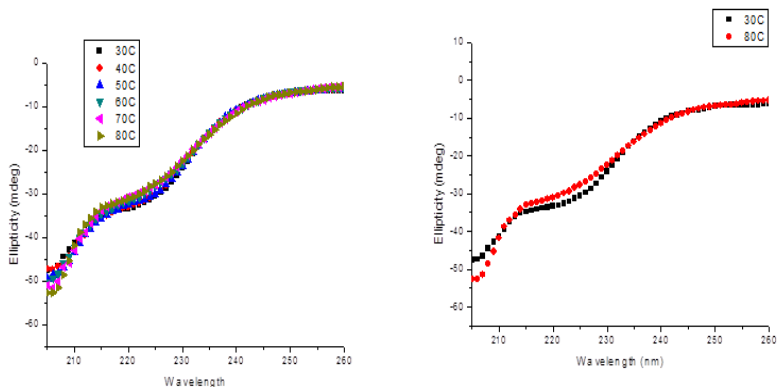


Figure xi. Circular dichroism spectra of Ub62 at different temperatures. On the left are circular dichroism spectra for a range of temperature, from 30-80 °C while on the right circular dichroism spectra at only two temperatures (30 °C and 80 °C) is shown to better illustrate the effect of temperature.

Moreover, we also observed the unfolding effect of Ub62 with temperature by following the change in CD at 222nm. The decrease in CD indicates loss of helicity. The protein loses all its helicity at around 65°C.

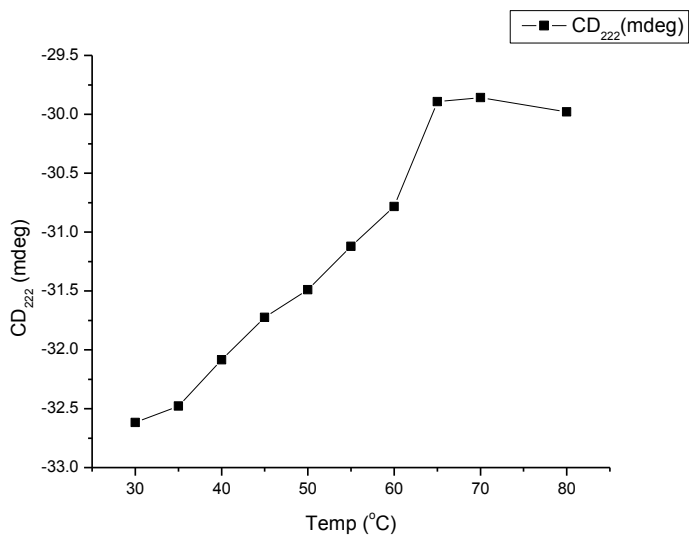


Figure xii. Change in ellipticity of Ub62 at 222nm as a function of temperature.

Since we could not capture a single conformer of Ub62 by any of the methods mentioned above, we hypothesized that if we add the peptide that is missing, it might

click into place and form the missing β -strand, and result in a single set of NMR amide signals comparable to those of ubiquitin. The peptide containing residues K63-G76 (referred to as C-terminal peptide) from Biomatik. It was dissolved in 20 mM Sodium phosphate (NaP) pH 6.8. Upon titrating it into Ub62, we did not detect any shifts in the signals of Ub62.

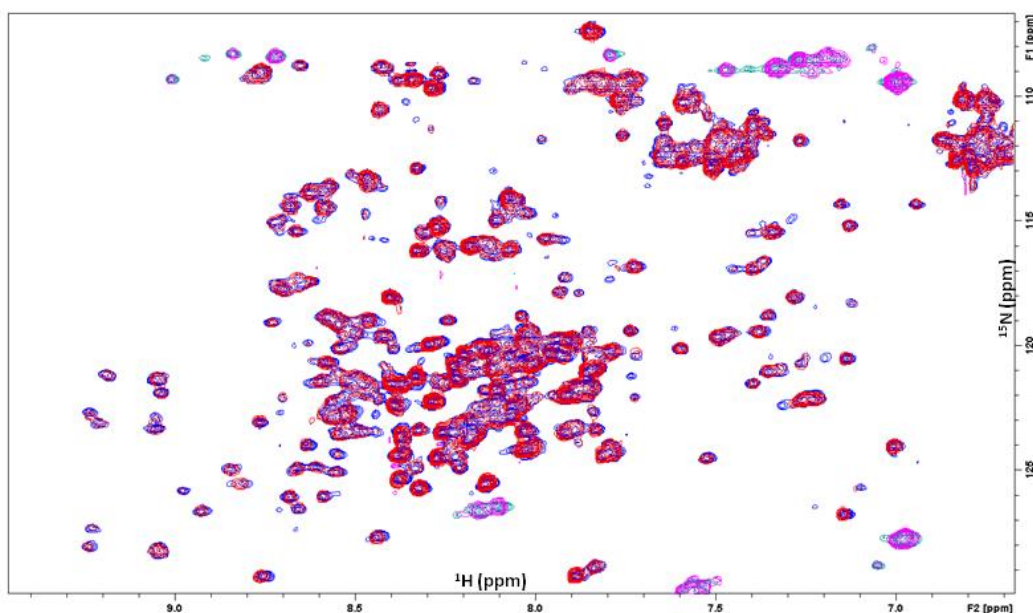


Figure xiii. Comparison of the ^1H - ^{15}N SOFAST HMQC spectra of Ub62 before (blue) and after (red) adding the C-terminal peptide.

One of the possible reasons the signals did not shift was that the peptide might not have dissolved well at pH 6.8, thus we added 10% (v/v) acetic acid to the NaP buffer containing the peptide. Upon titrating this into Ub62 and collecting ^1H - ^{15}N SOFAST HMQC spectrum, we observed that some signals shifted but we also noticed that some new signals started to show up (Figure xiv, black box) that are indicative of lower pH of the sample. Probably, the shift in signals of Ub62 was caused by the pH change and not by the interaction with C-terminal peptide.

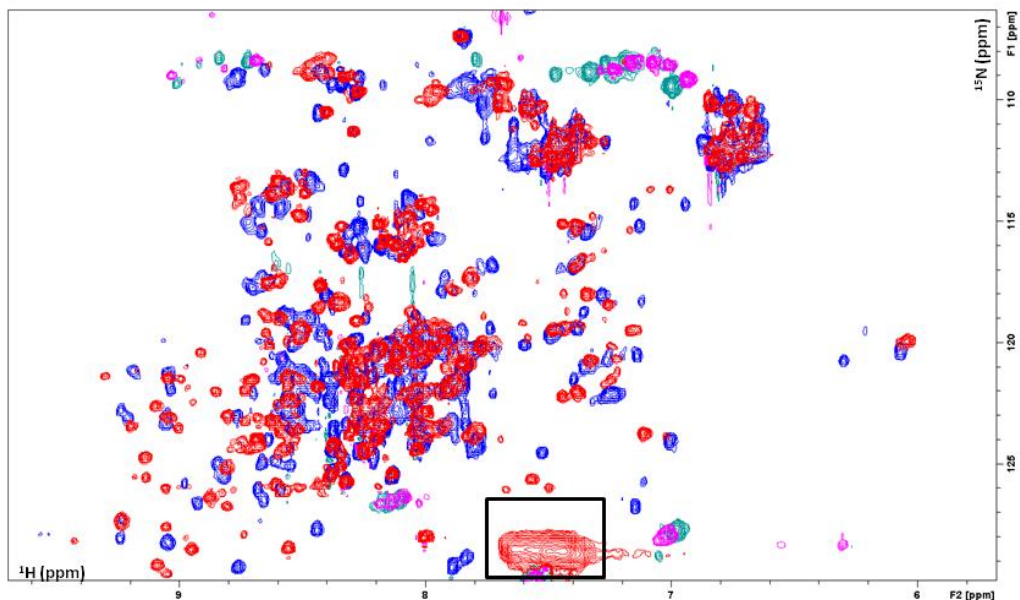


Figure xiv. Comparison of the ^1H - ^{15}N SOFAST HMQC spectra of Ub62 with C-terminal peptide in 20mM NaP pH 6.8 (blue) and upon addition of 10% v/v acetic acid (red). Black box illustrates new amide signals that start to show up indicating lower pH.

Next, we tested if for the peptide to click into place, it needs Ub62 to be completely denatured. Ub62 was denatured by heating the sample incrementally to a temperature of 345 K (72 °C) in the NMR magnet and then refolded by bringing the temperature back to 296 K (23 °C), however it still showed the same spectrum (Figure xv).

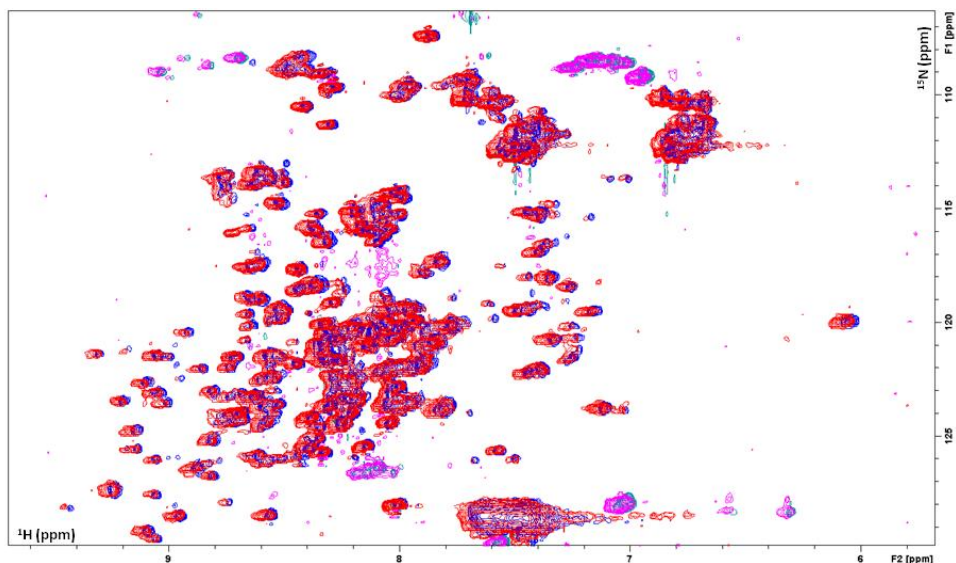


Figure xv. Comparison of ^1H - ^{15}N SOFAST HMQC spectra of Ub62 before (blue) and after (red) denaturing by increasing the temperature to 72 °C and refolding back by reducing temperature to 23 °C. The sample is in 10% v/v acetic acid in 20 mM NaP.

Another attempt was made to denature and renature Ub62 in the presence of C-terminal peptide, especially since in the previous attempt the buffer conditions were acidic. We denatured the protein in 8M urea and slowly refolded it in the presence of C-terminal peptide by incrementally diluting the denaturant. We used a dialysis bag of cutoff 1 kDa since the peptide is 1.5 kDa. After diluting out the denaturant by performing multiple dialyses, we collected ^1H - ^{15}N SOFAST HMQC spectrum. There was no significant change in the signal shifts. One of the possible reasons is that the peptide was lost from the dialysis bag.

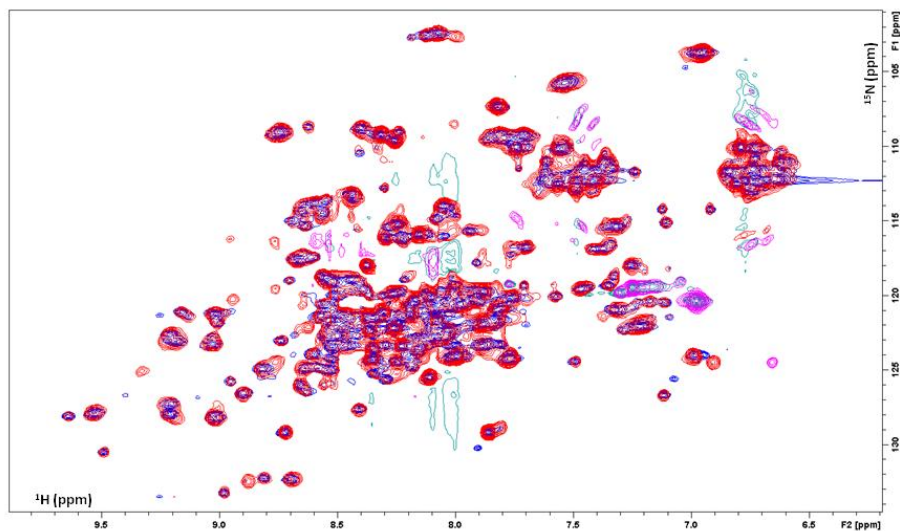


Figure xvi. Comparison of the ^1H - ^{15}N SOFAST HMQC spectra of Ub62 with C-terminal peptide before (blue) and after (red) denaturing by 8M Urea and refolding in 20 mM NaP pH 6.8.

We also attempted to crystallize Ub62. Crystallization screening experiments with Index and PEG screens were performed. No crystals were obtained.

In summary, although it is an interesting discovery that ubiquitin is capable of forming a folded structure without its β -5 strand and tail; we have been unable to find a way to capture it in a single conformer.

Immobilize K6-linked polyubiquitin chain and perform pull-down assays:

As shown before we can synthesize fully natural K6-linked polyubiquitin chains. In order to determine its function *in vivo* we performed pull-down assays to identify its novel binding ligands from the cell extracts of interest. The first step towards performing a pull-down assay is to attach an affinity tag to the protein that one wants to use as bait. In our case, it was K6-linked polyubiquitin chain. The

affinity tag we attempted to use was biotin because of its high specificity for its binding partner streptavidin or a similar strep-tagTM II which has been shown to be more specific than biotin for its binding partner.

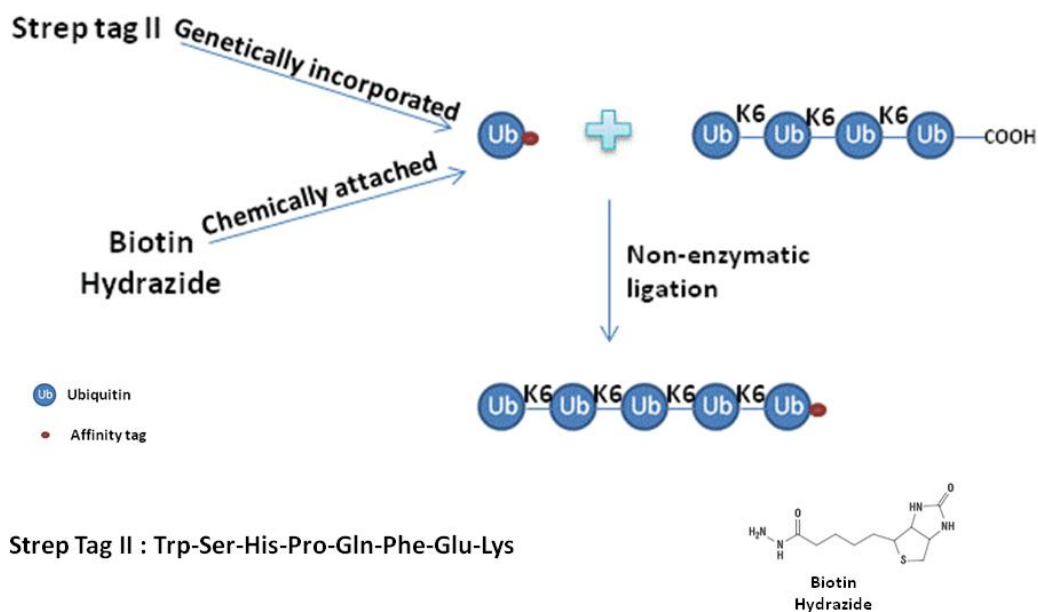


Figure xvii. Schematic representation of attaching either strep-tagTM II or biotin hydrazide to K6-linked polyubiquitin chains in order to immobilize the chains for pull-down assays.

EZ-Link Hydrazide-Biotin is a commercially available biotinylating agent. An attempt to attach biotin to the polyubiquitin chain using this chemical was performed in collaboration with Dr. Carlos Castañeda. The method we proposed was to use the same reaction used for ubiquitin ligation by using ubiquitin with activated C-terminus (UbCOSR) and biotin hydrazide. The $-NH_2$ group of biotin hydrazide will act like a nucleophile and attack the carbon of the thioester group. If the tag is linked successfully to the chain, the expected increase in molecular weight will be around 115 Dalton, since we are replacing the 125 Dalton MESNA by 240 Dalton biotin hydrazide ($240-125=115$ Da) and it can be confirmed using ESI-MS. Once the biotin

is attached to the polyubiquitin chain, we can immobilize it on a column containing streptavidin resin. Multiple attempts were made as described below:

Attempt 1:

The first condition we tried was the one mentioned in the document we obtained from Thermo Scientific with the Biotin Hydrazide material. In that protocol, instead of using EDC ((3-Dimethylaminopropyl)-3-ethylcarbodiimide Hydrochloride, a compound which activates carboxyl groups to bind to the $-NH_2$ group from the biotin molecule), we just used an activated Ub (UbCOSR). 5 mgs of UbCOSR in 500 μ l 0.1 M MES (2-(N-morpholino)ethanesulfonic acid buffer) + 25 μ l of 50 mM Hydrazide biotin solution (EZ-Link Hydrazide Biotin from Thermo in DMSO). It was incubated overnight at room temperature with mixing.

We did not observe the increase in mass as expected using ESI-MS. The COSR(R=MESNA) gives a mass addition of 125 Dalton to the WT Ub (final weight of 8689 Da) and EZ-link Biotin Hydrazide adds 240.11 Da. So the total mass added to WT Ub after the reaction should be $240-125 \approx 115$ Da (a final weight of 8804 Da). This was not observed as seen in Figure xviii

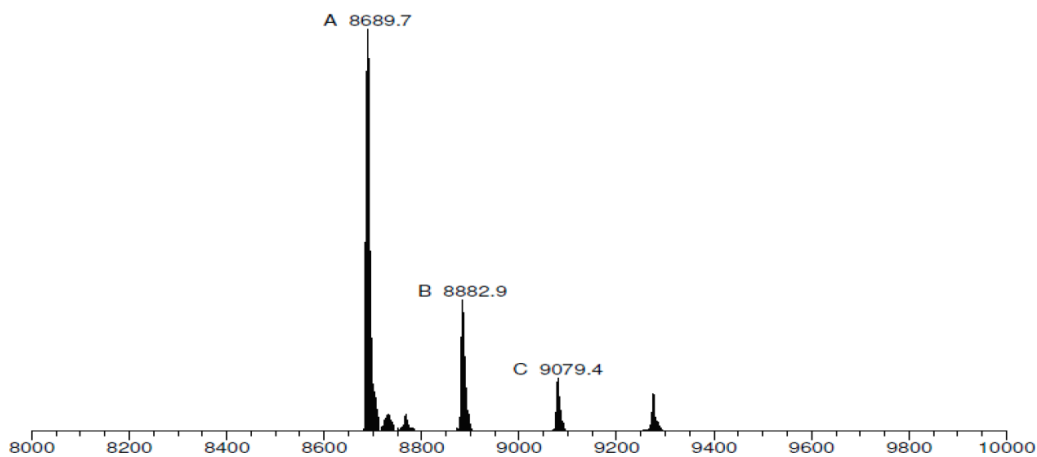


Figure xviii. Deconvoluted ESI-MS of the following reaction: 5mgs of UbCOSR in 500 μ l 0.1M MES buffer + 25 μ l of 50 mM Hydrazide biotin solution (EZ-Link Hydrazide Biotin from Thermo Scientific in DMSO). It was incubated overnight at room temperature with mixing. Expected mass is 8804 Da.

Just to confirm that the MES buffer is not affecting the signals, we buffer exchanged the sample to water and ran MS again. We obtained the same result as before, see Figure xix.

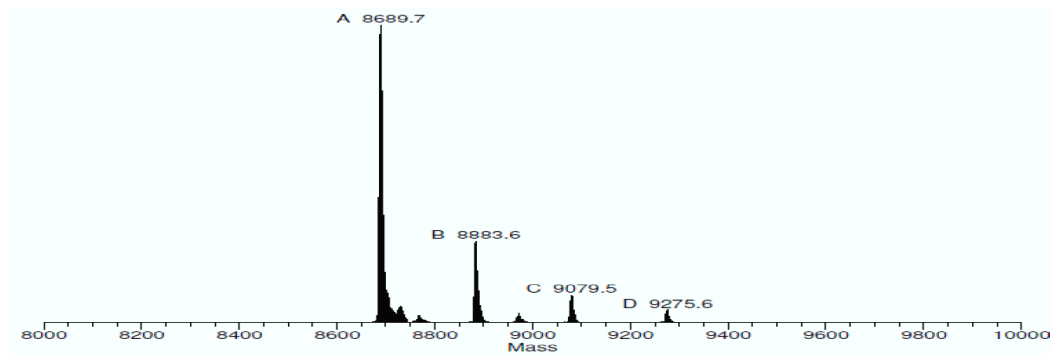


Figure xix. Deconvoluted ESI-MS of the following reaction: 5mgs of UbCOSR in 500 μ l 0.1 M MES buffer + 25 μ l of 50 mM Hydrazide biotin solution (EZ-Link Hydrazide Biotin from Thermo Scientific in DMSO). It was incubated overnight at room temperature with mixing. Buffer exchanged into water before performing ESI-MS. Expected mass was 8804 Da.

Attempt 2:

Next, to check if EDC can activate the carboxyl group and make it a better leaving group, thus helping in labeling Ub with Biotin Hydrazide, we tried these two protocols with different buffers and pH:

Protocol A:

2.5 mgs ^{15}N WT Ub in 970 μl 0.1 M MES buffer pH 4.8

25 μl 50 mM Biotin hydrazide in DMSO

12.5 μl of 100 mg/ml EDC solution in 0.1 M MES buffer pH 4.8

Incubated overnight at room temperature with mixing.

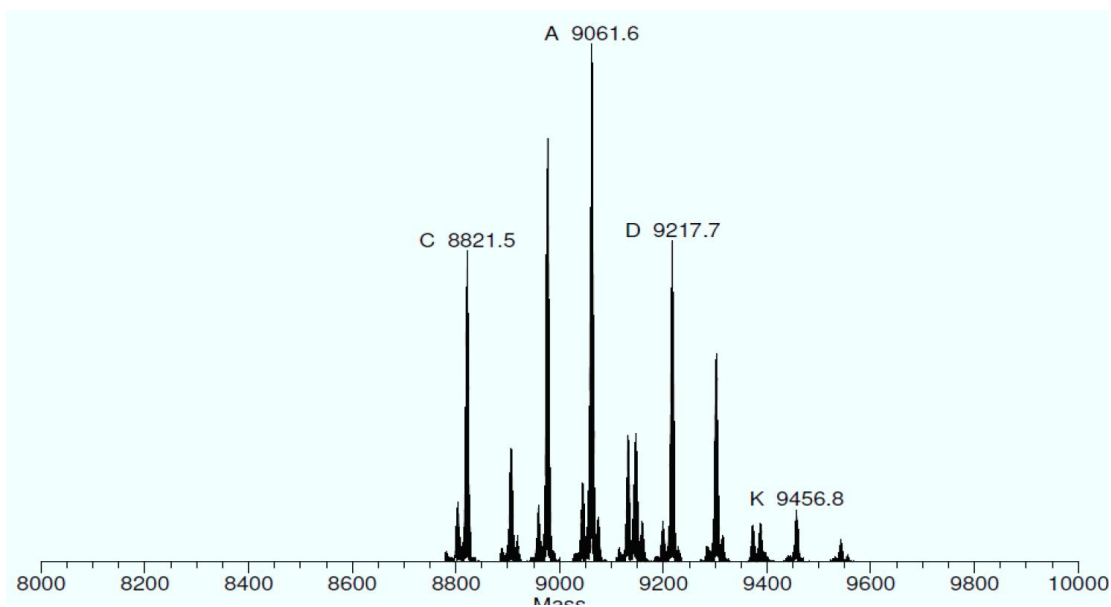


Figure xx. Deconvoluted ESI-MS of the following reaction 2.5 mgs ^{15}N WT Ub in 970 μl 0.1 M MES buffer pH 4.8 + 25 μl 50 mM Biotin hydrazide in DMSO + 12.5 μl of 100 mg/ml EDC solution in 0.1M MES buffer pH 4.8. The reaction was incubated overnight at room temperature with mixing. Final expected mass was 8904 Da since the starting ubiquitin is ^{15}N labeled.

We expected a net increase of 240 Da to the mass of the protein. In this scenario, we used ^{15}N WT Ub so our final expected mass was 8904 Da. It is evident from the ESI-MS deconvolution above that some reaction did take place, but many peaks were present. A couple of them show a mass difference that we were looking

for (e.g. the difference between 8821 Da and 9061 Da is the expected 240 Da) but the presence of extra peaks indicates non specific activation of Carboxyl group by EDC. It is unclear what has given rise to the starter molecular weight of 8821 (gain of 157 Da from the original ^{15}N WT Ub protein). EDC has a molecular weight of 191.7 Da and MES has a molecular weight of 195.2 Da.

Protocol B:

2.5 mgs Unlabeled WT Ub in 970 μl 20 mM NaP buffer pH 8

25 μl 50 mM Biotin hydrazide in DMSO

12.5 μl of 100 mg/ml EDC solution in 20 mM NaP buffer pH 8

Incubated overnight at room temperature with mixing.

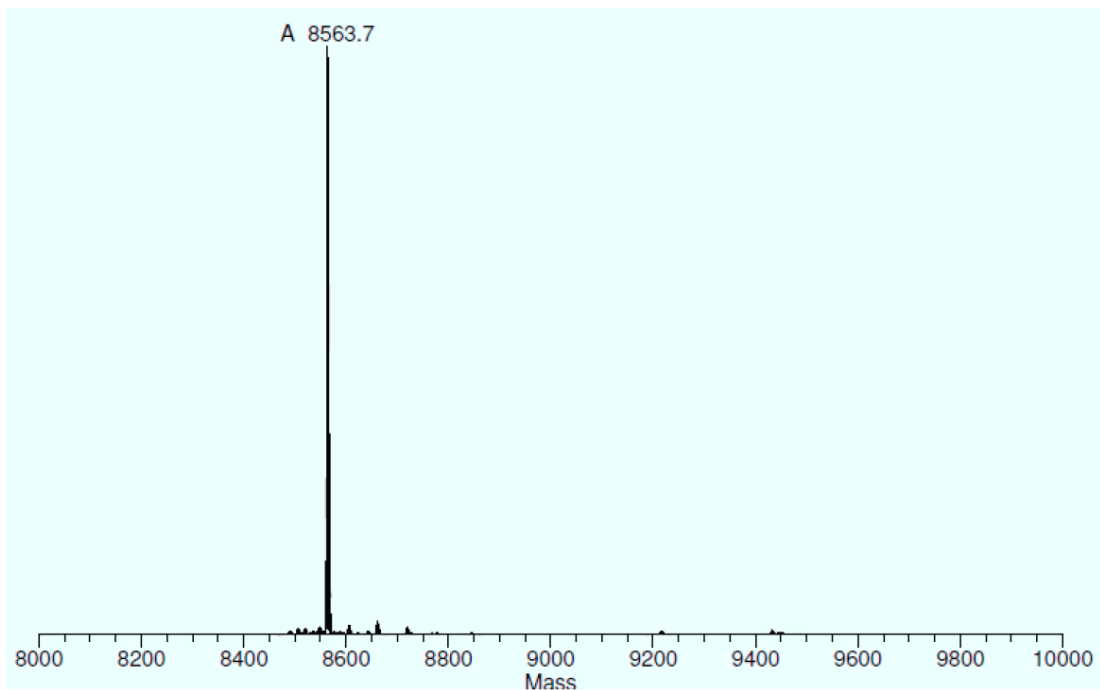


Figure xxi. Deconvoluted ESI-MS of the following reaction: 2.5 mgs Unlabeled WT Ub in 970 μl 20 mM NaP buffer pH 8 + 25 μl 50mM Biotin hydrazide in DMSO +12.5 μl of 100 mg/ml EDC solution in 20 mM NaP buffer pH 8 The reaction was incubated overnight at room temperature with mixing. Expected mass was 8804 Da.

No reaction took place with NaP buffer at the higher pH.

Attempt 3:

We wanted to see if we could use the ligation protocol used for making Ub chains to try and tag UbCOSR that has all amino groups protected by alloc groups (UbCOSR alloc) with biotin hydrazide. The -NH_2 group of biotin hydrazide acts as a nucleophile (instead of a NH_2 of Ub acting as a nucleophile) and attacks the carbon of the thioester moiety (however, the thioester has been replaced by an even better leaving group – the succinimide from H-OSu)

Reaction components:

~5 mgs Unlabeled UbCOSR Alloc

Dimethyl sulfoxide, DMSO 87.5 μl

N,N-Diisopropylethylamine (DIEA) 10 μl

Silver nitrate (AgNO_3) 2.5 μl

N-Hydroxysuccinimide (H-OSu) 2.5 μl

We covered the tube with aluminum foil and incubated overnight at room temperature with mixing.

If we looked at only the m/z after 1200 and transformed, we observed:

(We transformed only this region as Alloc-Ub exhibits only a few peaks at m/z ratios above 1200.)

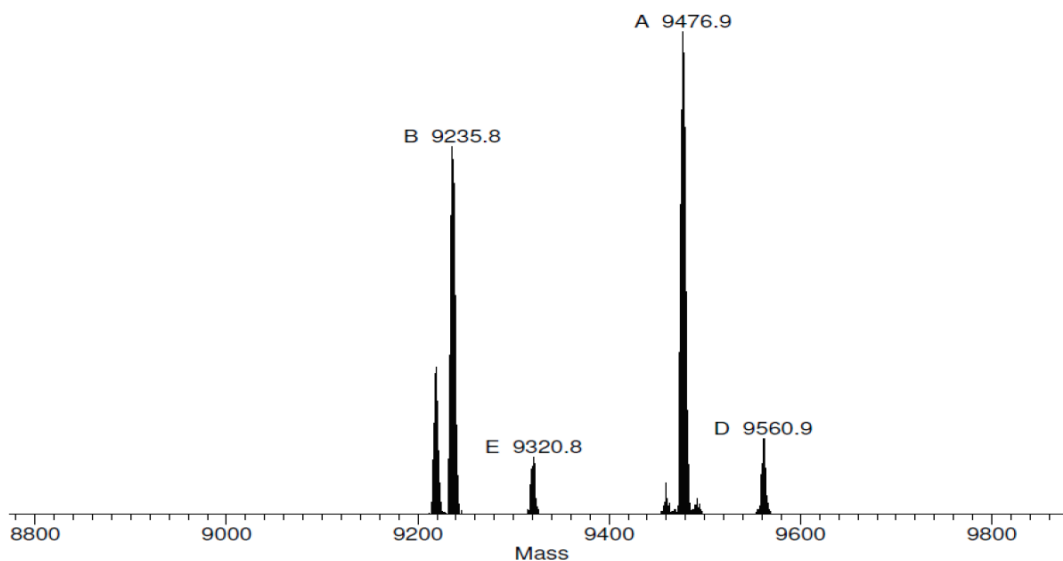


Figure xxii. Deconvoluted ESI-MS of the following reaction: ~5 mgs Unlabeled UbCOSR Alloc + DMSO 87.5 μ l + DIEA 10 μ l + AgNO₃ 2.5 μ l + H-OSu 2.5 μ l. Expected mass of WT Ub + 8 Allocs (where each Alloc is 84 Da) has an expected molecular weight of 9235 Da (peak B), while WT Ub + 9 Allocs has an expected molecular weight of 9321 Da (peak E).

WT Ub + 8 Allocs (where each Alloc is 84 Da) has an expected molecular weight of 9235 Da (peak B), while WT Ub + 9 Allocs has an expected molecular weight of 9321 (peak E). The thioester moiety has been lost, as no peak at 9360 (Ub-COSR + 8 Allocs) is observed or 9444 Da (Ub-COSR + 9 Allocs). We observed new peaks at 9476.9 (peak A: WT Ub + 8 Allocs + biotin hydrazide [mass of 240 Da]) and 9560 (peak D: WT Ub + 9 Allocs + biotin hydrazide [mass of 240 Da]). This suggests that we had a working reaction between biotin hydrazide and the C-terminus of WT Ub – however, the reaction was not at 100% completion, but perhaps more like 50/50.

Since we had so much trouble with this process and it was cumbersome, we decided to genetically incorporate Strep-tagTM II, to help immobilize the K6-linked diubiquitin chain. The tag consists of an eight amino-acid long sequence (Trp-Ser-His-Pro-Gln-Phe-Glu-Lys) that can bind to streptavidin and is fused to recombinant

proteins by genetically incorporating the above sequence into the gene of interest. It has been shown that this short, biologically inert sequence does not affect the proper folding of the recombinant protein. Moreover, the affinity of this peptide has been optimized to its ligand, a modified streptavidin: StrepTactin™. Thus, once it is attached to the polyubiquitin chain, it can be immobilized on a commercially available pre-packed StrepTactin™ column. We were successful in synthesizing K6-linked diubiquitin chains with Strep-tag™ II on the C-terminus of the proximal domain.

Once we had the diubiquitin chains that could be immobilized, we optimized the growth conditions of yeast, such that we could get a good proteomics profile. To avoid losing possible ligands to proteolytic activity, we used PEP4⁻ (Vacuolar aspartyl protease (proteinase A) deficient) yeast cells. Initially, protein profile of the yeast cell was checked using SDS PAGE at different stages of the growth curve to determine the stage with maximum number of possible ligands (Figure xxiii).

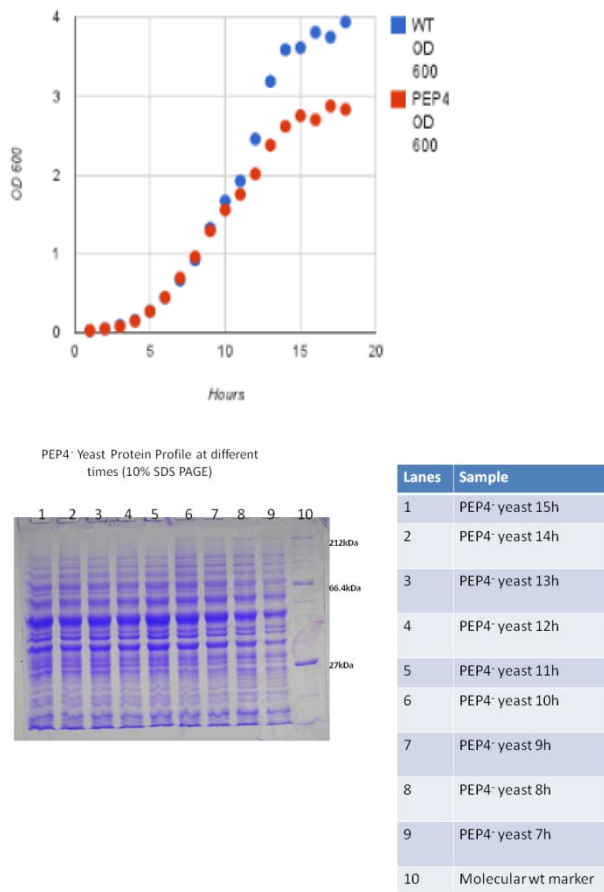


Figure xxiii. Growth curve of WT yeast and PEP4⁻ yeast (top), PEP4⁻ yeast protein profile at different time points during its growth curve (bottom).

Looking at the gel shown in Figure xxiv, the 10 hour time point was chosen and PEP4⁻ deficient cells were grown. The cells were lysed by freezing the cells using liquid nitrogen and grinding them using mortar and pestle.

The following protocol designed in collaboration with Andrew Timmons and Dr. Rajesh Singh was used for pull-down assay. It is based on Schmidt and Skerra 2007, Nature Protocols⁶⁹.

1. Washed column with 5 ml buffer 1 (50 mM Tris-HCl pH 7.4, 150 mM NaCl, 7.5% glycerol) at 1ml/min.

2. Loaded strep chains (K6-Ub₂- Strep-tagTM II). Made sure the strep chains are in buffer 1 before loading.
3. Washed column with 5 ml buffer 1 to remove any unbound strep chains. Collected flow through and stored it in +4 °C for later use.
4. At this point we switched to +4 °C. It is important to keep everything (buffer, lysate, column, etc.) at +4 °C. This way, we can keep most DUBs inactive.
5. Since the potential binding partners are expressed at endogenous level, as well as in few instances they are expressing only at certain stage(s) of the cell cycle of yeast (which can further reduce the amount of yeast cells expressing the potential binder), we used 500 ml of cultivated yeast culture in 10 ml of lysis buffer and then passed it through the column with a slow flow rate (say 0.2-0.3 ml/min). In this way, we passed through column a larger amount of potential binders, and so had greater chance of binding more and consequently seeing them on SDS-PAGE.
6. Incubated at 4 °C for 60 minutes. We can reduce it or keep it depending on the flow rate.
7. Washed column till Abs₂₈₀ drops to below 0.02 to remove any unbound proteins. Kept flowrate at 0.5 ml/min.
8. Eluted protein using 3 column volume (CV) buffer 2 (Buffer 1 + (Protease/phosphatase inhibitors if available) + 2.5 mM desthiobiotin). Aliquoted 0.5 ml each, such that we do not unnecessarily dilute the eluted proteins.

9. Regenerated the column using 15ml Buffer 3 (Buffer 1 + 1 mM 4'-hydroxyazobenzene-2-carboxylic acid (HABA)) and finally re-equilibrated with Buffer 1.
10. Also, ran a negative control excluding steps 2 & 3, in which we loaded yeast lysate onto the StrepTactin™ column with no chains bound to it. This control is to find out which of the proteins from the yeast lysate directly bind to StrepTactin™ and are eluted upon being treated by 2.5 mM desthiobiotin. We treated this column exactly as the positive column.
11. To analyze the eluates, we used 4X-5X concentrated sample loading buffer. e.g., 20 ul of elution + 5 ul of 5X buffer, boiled and then loaded everything in one lane of SDS-PAGE.
12. The different samples run on the gel were:

MW marker, Strep chain, lysate before loading, lysate flow through, lysate wash, elution fraction, control elution fraction.

We used both 10% and 15% SDS-PAGE for better separation in high and low molecular weight profile. Additionally, since many eukaryotic organisms have ca. 25-30% of mRNA expressing proteins which are < or equal to 3 KDa, it would have been interesting to see if our Ub chains pull out any of these small proteins. For this, we could pass the eluted proteins to a 3 KDa cut-off filter and subject the flow through to a trypsinized/ nontrypsinized mass spec. This way, hopefully, we can capture few small proteins which always eluded most pull down experiments (remember people widely use SDS-PAGE to separate the binders and running even 15% SDS-PAGE should land most of the small

proteins in the running tank).

K6-Ub₂ in which the proximal end is Strep-tagTM-II tagged was immobilized on the StrepTactinTM column. Upon passing through the PEP4⁻ yeast lysate, we found some binding partners. But similar binding profile was also seen in the negative control in which the yeast lysate was loaded directly on the StrepTactinTM column. Thus, the experiment was inconclusive. We later found that most likely K6-Ub₂-Strep-tagTM II was washed off while we tried to wash off the unbound lysate. This project was dropped due to unsuitable immobilization techniques.

Tail variants project

¹⁵N relaxation NMR data were collected for Ub and truncated tail variants, namely WT Ub (Ub76), ubiquitin with last two amino acids removed (Ub74) and ubiquitin with last four amino acids removed (Ub72) in 20 mM NaP buffer, pH 6.8 at 303.4 K (~30 °C). The data were analyzed using ROTDIF and is tabulated in Table i.

Ub Variant	τ_c (ns)	α (deg)	β (deg)	γ (deg)	Anisotropy	Rhombicity (ns)	D_{xx} rad s ⁻² (*10 ⁷)	D_{yy} rad s ⁻² (*10 ⁷)	D_{zz} rad s ⁻² (*10 ⁷)
Ub72	3.85 ±0.06	165 ± 26	170± 14	64 ± 30	1.10 ± 0.04	0.875 ± 0.22	4.06 ± 0.12	4.31 ± 0.09	4.62 ±0.15
Ub74	4.24 ±0.19	105 ± 14	158 ± 7	44 ± 98	1.21 ± 0.13	0.057 ± 0.020	3.65 ± 0.18	3.69 ± 0.21	4.43 ±0.46
Ub76	4.34 ±0.09	111 ± 10	156 ± 5	11 ± 27	1.25 ±0.06	0.165 +/- 0.022	3.50 ±0.11	3.59 ± 0.09	4.42 ± 0.18

Table i. Overall rotational diffusion tensor characteristics of ubiquitin tail variants determined from ¹⁵N relaxation data. Atom coordinates for each ubiquitin variant were taken from (PDB: 1D3Z). D_{xx} , D_{yy} , D_{zz} represent the principal components of the overall rotational diffusion tensors along the x, y and z principal axes respectively. τ_c represents the overall rotational correlation time. α , β , γ represent Euler angles that determine the orientation of the principal axes of the overall rotational diffusion tensor with respect to the coordinate frame of the protein.

Ub tail variants RDC analysis

Similarly, RDC data were collected for all the tail variants. The data were analyzed using PATI (Table ii).

Tail Variant	Variable	Calculated* (1e-04)	Predicted* (1e-04)	Scaled Predicted value* (1e-04)
Ub72	S_{xx}	0.194 ± 0.141	0.167	0.25
	S_{yy}	4.787 ± 3.353	3.181	4.754
	S_{zz}	-4.980 ± 3.436	-3.348	-5.004
Ub74	S_{xx}	1.067 ± 0.162	1.277	1.737
	S_{yy}	6.072 ± 0.321	4.117	5.599
	S_{zz}	-7.139 ± 0.299	-5.394	-8.062
Ub76	S_{xx}	2.360 ± 0.154	2.317	3.012
	S_{yy}	6.670 ± 0.282	4.731	6.15
	S_{zz}	-9.029 ± 0.246	-7.047	-9.161

Tail variant	Optimal Scaling factor
Ub72	1.4946
Ub74	1.3631
Ub76	1.3

Table ii. Alignment tensor characteristics for ubiquitin tail variants determined from the RDCs. Atom coordinates for each Ub variant were taken from PDB: 1D3Z. For Ub74, we removed the last two amino acids from the PDB file while for Ub72, we removed the last four. S_{xx} , S_{yy} , S_{zz} represent the principal components of the alignment tensors along the x, y and z axes respectively. α , β , γ represent Euler angles that determine the orientation of the principal axes of the alignment tensor with respect to the coordinate frame of the protein. The final column was calculated by multiplying the predicted value obtained from PATI using 1D3Z coordinates with the optimal scaling factor for S_{xx} , S_{yy} , S_{zz} of each variant.

Also, the rhombicity values are tabulated in Table iii.

Tail Variant	Variable	Calculated	Predicted
Ub72	Da	-2.490 +/- -1.718 * (1e-04)	-1.674* (1e-04)
	Dr	-1.531 +/- -1.091 * (1e-04)	-1.005* (1e-04)
	Rhombicity	0.615 +/- -0.033	0.60
Ub74	Da	-3.570 +/- -0.149 * (1e-04)	-2.697* (1e-04)
	Dr	-1.669 +/- -0.137 * (1e-04)	-0.947* (1e-04)
	Rhombicity	0.467 +/- -0.030	0.35
Ub76	Da	-4.515 +/- -0.123* (1e-04)	-3.524* (1e-04)
	Dr	-1.437 +/- -0.127* (1e-04)	-0.805* (1e-04)
	Rhombicity	0.318 +/- -0.024	0.23

Table iii. Rhombicity values of the tail variants.

Bibliography

1. Li, W. & Ye, Y. Polyubiquitin chains: functions, structures, and mechanisms. *Cell. Mol. Life Sci.* **65**, 2397–406 (2008).
2. Pickart, C. M. & Fushman, D. Polyubiquitin chains: polymeric protein signals. *Curr. Opin. Chem. Biol.* **8**, 610–6 (2004).
3. Ciechanover, A. & Iwai, K. The ubiquitin system: from basic mechanisms to the patient bed. *IUBMB Life* **56**, 193–201 (2004).
4. Lee, F. K. M. *et al.* The role of ubiquitin linkages on alpha-synuclein induced-toxicity in a *Drosophila* model of Parkinson's disease. *J. Neurochem.* **110**, 208–19 (2009).
5. Fushman, D. & Wilkinson, K. D. Structure and recognition of polyubiquitin chains of different lengths and linkage. *F1000 Biol. Rep.* **3**, 26 (2011).
6. Terrell, J., Shih, S., Dunn, R. & Hicke, L. A function for monoubiquitination in the internalization of a G protein-coupled receptor. *Mol. Cell* **1**, 193–202 (1998).
7. Hicke, L. Protein regulation by monoubiquitin. *Nat. Rev. Mol. Cell Biol.* **2**, 195–201 (2001).
8. Ulrich, H. D. & Walden, H. Ubiquitin signalling in DNA replication and repair. *Nat. Rev. Mol. Cell Biol.* **11**, 479–89 (2010).
9. Glickman, M. H. & Ciechanover, A. The ubiquitin-proteasome proteolytic pathway: destruction for the sake of construction. *Physiol. Rev.* **82**, 373–428 (2002).

10. Bachmair, A. & Varshavsky, A. The degradation signal in a short-lived protein. *Cell* **56**, 1019–32 (1989).
11. Al-Hakim, A. *et al.* The ubiquitous role of ubiquitin in the DNA damage response. *DNA Repair (Amst)*. **9**, 1229–40 (2010).
12. Kirkpatrick, D. S. *et al.* Quantitative analysis of in vitro ubiquitinated cyclin B1 reveals complex chain topology. *Nat. Cell Biol.* **8**, 700–10 (2006).
13. Jin, L., Williamson, A., Banerjee, S., Philipp, I. & Rape, M. Mechanism of ubiquitin-chain formation by the human anaphase-promoting complex. *Cell* **133**, 653–65 (2008).
14. Beal, R. E., Toscano-Cantaffa, D., Young, P., Rechsteiner, M. & Pickart, C. M. The hydrophobic effect contributes to polyubiquitin chain recognition. *Biochemistry* **37**, 2925–34 (1998).
15. Beal, R., Deveraux, Q., Xia, G., Rechsteiner, M. & Pickart, C. Surface hydrophobic residues of multiubiquitin chains essential for proteolytic targeting. *Proc. Natl. Acad. Sci. U. S. A.* **93**, 861–6 (1996).
16. Varadan, R., Walker, O., Pickart, C. & Fushman, D. Structural properties of polyubiquitin chains in solution. *J. Mol. Biol.* **324**, 637–47 (2002).
17. Datta, A. B., Hura, G. L. & Wolberger, C. The structure and conformation of Lys63-linked tetraubiquitin. *J. Mol. Biol.* **392**, 1117–24 (2009).
18. Eddins, M. J., Varadan, R., Fushman, D., Pickart, C. M. & Wolberger, C. Crystal structure and solution NMR studies of Lys48-linked tetraubiquitin at neutral pH. *J. Mol. Biol.* **367**, 204–11 (2007).
19. Varadan, R. *et al.* Solution conformation of Lys63-linked di-ubiquitin chain

- provides clues to functional diversity of polyubiquitin signaling. *J. Biol. Chem.* **279**, 7055–63 (2004).
20. Varadan, R., Assfalg, M., Raasi, S., Pickart, C. & Fushman, D. Structural determinants for selective recognition of a Lys48-linked polyubiquitin chain by a UBA domain. *Mol. Cell* **18**, 687–98 (2005).
 21. Groettrup, M., Pelzer, C., Schmidtke, G. & Hofmann, K. Activating the ubiquitin family: UBA6 challenges the field. *Trends Biochem. Sci.* **33**, 230–7 (2008).
 22. Ye, Y. & Rape, M. Building ubiquitin chains: E2 enzymes at work. *Nat. Rev. Mol. Cell Biol.* **10**, 755–64 (2009).
 23. David, Y. *et al.* E3 ligases determine ubiquitination site and conjugate type by enforcing specificity on E2 enzymes. *J. Biol. Chem.* **286**, 44104–15 (2011).
 24. Reyes-Turcu, F. E. & Wilkinson, K. D. Polyubiquitin binding and disassembly by deubiquitinating enzymes. *Chem. Rev.* **109**, 1495–508 (2009).
 25. Raasi, S., Orlov, I., Fleming, K. G. & Pickart, C. M. Binding of polyubiquitin chains to ubiquitin-associated (UBA) domains of HHR23A. *J. Mol. Biol.* **341**, 1367–79 (2004).
 26. Zhang, D., Raasi, S. & Fushman, D. Affinity makes the difference: nonselective interaction of the UBA domain of Ubiquilin-1 with monomeric ubiquitin and polyubiquitin chains. *J. Mol. Biol.* **377**, 162–80 (2008).
 27. Bennett, E. J. & Harper, J. W. DNA damage: ubiquitin marks the spot. *Nat. Struct. Mol. Biol.* **15**, 20–2 (2008).
 28. Nowicka, U. *et al.* DNA-Damage-Inducible 1 Protein (Ddi1) Contains an

- Uncharacteristic Ubiquitin-like Domain that Binds Ubiquitin. *Structure* **23**, 542–557 (2015).
29. Dolinsky, T. J., Nielsen, J. E., McCammon, J. A. & Baker, N. A. PDB2PQR: an automated pipeline for the setup of Poisson-Boltzmann electrostatics calculations. *Nucleic Acids Res.* **32**, W665–W667 (2004).
 30. Singh, R. K. *et al.* Recognition and Cleavage of Related to Ubiquitin 1 (Rub1) and Rub1-Ubiquitin Chains by Components of the Ubiquitin-Proteasome System. *Mol. Cell. Proteomics* **11**, 1595–1611 (2012).
 31. Xu, P. *et al.* Quantitative proteomics reveals the function of unconventional ubiquitin chains in proteasomal degradation. *Cell* **137**, 133–45 (2009).
 32. Ikeda, F. & Dikic, I. Atypical ubiquitin chains: new molecular signals. ‘Protein Modifications: Beyond the Usual Suspects’ review series. *EMBO Rep.* **9**, 536–42 (2008).
 33. Kumar, K. S. A., Spasser, L., Erlich, L. A., Bavikar, S. N. & Brik, A. Total chemical synthesis of di-ubiquitin chains. *Angew. Chem. Int. Ed. Engl.* **49**, 9126–31 (2010).
 34. Castañeda, C. *et al.* Nonenzymatic assembly of natural polyubiquitin chains of any linkage composition and isotopic labeling scheme. *J. Am. Chem. Soc.* **133**, 17855–68 (2011).
 35. Fushman, D. & Walker, O. Exploring the linkage dependence of polyubiquitin conformations using molecular modeling. *J. Mol. Biol.* **395**, 803–14 (2010).
 36. Virdee, S., Ye, Y., Nguyen, D. P., Komander, D. & Chin, J. W. Engineered diubiquitin synthesis reveals Lys29-isopeptide specificity of an OTU

- deubiquitinase. *Nat. Chem. Biol.* **6**, 750–7 (2010).
37. Morris, J. R. & Solomon, E. BRCA1 : BARD1 induces the formation of conjugated ubiquitin structures, dependent on K6 of ubiquitin, in cells during DNA replication and repair. *Hum. Mol. Genet.* **13**, 807–17 (2004).
 38. Wu-Baer, F., Lagrazon, K., Yuan, W. & Baer, R. The BRCA1/BARD1 heterodimer assembles polyubiquitin chains through an unconventional linkage involving lysine residue K6 of ubiquitin. *J. Biol. Chem.* **278**, 34743–6 (2003).
 39. Sobhian, B. *et al.* RAP80 targets BRCA1 to specific ubiquitin structures at DNA damage sites. *Science* **316**, 1198–202 (2007).
 40. Nguyen, L. K. *et al.* Switches, excitable responses and oscillations in the Ring1B/Bmi1 ubiquitination system. *PLoS Comput. Biol.* **7**, e1002317 (2011).
 41. Castañeda, C. A. *et al.* Linkage via K27 Bestows Ubiquitin Chains with Unique Properties among Polyubiquitins. *Structure* **24**, 423–436 (2016).
 42. Castañeda, C. A. *et al.* Linkage-specific conformational ensembles of non-canonical polyubiquitin chains. *Phys. Chem. Chem. Phys.* **18**, 5771–5788 (2016).
 43. Birsa, N. *et al.* Lysine 27 Ubiquitination of the Mitochondrial Transport Protein Miro Is Dependent on Serine 65 of the Parkin Ubiquitin Ligase. *J. Biol. Chem.* **289**, 14569–14582 (2014).
 44. Cao, Z. *et al.* Ubiquitin Ligase TRIM62 Regulates CARD9-Mediated Anti-fungal Immunity and Intestinal Inflammation. *Immunity* **43**, 715–726 (2015).
 45. Arimoto, K.-I. *et al.* Polyubiquitin conjugation to NEMO by tripartite motif protein 23 (TRIM23) is critical in antiviral defense.

doi:10.1073/pnas.1004621107

46. Liu, J. *et al.* Rhbdd3 controls autoimmunity by suppressing the production of IL-6 by dendritic cells via K27-linked ubiquitination of the regulator NEMO. *Nat. Immunol.* **15**, 612–622 (2014).
47. Gatti, M. *et al.* RNF168 Promotes Noncanonical K27 Ubiquitination to Signal DNA Damage. *Cell Rep.* **10**, 226–238 (2015).
48. Walker, O., Varadan, R. & Fushman, D. Efficient and accurate determination of the overall rotational diffusion tensor of a molecule from (15)N relaxation data using computer program ROTDIF. *J. Magn. Reson.* **168**, 336–45 (2004).
49. Rückert, M. and & Otting, G. Alignment of Biological Macromolecules in Novel Nonionic Liquid Crystalline Media for NMR Experiments. (2000).
doi:10.1021/JA001068H
50. Clore, G. M. & Garrett, D. S. R-factor, Free R, and Complete Cross-Validation for Dipolar Coupling Refinement of NMR Structures. (1999).
doi:10.1021/JA991789K
51. Berlin, K., P O’Leary, D. & Fushman, D. Structural assembly of molecular complexes based on residual dipolar couplings. *J. Am. Chem. Soc.* **132**, 8961–8972 (2010).
52. Berlin, K. *et al.* Recovering a representative conformational ensemble from underdetermined macromolecular structural data. *J. Am. Chem. Soc.* **135**, 16595–609 (2013).
53. Curtis, J. E., Raghunandan, S., Nanda, H. & Krueger, S. SASSIE: A program to study intrinsically disordered biological molecules and macromolecular

- ensembles using experimental scattering restraints. *Comput. Phys. Commun.* **183**, 382–389 (2012).
54. Dickinson, B. C., Varadan, R. & Fushman, D. Effects of cyclization on conformational dynamics and binding properties of Lys48-linked di-ubiquitin. *Protein Sci.* **16**, 369–378 (2007).
55. Lin, D. Y., Diao, J., Zhou, D. & Chen, J. Biochemical and Structural Studies of a HECT-like Ubiquitin Ligase from *Escherichia coli* O157:H7. *J. Biol. Chem.* **286**, 441–449 (2011).
56. Hospenthal, M. K., Freund, S. M. V & Komander, D. Assembly, analysis and architecture of atypical ubiquitin chains. *Nat. Struct. Mol. Biol.* **20**, 555–565 (2013).
57. Sobhian, B. *et al.* RAP80 targets BRCA1 to specific ubiquitin structures at DNA damage sites. *Science* **316**, 1198–202 (2007).
58. Sims, J. J. & Cohen, R. E. Linkage-specific avidity defines the lysine 63-linked polyubiquitin-binding preference of rap80. *Mol. Cell* **33**, 775–83 (2009).
59. Varadan, R. *et al.* Solution conformation of Lys63-linked di-ubiquitin chain provides clues to functional diversity of polyubiquitin signaling. *J. Biol. Chem.* **279**, 7055–63 (2004).
60. Sekiyama, N. *et al.* NMR analysis of Lys63-linked polyubiquitin recognition by the tandem ubiquitin-interacting motifs of Rap80. *J. Biomol. NMR* **52**, 339–50 (2012).
61. Zhang, N. *et al.* Structure of the S5a:K48-Linked Diubiquitin Complex and Its Interactions with Rpn13. *Mol. Cell* **35**, 280–290 (2009).

62. Castañeda, C. A., Kashyap, T. R., Nakasone, M. A., Krueger, S. & Fushman, D. Unique Structural, Dynamical, and Functional Properties of K11-Linked Polyubiquitin Chains. *Structure* **21**, 1168–1181 (2013).
63. Wiener, R., Zhang, X., Wang, T. & Wolberger, C. The mechanism of OTUB1-mediated inhibition of ubiquitination. *Nature* **483**, 618–622 (2012).
64. Pickart, C. M. & Raasi, S. Controlled Synthesis of Polyubiquitin Chains. in *Methods in enzymology* **399**, 21–36 (2005).
65. Castañeda, C. A. *et al.* Controlled enzymatic synthesis of natural-linkage, defined-length polyubiquitin chains using lysines with removable protecting groups. *Chem. Commun.* **47**, 2026 (2011).
66. T. D. Goddard and D. G. Kneller. No Title. *SPARKY 3, University of California, San Francisco*
67. Keller, R. L. J. The Computer Aided Resonance Assignment Tutorial.
68. Ryabov, Y. & Fushman, D. Interdomain mobility in di-ubiquitin revealed by NMR. *Proteins Struct. Funct. Bioinforma.* **63**, 787–796 (2006).
69. Schmidt, T. G. M. & Skerra, A. The Strep-tag system for one-step purification and high-affinity detection or capturing of proteins. *Nat. Protoc.* **2**, 1528–35 (2007).